2001

Weathering crust processes on melting glacier ice (Alberta, Canada)

Corinne Joanne Schuster
Wilfrid Laurier University

INFORMATION TO USERS

This manuscript has been reproduced from the microfilm master. UMI films the text directly from the original or copy submitted. Thus, some thesis and dissertation copies are in typewriter face, while others may be from any type of computer printer.

The quality of this reproduction is dependent upon the quality of the copy submitted. Broken or indistinct print, colored or poor quality illustrations and photographs, print bleedthrough, substandard margins, and improper alignment can adversely affect reproduction.

In the unlikely event that the author did not send UMI a complete manuscript and there are missing pages, these will be noted. Also, if unauthorized copyright material had to be removed, a note will indicate the deletion.

Oversize materials (e.g., maps, drawings, charts) are reproduced by sectioning the original, beginning at the upper left-hand corner and continuing from left to right in equal sections with small overlaps.

Photographs included in the original manuscript have been reproduced xerographically in this copy. Higher quality 6" x 9" black and white photographic prints are available for any photographs or illustrations appearing in this copy for an additional charge. Contact UMI directly to order.

ProQuest Information and Learning
300 North Zeeb Road, Ann Arbor, MI 48106-1346 USA
800-521-0600

Weathering Crust Processes

on Melting Glacier Ice

by

Corinne J. Schuster

(BSc, Leicester University, England, 1993)

THESIS

Submitted to the Department of Geography and Environmental Studies
in partial fulfilment of the requirements
for the degree of
Doctor of Philosophy
Wilfrid Laurier University
2001

ABSTRACT

This thesis examines the relationship between the energy balance and hydrology of a glacier at the ice surface interface during the melt season. Experimental sub-catchments were established on the ablation area of the Peyto Glacier, Alberta, Canada, during the summers of 1994, 1995 and 1997. These sub-catchments were equipped with meteorological and hydrological instrumentation to examine relationships in the surface layer.

Specifically, the development of a phenomenon known as the weathering crust is followed by examining the ratio between potential surface lowering (calculated from energy available for melt) and actual surface lowering (as measured in the field). This enables an indirect division of weathering crust development into growth and decay stages. Weathering crust growth is driven by K^* while decay is driven by positive inputs of $Q_H + Q_E + L^*$. Analysis was undertaken within periods of weathering crust growth, crustal decay and when little or no apparent melt was occurring. Actual differences between measured and potential surface lowering were also calculated. Further, associated stage records for the 1997 field season were examined for periods of weathering crust growth and decay in order to examine lags within the system.

This analysis led to the simulation of ice densities at increasing depths within an ice column, based on weathering crust processes. The simulation was driven by data collected in the field. An addition to the simulation which allows for re-freezing of water within the crust indicates that the effect of re-freezing of ice during the melt season is virtually negligible. Further, subsurface priming is indicated under daytime conditions when there is a net energy loss at the surface. It is proposed that the results from the simulations produce a suitable surrogate for indicating the resultant changes in ice density given weathering crust development, thus providing an insight into events in the field.

It is concluded that the weathering crust phenomenon is a complex relationship between energy inputs, initial crustal conditions and mechanical thresholds. Daytime weathering crust decay is the most complicated to analyse, as growth and decay are occurring simultaneously, even though decay is the dominant process. Daytime growth and nocturnal decay are the most straightforward cases. Weathering crust development appears to dampen catchment response by increasing storage in the lower density ice in the late morning. Further, the storage capacity of a highly developed weathering crust can result in drainage from the system overnight. This overnight drainage can be compounded by nocturnal crustal decay.

ACKNOWLEDGEMENTS

In the undertaking of this thesis there are many people who have provided help and support and who deserve my thanks. Dr. Scott Munro (University of Toronto, Erindale) and Dr. Eric Mattson (Nipissing University) were instrumental in the completion of the thesis. I would like to thank Dr. Gordon Young (WLU) for his financial support and guidance and Dr. Mike English (WLU), Dr. Dan Moore (University of British Columbia) and Dr. Chris Smart (University of Western Ontario) for their contributions.

My thanks go to Scott Munro for teaching me the art of tinkering and other field necessities over the years as well as his ongoing friendship. Further thanks go to Alistair Wallace, Eric Mattson, Mike Demuth, Gary, Alexi, Ty, Mike, Coolcat and Chris for their help in the field. The National Hydrological Research Institute provided access to the Peyto Glacier Research huts and logistical support through Mike Demuth and Environment Canada provided field equipment in 1997. I would like to thank the Cold Regions Research Centre at WLU, and Dr. Mike English for logistical support. Financial support was provided by Dr. Gordon Young, Mountain Equipment Co-Op through their Environmental Research Grants and the Graduate Student Union, WLU.

Pam Schauss and Grant Simpson provided cartographic and computer support and were always around for a chat. Michael was my personal graphics consultant and Liz just makes me laugh.

Special thanks go to Krusty for being my right hand man, a great field guy and for putting up with me throughout this whole process. Iceman always had faith in me, livened up the field seasons and kept me focussed on the big picture. Thanks to my Buddy for keeping me safe in the wilderness and sane the rest of the time!

Finally, my thanks go to my parents for everything that has brought me to this point.

TABLE OF CONTENTS

LIST OF TABLES

LIST OF FIGURES

CHAPTER 1 INTRODUCTION

Glaciers have a considerable hydrological impact on their drainage basins. Glaciers regulate stream flow on a seasonal basis by storing winter precipitation and releasing water during the summer months. The melt water produced by glaciers is important for the water resources of these regions and adjacent lowlands. Spring and summer melt of the snow cover and ice surface can result in large volumes of melt water entering the hydrological system. Due to the importance of glaciers as a water resource, and in the light of probable global warming, it is becoming increasingly more important to examine the hydrological processes which occur as a result of a glacier cover.

1.1. Rationale

In recent research, glacial hydrologists have been mainly interested in englacial and subglacial processes. Research into these areas has provided many insights into the relatively unknown glacial drainage system beneath the ice surface. However, the surface hydrology of glaciers, and the processes at work, have not been accorded such detailed examination, even though it has been recognised that surface melt water contributes up to ninety percent of the melt water in the system. As far back as the mid-1970's attention has been drawn to the lack of investigation into the relationship between glacier melt and actual mass loss at the ice surface (Golubev, 1975).

Melt water production from a glacier can be predicted with reasonable accuracy over a melt season, but at the diurnal scale variations in discharge are more difficult to model with the same degree of accuracy, so fewer studies have been undertaken. One probable reason for these inaccuracies is the cycle of weathering crust development, an integral process in surface lowering, which occurs as a result of the penetration of short-wave radiation into an ice surface. Ice

transmits short-wave radiation through its medium according to an exponential decay curve. As a result, melt not only occurs on a plane, but in a volume, and this is very difficult to measure.

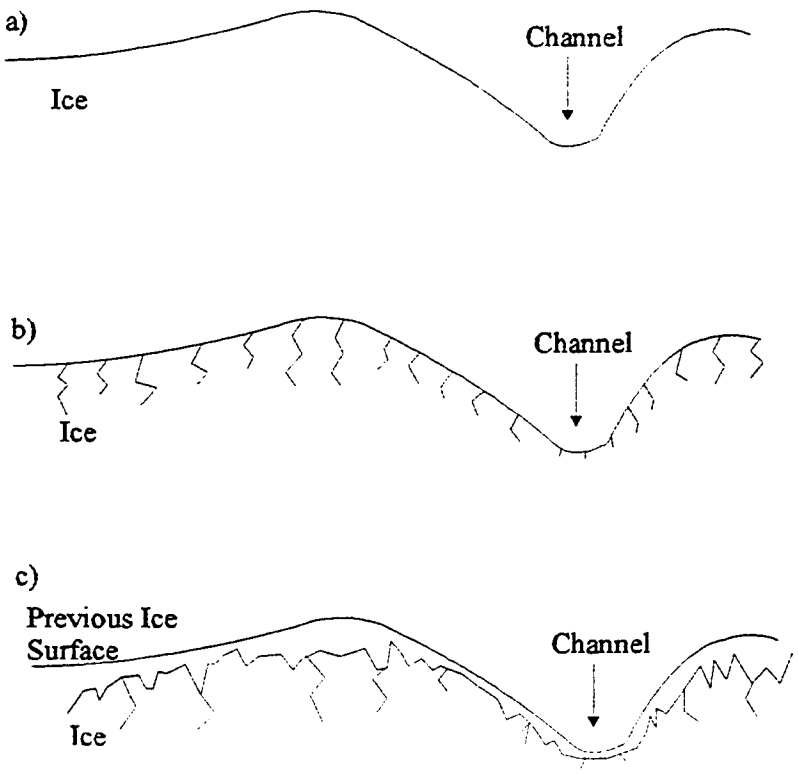

Fig. 1.1. The progression from a) no weathering crust to c) surface lowering as a result of weathering crust growth

The weathering crust is a surface layer of ice that is less dense than typical glacier ice, which has a density of 0.89 kg m^{-3} x 10^3. Measurements of core sample ice densities suggest densities in the weathering crust as low as 0.30 kg m^{-3} x 10^3 (from measurements taken on the Peyto Glacier in August 1994). Ice densities within the weathering crust will decrease as internal melt occurs and, as a result of this, surface roughness will increase. Eventually, internal melt will lead to enhanced surface lowering (Fig. 1.1), either as a result of further melt of the lower density

layer or through mechanical collapse of the ice. This can be identified through greater measured surface lowering than would be expected given the amount of energy available for melt. The process is cyclic because, as surface lowering occurs, a new layer of ice becomes available for melt at depth. A complicating factor in this process is that, given a series of overcast days, the short-wave energy source decreases and the weathering crust will not develop. Indeed, if the sensible heat flux becomes the dominant energy source and energy is available for melt, the weathering crust will decay. This results in a very smooth glacier surface because turbulent heat fluxes and long-wave radiation cannot penetrate the ice, so melt will only occur at the surface.

Weathering crust processes will directly affect surface lowering measurements. During periods of weathering crust growth, the amount of ice mass lost from the surface will be underestimated by straightforward surface lowering techniques. This mass loss will be overestimated during periods of crustal decay. The processes will also affect water movement at the ice surface. A less dense surface layer will provide storage for surface meltwater and introduce a lag into the system between the point of ice melt and flow within a supraglacial channel. Under highly developed weathering crust conditions, in addition to water storage, water will flow within this upper layer.

Processes acting at the air-ice interface are important in quantifying amounts of ice lost and therefore amounts of melt water generated from a glacier surface. It is this surface water which drives the rest of the glacial hydrologic system. Important implications include those for glacier sliding, which in turn may be a major factor in glacier surges, and for provision of water flowing in the proglacial stream, which is a resource for many users downstream.

1.2. Research Goal

The goal of this research is to examine and explain the weathering crust phenomenon on a bare ice surface and to track its development under changing meteorological conditions.

This is achieved through:

1) collection and analysis of relevant data;

2) determination of the effect of weathering crust development on the accuracies of standard ablation measurement techniques (specifically, surface lowering);

3) discrimination of conditions for weathering crust growth and decay for widespread application; and

4) simulation of ice densities over time from measured energy inputs.

1.3. Field Location

The glacier chosen for this study is the Peyto Glacier (51°40' N, 116°35' W). It is a mid-latitude glacier located in Banff National Park, Alberta, approximately 30 km north-west of Lake Louise. It is part of the Wapta Icefield, which straddles the Continental Divide. The basin is in the headwaters of the Mistaya Basin, a larger basin which forms a tributary of the North Saskatchewan River. The Peyto Glacier covered an area of 11.74 km^2 in 1995 (IAHS, 1998) in a total basin area of 22.8 km^2 (Fig. 1.2.). The glacier has been shrinking fairly rapidly over the past decade. The glacier has retreated approximately 500 m over the last thirty years and Young (1991) calculated glacier shrinkage between 1966 and 1989 to be 1.3 km^2.

The study site is located at an elevation of approximately 2 230 metres above sea level (m asl) on the glacier tongue. The total altitudinal range of the glacier is 2 100 to 3 100 m asl with a mean elevation of 2 635 m asl (Ommanney, 1990). The Peyto Glacier was chosen for several

reasons. First, the glacier has been well monitored for a long time, particularly after it was designated to be studied as part of the International Hydrological Decade (IHD) from 1965 to 1974. Although part of a much broader spectrum of scientific investigation, experiments conducted and data collected under the auspices of the IHD have facilitated intense studies, particularly in Canada and especially on the Peyto Glacier. The main reason for its choice in the IHD study was its well defined catchment area with a single proglacial channel which did not pond up and which was not heavily braided (Young, pers. com.). The glacier is also easily accessed by foot off the main highway and the lower ablation area consists of a large, relatively flat area on which experiments can be conducted without hazard.

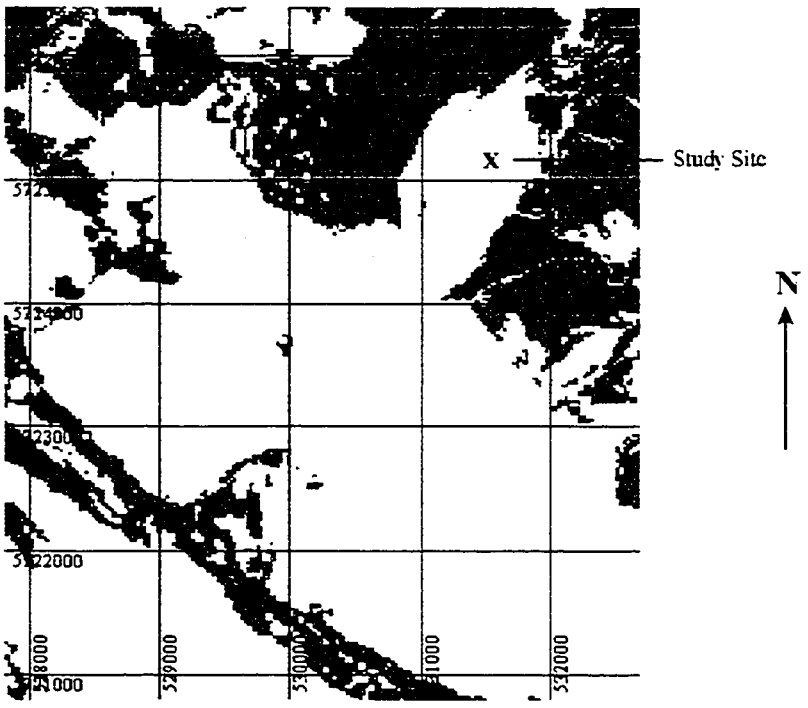

Fig. 1.2. Location map of Peyto Glacier and field site

The following is an overview of literature relating to the interaction between the near-surface atmosphere and the skin layer of a glacier ice surface. An examination of the surface energy balance of a glacier is undertaken, with respect to the effects on glacial surface melt and runoff processes and the resultant micro hydrologic regime.

2.1. The Relationship between Glaciers and Meteorology

Glacial meteorology is concerned with determining relationships between the prevailing meteorological situation and glacier behaviour (Müller and Keeler, 1969). Climate, along with the physical properties of ice and the surface topography, determines the extent and behaviour of a glacier. The relationships are complex because glaciers are found in many geographic locations and the factors acting upon them exert their influence in varying ways.

Climate is important because it determines the annual mass balance of a glacier. Lawson (1993) defines the production of ice melt as a function of climate, or the result of energy and the amount and type of precipitation. However, the variability of climate means that knowledge of the mass balance is necessary for studying the hydrology of the glacier (Röthlisberger and Lang, 1987). Lawson (1993) suggests that long term runoff trends reflect the effects of climate on mass balance rather than the effects of daily and seasonal energy variations. Changes in mass balance are reflected by changing volume and distribution of ice within the basin and this may affect runoff over a time period of decades and longer.

A glacier induces a micro-climate of its own, producing katabatic winds. Slope, aspect and surface characteristics also modify the climate, as does altitude through its effect on

temperature. One result of the effect of altitude on air temperature is that a precipitation event may fall as rain on the lower portions of a basin while it falls as snow at the higher elevations. This is important for high mountain glaciers, particularly during the melt season because of the elevated albedo values of snow compared to ice. Snow effectively insulates or 'protects' the ice beneath it from melt because, although the same amount of absorbed energy is required to melt both snow and ice, a unit of snow requires a larger irradiance to absorb a similar amount of energy because it reflects up to 90 % of the incoming energy compared to ice which only reflects about 40 %. Thus a snow surface needs to receive more energy than ice for comparable melt to occur.

A summer snowfall temporarily depresses the snowline elevation. It is capable of slowing down melt water production on a glacier for up to several days, until the snow has melted, because of the difference in albedo between snow and ice. This was experienced on the Peyto Glacier at the end of the 1997 field season.

Processes which result in ice and snow loss from a glacier are defined as ablation processes. The water being discharged from a glacier is mainly produced by melting of the glacier surface although sublimation and geothermal melt can also occur. The factors involved in melt and runoff fall into two groups: meteorological and morphological. According to Konzelmann and Ohmura (1995), the energy balance determines melt processes at the surface and these processes depend not only on atmospheric conditions but also on surface properties. Many other studies have been undertaken to examine the factors involved (e.g. Hoinkes, 1955; LaChapelle, 1961; Lang, 1973; Wendler and Ishikawa, 1973; Escher-Vetter, 1985; Müller, 1985; Hannah and McGregor, 1997).

2.1.1. The Surface Energy Balance

The surface energy balance during the melt season determines the main factors contributing to melt. As a result, it is an important aspect of glacial meteorology (Müller and Keeler, 1969). One of the most important of these variables in relation to the examination of melt rates on a glacier is the net radiation at the glacier surface, consisting of incoming and outgoing short-wave (solar) and long-wave (terrestrial) radiation. It should be noted that all energy components within this study are termed positive when they act towards the surface and negative when they act away from the surface, with the exception of Q_M which is positive when melt is occurring. Net radiation (Q*) is usually dominated by incoming solar radiation during the day and therefore has a positive value. At night outgoing long-wave radiation is the dominant energy flux and thus Q* has a negative value. It is calculated as:

$$Q^* = K\downarrow(1-\alpha) + L\downarrow - \varepsilon\sigma T_o^4 = K^* + L^* \qquad (2.1)$$

where K↓ is incoming short-wave radiation; α is albedo; L↓ is incoming long-wave radiation; ε is emissivity; σ is the Stefan-Boltzmann constant ($5.67*10^{-8}$ W m^{-2} K^{-4}); T_o is surface temperature (273.15 K for a melting ice surface); K* is net short-wave radiation; and L* is net long-wave radiation.

The total melt energy (Q_M) at the surface of a glacier is defined as:

$$Q_M = Q^* + Q_H + Q_E + Q_R + Q_G \qquad (2.2.a.)$$

where Q_H is the sensible heat flux; Q_E is the latent heat flux; Q_R is the energy provided by rainfall events; and Q_G is the heat flux into the ice. Terms on the right hand side of the equation can be positive or negative.

As Q_R and Q_G are negligible within the parameters of this study, equation 2.2.a. can be rewritten as:

$$Q_M = Q^* + Q_H + Q_E = K^* + L^* + Q_H + Q_E \qquad (2.2.b.)$$

Q_M is calculated as the residual of all other energy balance terms. As a residual, it incorporates any measurement errors associated with individual energy terms. Equations 2.1. and 2.2.b. are the basis for all subsequent analysis within this thesis.

Table 2.1.demonstrates the varying contributions of the main energy sources for different glaciers and geographic regions. Although it varies in both space and time, it is useful to be able to determine which is the most important source of energy available for melt. A study by Hoinkes (1955) looked at the amounts of energy and their sources contributing to melt on flat glaciated areas and glacier tongues in the Alps. The results show that for a flat glaciated area approximately 81 to 84 % of energy causing ablation is short-wave radiation and 16 to 19 % is from a combination of sensible and latent heat fluxes. On a glacier tongue, approximately 2 300 m asl, 58 to 65 % of melt energy is from short-wave radiation and 15 to 30 % is from the sensible and latent heat fluxes. The difference between the two can be explained by the decreased amount of short-wave radiation reaching the valley tongue, due to the shadowing effect of surrounding mountains.

Table 2.1. A summary of energy partitioning for various studies of summer melt

Observer	Notes	Q*	K*	Q_H	Q_E
Hoinkes (1955) Alps	3 000 m asl (flat area)	--	81-84 %	16-19 %	
	2 300 m asl (tongue)	--	58-65 %	15-30 %	
LaChapelle (1959) Blue Glacier, Washington†		69 %	--	25 %	6 %
Ambach (1963) Greenland Icesheet†		78 %	--	22 %	-8 %
Ambach and Hoinkes (1963) Alps†		68 %	--	32 %	-2 %
Streten and Wendler (1968) Alaska Glacier†		51 %	--	29 %	20 %
Föhn (1973) Peyto Glacier, Alberta		44 %	--	48 %	8 %
de la Cassinière (1974) Valleé Blanche, Alps†	July melt	84.6 %	--	15.4 %	-15.4 %
Martin (1975) Glacier de Saint-Sorlin, France†		57 %	--	43 %	-6.2 %
Lang (1986) Aletschgletscher, Alps	2 200 m asl	71 %	--	21 %	8 %
	Rain snowmelt event (Q_R 6 %)	14 %		56 %	24 %
Munro (1990) Peyto Glacier, Alberta	Snow	51 %	--	42 %	7 %
	Ice	65 %	--	34 %	1 %
Owens and others (1992) Franz Josef Glacier, New Zealand	Day	50-60 %	--	30 %	10-20 %
	Night	slightly negative	--	60-80 %	20-40 %

† from Male and Granger 1981

2.1.1.1. Incoming Solar Radiation (K↓)

Solar radiation is the energy emitted by the sun. It is typically short-wave radiation which is emitted in the range 0.15 μm (ultra violet) to 3.0 μm (near infrared). The solar beam is scattered, absorbed and transmitted as it passes through the atmosphere as a result of atmospheric constituents such as gases, dust particles, ice and salt crystals, water vapour and clouds. As a result, both direct and diffuse short-wave radiation reach the earth's surface. Gratton and others (1994) studied the proportion of direct to diffuse K↓ on Athabasca Glacier, Alberta. They concluded that approximately 11 % of total incoming solar radiation was diffuse.

Anomalies can exist in the atmosphere as a result of these relationships. For example, cloud presence generally decreases the amount of short-wave radiation reaching the surface through absorption by water vapour and droplets and reflection at the top of the clouds back out to space. However, under partial cloud conditions short-wave energy can be reflected off the sides of clouds towards the earth's surface, rather than back out to space, enhancing solar radiation amounts at the surface.

Topography has an impact on all climate variables through its influence on elevation, slope, aspect and the sky-view factor (Gratton and others, 1994). At a micro scale, slope angle and aspect will affect the amount of incoming solar radiation received. The steeper the slope, the less concentrated the radiation intensity per unit area in comparison to an horizontal surface. Aspect plays an important role as a result of the tilt of the earth's axis. In the northern hemisphere north facing slopes receive less solar radiation because they face away from the path of the sun. The sky-view factor determines the length of time a location will receive direct solar radiation, as opposed to being in shadow from surrounding peaks.

2.1.1.2 Outgoing Solar Radiation (K↑)

A proportion of incoming short-wave radiation is reflected back out to space off clouds and through scattering and reflecting of other atmospheric constituents. However, the greatest source of outgoing short-wave radiation over snow and ice surfaces is the portion reflected back from the surface.

Albedo is a major factor in surface melt because the amount of energy absorbed by a surface for melt to occur depends on the amount of energy reflected from the surface. Snow and ice surfaces have very high albedos. As a result, a greater irradiance is needed for the same absorption of energy, compared to other surface types. Further, given the microtopography of a glacier surface, the large degree of reflection will result in scattering and absorption of the diffuse beam by the surrounding surface.

Albedo varies with varying solar incidence angle. This variation becomes important at incidence angles greater than 70° (Gratton and others, 1993). However, the amount of radiation received under these conditions is quite small. It is to be assumed that variations in albedo have a limited effect on daily short-wave radiation over snow and ice surfaces. However, Van de Wal and others (1992) suggest that differences in ablation rates over the tongue of a glacier are directly attributable to differences in albedo both along and across the tongue. A minor influence is also imposed by advection started by the thermal contrasts between a glacier and its surroundings.

Cutler and Munro (1996) examined albedo on the Peyto Glacier for a melt season. The albedo values of different surface types on the glacier were cited as having an important temporal and spatial control on melt water generation. It was concluded that surface roughness is of minor importance in albedo variations compared to surface impurities. However, the development of the surface microtopography over the melt season may reduce surface albedo. The presence of liquid

water will also decrease albedo because melting ice crystals are less able to specularly reflect incident solar radiation.

Gratton and others (1994) emphasised the importance of terrain reflected radiation in the computation of surface albedo and net short-wave radiation. Topography gives rise to terrain irradiance as a result of the short-wave radiation reflected from neighbouring surfaces. The proportion of terrain irradiance increases when a surface sloping away from the sun is receiving little direct radiation, while the neighbouring terrain receives large amounts of incoming radiation. It is also increased on shallower slopes, as steeper slopes are more likely to be in prolonged shade. It is further increased if surrounding areas have a high surface absorptivity. In shaded areas, terrain irradiance can contribute as much as 20 - 25 % of total irradiance as compared with 10 % in non-shaded areas (Gratton and others, 1993). This phenomenon is more marked early and late in the day when the glacier may be in shadow but surrounding rock slopes may not.

2.1.1.3. Outgoing Terrestrial Radiation ($L\uparrow$)

The earth-atmosphere system emits less total energy than the sun and it is also in a different wavelength band (3.0 μm to 100 μm). Thus the main source of outgoing long-wave radiation is the earth's surface. In the case of a glacier surface during the melting season, it can be assumed that surface temperature is at melting point (273.15 K) and, as ice can be considered to approximate a black body radiator, the long-wave emissions are approximately 316 W m^{-2}, according to the Stefan-Boltzmann equation:

$$L\uparrow = \sigma T_o^4 \qquad (2.3.)$$

wherein T_o is surface temperature (273.15 K for a melting ice surface); and σ is the Stefan Boltzmann constant ($5.67*10^{-8}$ W m^{-2} K^{-4})

2.1.1.4. Incoming Terrestrial Radiation (L↓)

Incoming long-wave radiation is the re-radiation of outgoing radiation back to the surface before it can be lost to space. This effect is enhanced in the presence of clouds, as water droplets are good absorbers of long-wave radiation. Incoming long-wave radiation can also be a result of absorption and re-radiation of outgoing solar radiation. Topography increases incoming terrestrial radiation to a glacier surface as a result of the emitted long-wave radiation from neighbouring surfaces. As a result, high surface temperatures of surrounding rock surfaces can significantly increase both snow and ice melt.

Konzelmann and Ohmura (1995) examined melt under cloud conditions on the Greenland ice sheet. They suggest that the decrease in global radiation as a result of cloud cover is compensated for by the increase in incoming long-wave radiation from the cloud base. Although this may mean that there is no significant change in the energy available for melt, it will have a large impact on the type of melt occurring at the surface with respect to weathering crust development. Under exclusively long-wave radiation conditions, sub-surface melt cannot occur, so the weathering crust will degrade.

2.1.1.5 Turbulent Heat Fluxes (Q_H and Q_E)

Sensible (Q_H) and latent (Q_E) heat fluxes depend on wind speed, temperature and humidity. In the glacier environment, because the surface during the melt season is at 273.15 K, sensible heat fluxes are positive unless air temperatures are below freezing. As previously stated, temperature

decreases with elevation. Humidity also decreases with elevation because vapour pressure decreases with decreasing temperatures (Barry, 1992).

Morris (1989) reviewed turbulent heat transfers over snow and ice and found that they transfer a significant proportion of the amount of the total energy available for snowmelt from the atmosphere. Morris suggests that Q_H is usually 40 % of Q*, although it can be as much as twice Q*, and Q_E is usually 10 % of Q*, but is capable of being equal to Q*.

The driving force for turbulent heat fluxes is a critical windspeed causing turbulence near the surface. Turbulent transfers between the atmosphere and the ground govern many of the physical processes occurring at the ground surface (Granger and Lister, 1966) but are difficult to measure in the field, so various methods of calculation have been used over time. For the purpose of this study, the bulk aerodynamic transfer method is used.

The bulk aerodynamic transfer method for calculating sensible and latent heat fluxes is the most practical method for the field. The only data requirements over a melting ice surface are temperature, humidity and windspeed measurements at a fixed height above the ice surface. The most sensitive parameter within the calculations is roughness length. Fortunately, detailed studies of surface roughness have been undertaken on the Peyto Glacier by Munro (1989) using a roughness element description approach (Lettau, 1969).

The bulk aerodynamic transfer method for calculating the sensible heat flux (Q_H) is (Munro, 1990):

$$Q_H = \frac{\rho c_p k^2 u_z (T_z - T_o)}{[\ln(z/z_o) + (\alpha z/L)][\ln(z/z_t) + (\alpha z/L)]} \qquad (2.4.)$$

in which ρ is air density; c_p is the specific heat of air at constant pressure (1010 J kg^{-1} K^{-1}); k is von Kármán's constant = 0.41; u_z and T_z are windspeed and temperature, respectively, measured at height z; T_o is temperature measured at the surface (assumed to be 0 °C for melting ice surface); z_o and z_t are roughness lengths for windspeed and temperature, respectively; and α is an empirical constant (= 5) which is part of the stability correction and varies according to L.

L is the Monin-Obukhov length scale and is calculated in the following manner:

$$L = \frac{\rho c_p u_*^3 T}{kgQ_H} \tag{2.5.}$$

where u_* is a wind-speed scalar or friction velocity; T is the absolute temperature of the air between the surface and the measurement height; and g is acceleration due to gravity (9.8 m s^{-2}).

Over a melting ice surface, surface temperature (T_o) is 0 °C. As a result, the scalar, u_*, can be estimated from u_z, windspeed measured at a height z above the ground. Thus:

$$u_* = \frac{ku_z}{[\ln(z/z_o) + (\alpha z/L)]} \tag{2.6.}$$

z_o is treated as a fixed property of the surface, while the roughness length for temperature is modelled as a function of the roughness Reynolds number ($Re_* z_o/v$) where v is the kinematic viscosity of the air. According to Munro (1990), when flow is rough, as expected over a melting ice surface, the function takes the form:

$$\ln z_t = \ln(z_o) + 0.317 - 0.565\ln(Re_*) - 0.183[\ln(Re_*)]^2 \tag{2.7.}$$

Equation (2.4.) has to be solved iteratively because values for Q_H and u_* are needed in order to solve for L which in turn is needed to solve for Q_H and u_*. The iteration process is initiated by setting z/L equal to zero in equations (2.4.) and (2.6.). The results are used to calculate the first estimation of L from equation (2.5.) and this is substituted back into the two equations. According to Munro (1990) five iterations will produce a stable value for L.

The latent heat flux (Q_E) is calculated in a similar manner (Munro, 1990):

$$Q_E = \frac{\rho\varepsilon\lambda k^2 u_z[(e_z - e_o)/p]}{[\ln(z/z_o)+(\alpha z/L)][\ln(z/z_e)+(\alpha z/L)]} \qquad (2.8.)$$

where ε is the ratio of the molecular weight of water vapour to air; λ is the latent heat of vaporisation (250.1 kJ kg^{-1} at 0 °C); e_z is vapour pressure measured at height z; e_o is surface vapour pressure; p is air pressure; and z_e is the roughness length for humidity.

In a similar manner to equation (2.4.) z_e can be calculated from the following function:

$$\ln z_e = \ln(z_o) + 0.396 - 0.512\ln(\mathrm{Re}_*) - 0.180[\ln(\mathrm{Re}_*)]^2 \qquad (2.9.)$$

2.1.1.6. Neglected Terms: Q_G and Q_R

At high latitudes total melt energy is reduced by the ground flux, Q_G, which is needed to bring the glacier surface up to 0 °C before melting can occur (Owens and others, 1992). This is less important in mid-latitudes because the cold content of the ice is significantly less at the beginning of the melt season, mainly a result of snow insulation, and the ice surface is usually around 273.15 K. All data used in this study were collected during the melt season when the surface temperature of a temperate glacier is 273.15 K. As a result, Q_G will be zero.

Rain falling on a glacier surface will provide heat energy proportional to its temperature, but even high intensity, warm rain does not provide a large amount of energy to the ice surface. It can be demonstrated that rain, with a temperature (T_p) of 10 °C and a mass (m_p) of 4 kg m^{-2} s^{-1} x 10^1, falling on a melting ice surface (T_o = 0 °C) can only provide enough heat energy to melt 5 mm w.e. (Röthlisberger and Lang, 1987; p.217):

$$Q_R = Cm_p(T_p - T_o) = 167.4J\ m^{-2}s^{-1}x10^4 \qquad (2.10.)$$

wherein C is the specific heat of water (4.1868 x 10^3 J kg^{-1} $°C^{-1}$).

As a temperate glacier has a surface temperature of 0 °C during the melt season, Q_R can be assumed negligible.

2.1.1.7. Using an Energy Balance Approach to Modelling Glacier Melt and Runoff

Many studies have been undertaken to produce models which simulate the processes of glacier melt and runoff. The energy balance approach calculates the residual energy from the net balance and applies this to melt at the surface. This approach has tended to become more popular in modelling today as it most closely approximates the processes occurring. Models incorporating this approach include Kraus (1975), Munro and Young (1982), Munro (1991) and Arnold and others (1998).

Kraus (1975) suggested that it was possible to use an energy balance model for computing ablation as a function of meteorological and surface parameters. Special circumstances can be

incorporated within the model: orographic wind systems and their influence on turbulent fluxes; the energy balance on mountain slopes; air pressure influence on ablation; and dirt on the ice.

Munro (1991) modelled melt processes so that the annual mass balance of a glacier could be estimated from winter accumulation. Global radiation was modelled after Munro and Young (1982). The model incorporated a two surface approach, with cloud sensitivity and the introduction of a seasonal thermal lag caused by heat exchange between the surface and a deep layer.

Arnold and others (1998) have produced a digitally based, distributed model of glacial hydrology. Surface melt is driven by an energy balance submodel and calculated at hourly intervals. Other submodels route the melt water through the glacier system.

In conjunction with monitoring glacier discharge in hydrological basins, smaller intensive studies of melt water runoff have also been undertaken in the past (e.g., Campbell and Rasmussen, 1973; and Derikx, 1973). These early studies specifically examined water generation and movement through the glacier.

Derikx (1973) simulated glacier discharge by treating it in a similar manner to groundwater flow. The aim of the paper was to predict glacier runoff in response to variable weather conditions. Boussinesq's equation was used, a partial differential equation which explains one dimensional, unconfined, non-steady flow through a homogeneous, porous material. The formula produced was used to predict basin wide melt. It was described as performing with a "crude approximation of the actual situation" (p.38).

In the paper, Derikx proposed three zones of flow: vertical percolation of melt and rain water through the snow pack and firn; turbulent flow in melt water channels; and probable lateral

saturated flow in the snow pack, firn and porous ice. It is suggested that the latter represents the bulk of water movement within the system. The study concluded that greater investigation of the significant physical processes occurring at the surface is required.

Along similar lines, Campbell and Rasmussen (1973) looked at aspects of melt water in a glacier by assuming that it was a porous medium and therefore governed by Darcy flow. The porous medium flow model that was developed was linked to an input model to enable computation of melt over the glacier surface for relatively short periods of time (24 hours). It was concluded that the model gave a reasonable approximation of actual glacier discharge.

2.1.1.8. Summary

On the whole, melt on temperate glaciers is dominated by radiation energy. Sensible heat is usually the next most significant energy source for melt. Latent heat energy is usually quite small, but obviously becomes more important under conditions favouring significant evaporation or condensation. Sensible heat also becomes important for nocturnal melt. Usually if there is energy available for melt at night, it is a result of a significant positive sensible heat flux.

Based on the different energy types contributing to melt, Q_M can be divided into the portion of energy contributing to internal melt $[K\downarrow(1 - \alpha)]$ and the portion of energy contributing to surface lowering $[L\downarrow - \sigma T^4 + Q_H + Q_E]$.

2.2. Surface Hydrology and Weathering Crust Processes

Runoff depends on melt processes. These processes determine water amounts and physical mechanisms which, in turn, determine the routing and timing of runoff (Röthlisberger and Lang, 1987). Water routing through the glacier system is complex and changes over the course of the

melt season. Water can travel in one of three zones: supraglacial; englacial; and subglacial. The three are linked by crevasses, moulins and tunnels. Water may be routed through a combination of these zones in many different and complex ways. These, along with surface storage, snowpack retention and firn storage, combine to vary the response, or lag time, of the glacier.

The ice surface, or skin layer, is the interface between climate and glacier hydrology. This is the layer where energy inputs are converted into meltwater runoff. As a result, the behaviour of this layer determines glacier system response. Many studies have been undertaken to examine the internal hydrology of the glacier but very little work has been carried out to examine the specifics of this skin layer. Most surface investigations have been undertaken to simulate the conversion of energy inputs into melt as a driving force for the rest of the glacier system. Fountain and Walder (1998) reviewed all aspects of glacial hydrology and concluded that further research into the coupling between near-surface, or skin layer, and englacial systems is needed.

Weathering crust development is a phenomenon arising out of the ablation process. It has been identified and examined by LaChapelle (1959; 1961), Müller and Keeler (1969), Derikx (1975) and Munro (1990). The weathering crust is a surface layer of ice with densities less than 0.89 g cm^{-3}. Its development results from the penetration of solar radiation into the ice surface. The decay of the short-wave flux into an ice surface can be calculated according to Beer's Law (Oke, 1987, p.84) (Fig. 2.1):

$$K^*_z = K^*_o e^{-\alpha z} \qquad (2.11.)$$

where K^*_z is the short-wave radiation incident at depth z (cm); e is the base of natural logarithms; and a is the extinction coefficient a = 0.06 cm^{-1} for ice (Geiger, 1965; p.207)

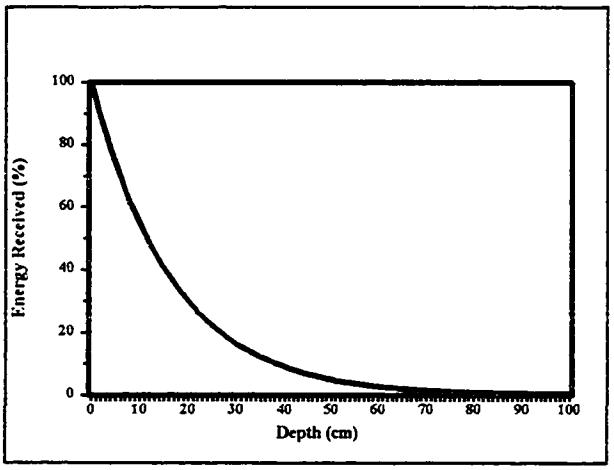

Fig. 2.1. Percentage extinction rate of short-wave radiation for an ice surface

It can be seen that only 50 % of the energy received at the surface reaches a depth of 11 cm (Fig. 2.1.). By 20 cm, there is only 30 % of surface energy and by 38 cm, the value is 10 % of the original input.

Weathering crust processes vary greatly on small spatial and temporal scales. Visual evidence from the field, in the form of stereophotographs, demonstrates the effect of radiation penetration on the skin layer (Appendix II). The photographs depict surface changes through time resulting from both weathering crust processes and cryoconitic melt. Factors such as ice density, crystal size and orientation, and water movement, all play a part in determining why some areas ablate faster than others at certain times.

LaChapelle (1959) examined errors in ablation measurements resulting from subsurface melting. A direct measurement of ice melt (I) was calculated using two successive ice density profiles according to the following equation:

$$I = \int_{o}^{h_o} \rho_i(h,t_o)dh - \int_{o}^{h_o} \rho_i(h,t_I)dh \qquad (2.12.)$$

in which h_o is the original ice surface at time t_o; h is the thickness between the surface and a sub-surface reference point; the initial and subsequent density profiles are designated by the relation $\rho_i(h,t_o)$ and $\rho_i(h,t_l)$, respectively.

While this equation accounts for internal melt resulting from short-wave penetration into the ice, it does not differentiate between the two sources of melt - internal (Q_{Mi}) and surface lowering (Q_{Ma}).

LaChapelle (1961) noted subsurface snow melt on the Blue Glacier, Washington, to a depth of 15 - 20 cm. As a result, a distinction was made in the study between melt and wastage. The effect of the weathering crust was also identified in a study by Munro (1990). A temporal discrepancy was observed between absorbed energy and surface lowering when computations of hourly ablation measurements from melt energy calculations were compared to field measurements.

Brandt and Warren (1993) briefly discussed internal melt within ice when examining subsurface temperature maxima in antarctic snow packs. Puddles beneath the ice surface have been observed at depths of 10 to 20 cm on Antarctic shelf ice and fast sea ice where the protective snow layer has been blown away. Other observations have been made on the Ross Ice Shelf where melt pools between 10 and 15 m in diameter occur at a depth of 7 to 40 cm below the ice surface. It is suggested that this is observed in ice and not in snow because of the lower albedo of ice which reduces scattering within the layer, allowing for absorption with depth.

Derikx (1975) established an artificial catchment on the Peyto Glacier in order to determine the hydrological response time of the weathering crust layer. The time constant of the site was determined to be close to one hour, the sampling time used in the study. Melt was calculated from the energy balance as the glaciological method (ablation stakes) is inaccurate for small time periods. Conclusions from this study suggest that runoff delay is a result of

supraglacial channel flow and not lateral flow through the porous ice layer, particularly in the upper portion of a catchment where channels are less well developed.

Most of the information regarding the properties of the skin layer at the glacier surface is a result of a study by Müller and Keeler (1969). The study examined differences between measured and predicted ablation and concluded that these errors were mainly due to a process of internal melt. Thermocouples and thermistors were placed into the ice to a depth of 15 m in order to examine the effects of what they termed the weathering crust. This crust develops during sunny periods and ablates away during overcast, warm weather. It was further established that this crust does not develop uniformly and is thicker over ridges than in depressions, where radiation has less access and where running water erodes it. The study was based on discreet data collected during daytime periods. In the study, weathering crust development is broken down into periods of growth and decay. Periods of growth are characterised by decreasing density of the surface layer while periods of decay are characterised by surface lowering and therefore increasing densities over time as the less dense layers are ablated away.

The work of Müller and Keeler (1969) aids in our understanding of weathering crust development on a day to day basis. However, there does not appear to be literature pertaining to time periods less than a day. Such studies would require continuous ablation measurements which were not available until Lewkowicz (1985). It is now possible to undertake analysis at sub-daily intervals and, through continuous data collection, examine nocturnal processes. It is intended that this study will build upon previous information through the use of continuous, sub-hourly data collection in order to provide a greater understanding of the processes occurring within the glacier surface layer.

CHAPTER 3 METHODS

The following chapter describes the techniques employed within this study. The chapter is broken down into two main parts: field and data calibration techniques; and data processing techniques. The field and data calibration section is broken down into meteorological and hydrological sections. The hydrological section is further broken down into surface lowering, weathering crust formation and stage (discharge). The data processing section describes computation undertaken on the data set prior to analysis of the data.

3.1. Introduction

This research was undertaken to investigate the relationship between energy balance and melt at the glacier surface at small spatial and temporal scales. Thus data collection was intensive and site specific. An area of relatively clean ice in the general locale of stake 40, on the Peyto Glacier, was chosen for the location of the study site (Fig. 1.2.).

The amount of radiation received on the Peyto Glacier is affected by surrounding mountains. Local shadowing delays sunrise and advances sunset, reducing the number of sun hours. This effect is greater early and late in the season.

Sub-catchments were established each season in the same area, the specific location varying according to channel location and surface features which would cause difficulty in closing a catchment. In 1994 and 1995 two catchments were established side by side and a meteorological mast was set up between the two. The mast held the meteorological instruments as well as the data logger and tape recorder that collected and stored data from the meteorological instruments, ablatometers and stage recorders placed in each plot (Fig. 3.3.b.). Only one sub-catchment was

established during the 1997 field season. The area of each sub-catchment varied for the different seasons (Table 3.1.). The slope of the ice surface varied between 4 and 7 %. Fig. 3.1. a, b and c, depict plan views of the plots established in each of the field seasons.

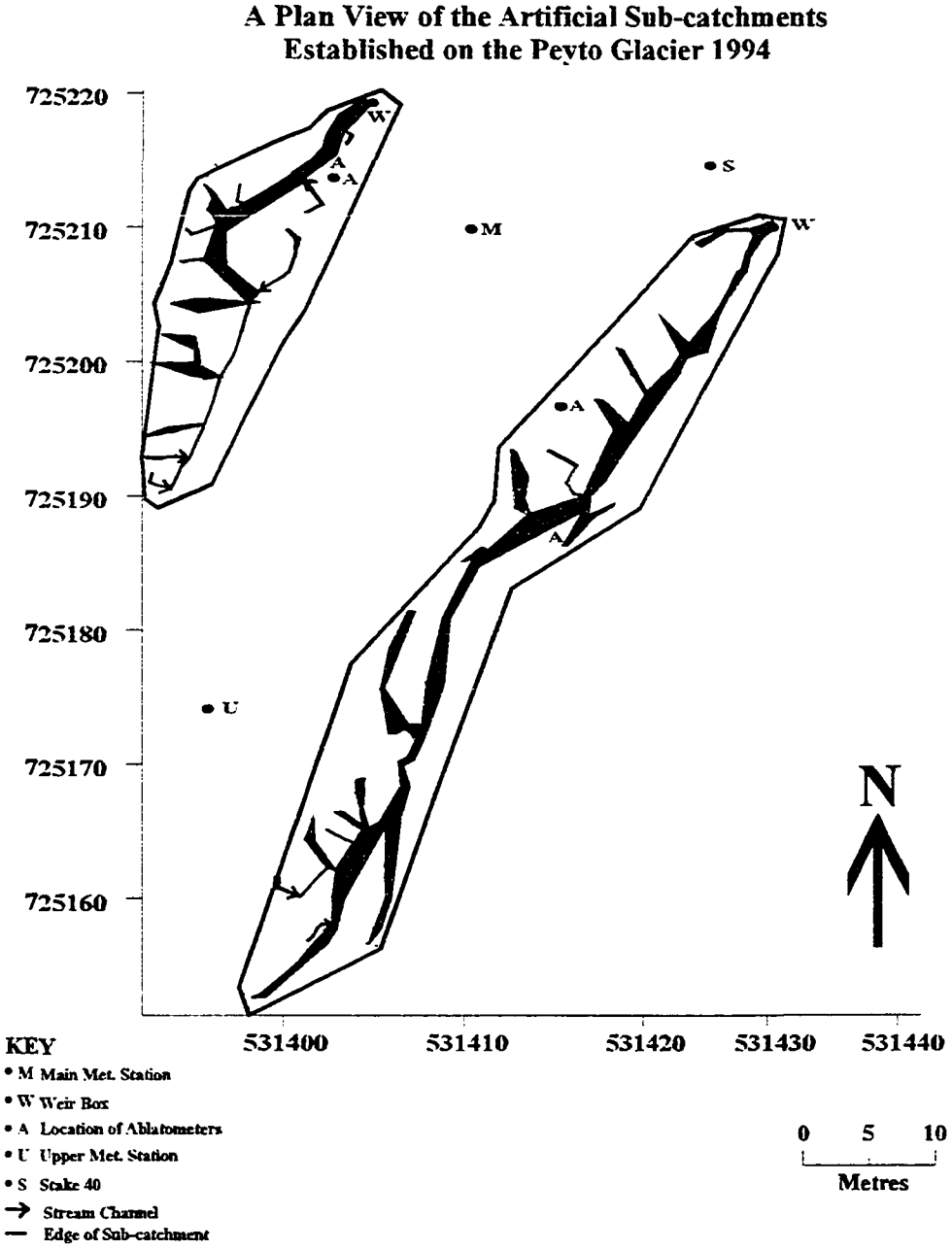

A Plan View of the Artificial Sub-catchments Established on the Peyto Glacier 1995

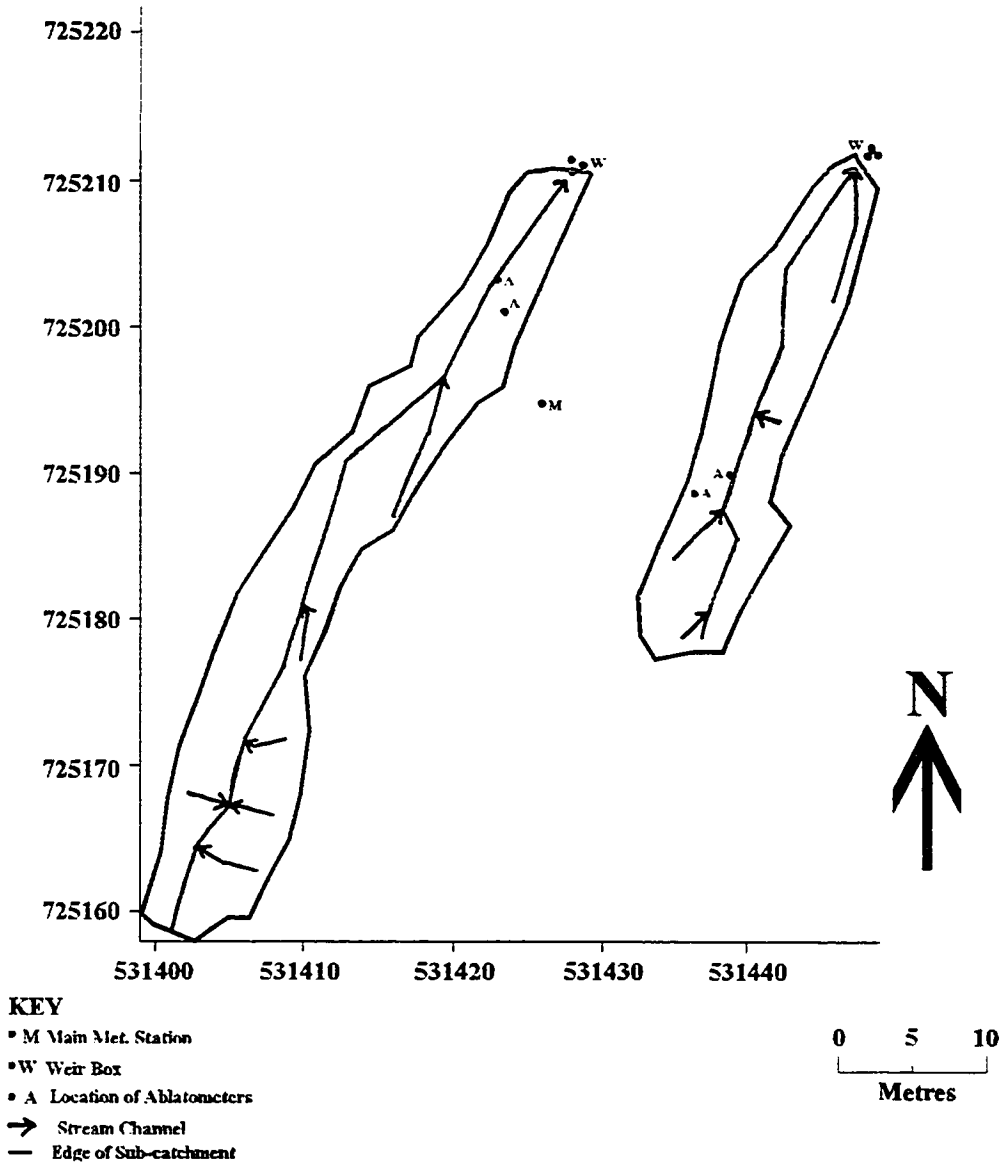

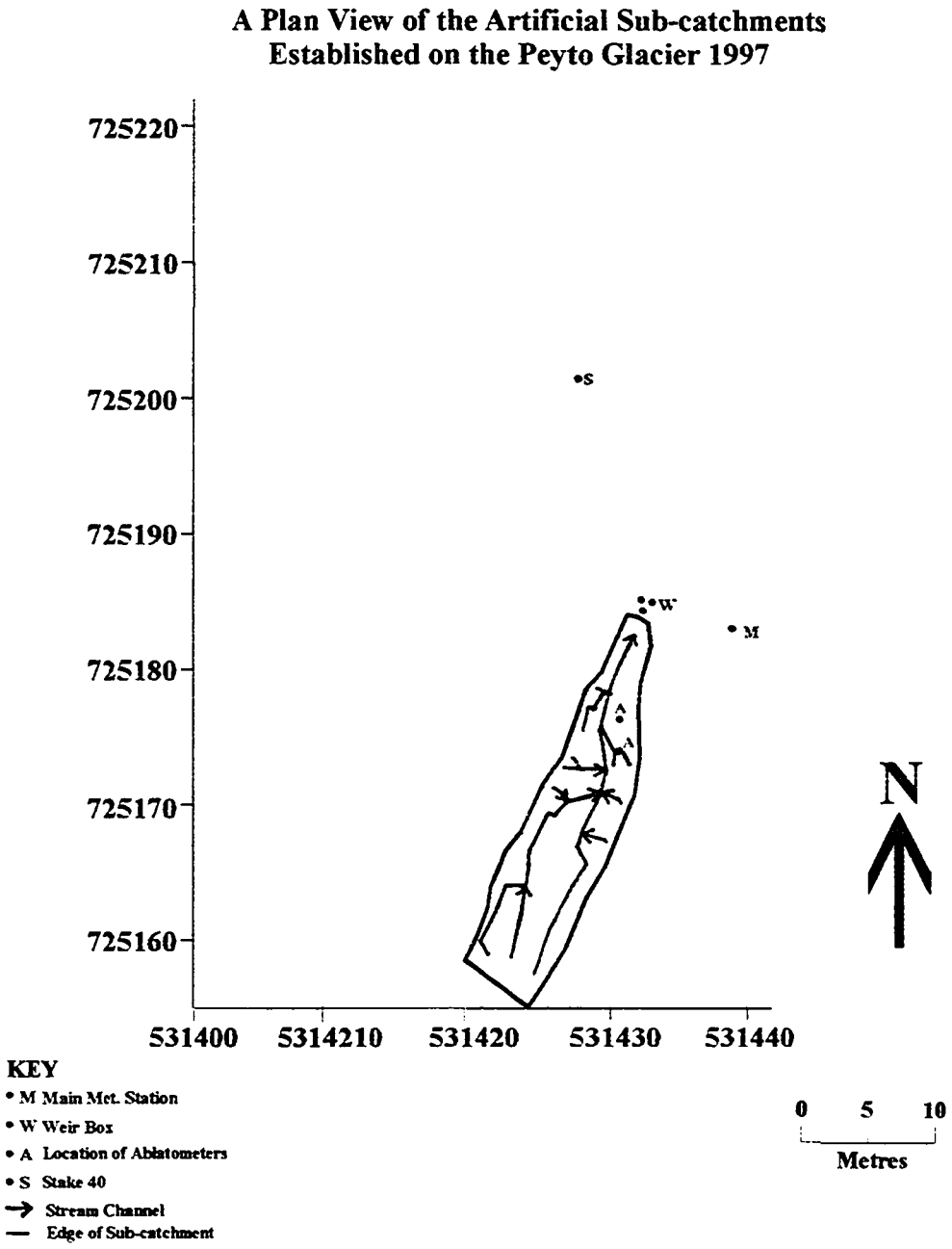

Fig. 3.1. Plan view of the a) 1994 b) 1995 and c) 1997 sub-catchment setup

Table 3.1. Areas of the sub-catchments established on the Peyto Glacier, 1994, 1995 and 1997

YEAR	PLOT	AREA (m^2)
1994	small plot	191
	large plot	434
1995	small plot	222
	large plot	362
1997	small plot	153

Once it had been decided that the type of data required could be gathered from small artificial catchments on the ice, suitable characteristics for the sub-catchments were determined. This was done by assuming that melt would occur during twelve hours of daylight, average ablation would be in the order of 0.05 m d^{-1} and the density of ice would be 0.89 kg m^{-3} x 10^3. Hence, it was possible to calculate the expected volume of ice ablated per day and the discharge rate as shown in Table 3.2.

Table 3.2. Initial discharge calculations for varying catchment area

Area (m^2)	Ablation (m^3 w.e.)	Discharge (l d^{-1})†	Discharge (l s^{-1})§
500	22.25	22 250	0.52
1 500	66.75	67 750	1.55
2 000	89	89 000	2.06
2 500	111.25	111 250	2.58

†1 l = 1 000 cm^3; 1 m^3 = 1 000 000 cm^3 ; 1 m^3 = 1 000 l

§ 43 200 seconds in 12 hours

To create a hydrograph for the day, it was assumed that maximum discharge was twice the average discharge and that maximum discharge would occur between 12:00 p.m. and 3:00 p.m. Minimum discharge was assumed to be zero. This meant that, for calculation purposes, catchment

areas would have to be chosen based on a maximum discharge of twice that calculated in the previous table. Thus an area of no more than 500 m^2 was considered to be large enough for data collection, yet reasonable for daily management and upkeep in the field.

It was decided to create two sub-catchments each season, one large, one small. Actual areas were smaller than the maximum limit due to the location of existing streams on the glacier surface and the decision, in the field, to seal off a single stream rather than to attempt to converge several into one exit from the sub-catchment (Table 3.1.). As a result, the artificial catchments established on the ice were long and narrow (Fig. 3.1.).

Meteorological data were measured using instruments mounted on a mast and surface lowering was measured using ablatometers. Discharge from the plots was measured by a weir box system in which a syphon was used to bring water out of the sub-catchment into a box.

3.2. Data Collection and Calibration

The field component of this study involved the collection of data over three ablation seasons. The first season, a preliminary investigation into data collection procedures, comprised the period from July 26th to August 22nd, 1994. The second and third seasons, 1995 and 1997, encompassed the periods July 5th to August 14th and June 11th to September 10th, respectively.

All meteorological instruments, stage recorders and ablatometers were connected to a datalogger (Campbell Scientific, 21X, USA) and were automatically downloaded onto a cassette tape in the field. The data were sampled every ten seconds and averaged over five minute periods. This was effected to indicate small scale variations which occur over time and to examine probable lags in the system which were not found in a similar study undertaken by Derikx (1975), in which data were averaged at hourly intervals. Data were retrieved from the magnetic tapes using a

Campbell Scientific C20 cassette interface. Data transformations were undertaken using *PFE32 for Windows* and *Quattro Pro 8 for Windows*.

3.2.1. Meteorology

During each field season an instrument mast, mounted on a stone base and secured with guy wires, was established to record meteorologic information on the ice. The mast was always located near the experimental plots. The stone base was of sufficient size that it melted at the same rate as the surface lowered. Thus the mast, and instruments attached to the mast, was at the same height above the surface throughout a season (Fig. 3.2.).

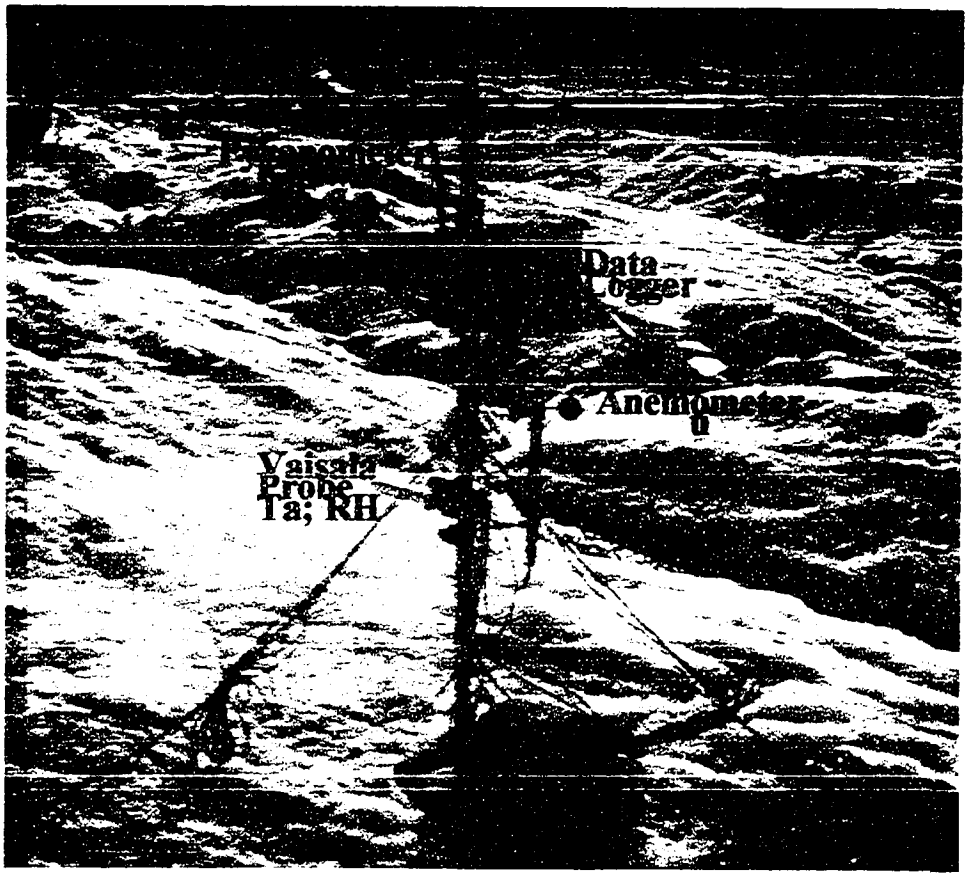

Fig. 3.2. Typical meteorological mast established for each of the three seasons

The standard variables measured were incoming and outgoing short-wave radiation, net radiation, air temperature, relative humidity, wind speed and rainfall. Changes in instrumentation between seasons reflected the availability of instruments. Continuity was maintained through the course of the study period by measurement of the same set of variables each season and by comparison with the base-camp station. The variables measured and instrumentation types are tabulated in Appendix III.

Temperature, windspeed and relative humidity measurements were recorded in °C, m s^{-1} and percent, respectively, in the field. The relative humidity data for all seasons and the wet and dry bulb temperatures (T_w, T_d) from the 1997 field season were converted to vapour pressures based on the following (Dilley, 1968):

$$e_s = 6.1078 * e^{\left(\frac{17.269 T_a}{237.3 + T_a}\right)} \qquad (3.1.)$$

where e_s is saturation vapour pressure at 100 %; and T_a is air temperature ($T_a = T_D$)

Vapour pressure (e), measured in millibars (mb), is calculated from RH:

$$e = \frac{RH}{100} * e_s \qquad (3.2.)$$

or, using wet and dry bulb temperatures:

$$e = e_w - \gamma (T_D - T_W)(p / p_o) \qquad (3.3.)$$

where e_w is saturation vapour pressure (mb) at T_w, calculated from equation (3.1.) by substituting T_W for T_a; γ is the psychrometric constant (0.66 mb $°C^{-1}$); p is atmospheric pressure at measurement site (775.774 mb); and p_o is atmospheric pressure at sea level (1013.25 mb).

Radiation data were recorded in millivolts (mV) on the datalogger and converted to W m^{-2}. The data were multiplied by the individual instrument calibrations. Further, the data were used to calculate sensible and latent heat fluxes using the bulk transfer method (Munro, 1990; 1991). Program details for the flux calculations are in Appendix IV. The energy available for melt (Q_M) was calculated as a residual in the energy balance equation.

3.2.2. Hydrology

Artificial sub-catchments were established on the ice surface using white polyethylene sheeting to delimit boundaries (Derikx, 1975). The polyethylene sheeting protects the ice beneath it from melting and over a short period of time, ice walls build up around the plot (Fig. 3.3.). These walls are assumed to be impermeable, as verified by the fact that food dye placed on the outside of one wall did not enter into the plot within a three hour monitoring period. As crevasses and moulins were deliberately kept out of the catchments, the surface of each sub-catchment is assumed to be impermeable thus preventing water loss by percolation into the englacial environment. This assumption is corroborated by Lliboutry (1996) who states that as a result of pressure being atmospheric at the ice surface and greater beneath the surface, the melt water in an upper boundary layer, with a thickness of approximately 2 m, will flow upwards. It is also suggested that ice must be more impermeable at its surface in order to maintain a high internal pressure.

a)

b)

Fig. 3.3. Plastic delimited sub-catchments (a) initially and (b) after 1 week

3.2.2.1. Surface Lowering

Surface lowering due to ablation of the ice was measured continuously with a set of ablatometers. An ablatometer designed by Lewkowicz (1985), consisting of a vertical pole attached to an horizontal bar, was mounted between two poles drilled into the ice to a depth of two metres (Fig. 3.4.). The vertical pole rests on the ice, either on a plastic foot or a wood foot and is attached to a potentiometer, which changes voltage as the foot lowers with the ice surface. Three ablatometers were established in each plot. Two were placed next to each other on the ice surface and the third was placed in a stream channel in order to examine the effects of running water on ablation. The wood foot was used in the stream and on the ice surface while the plastic foot was only used on the ice. In all future references, the ablatometers will be differentiated by use of the term wood, for the wood foot on the ice; plastic, for the plastic foot on the ice; and water, for the wood foot in the water. Further, *s* will denote ablatometers located in the small plot and *l* will denote ablatometers located in the large plot.

Different ablatometer feet were used in the anticipation that the wood foot would melt down into the ice and rest near the base of the weathering crust, while the plastic foot would rest on the surface of the ice at all times. The plastic foot is clear plexiglass and, as such, is assumed to interfere very little with the absorption of radiation, providing an accurate indication of weathering crust development. The wood foot melted into the ice as a result of its enhanced thermal properties and the fact that its small, circular, surface area, will break through the ice at higher densities than the plastic foot with its larger, cross-shaped, surface area.

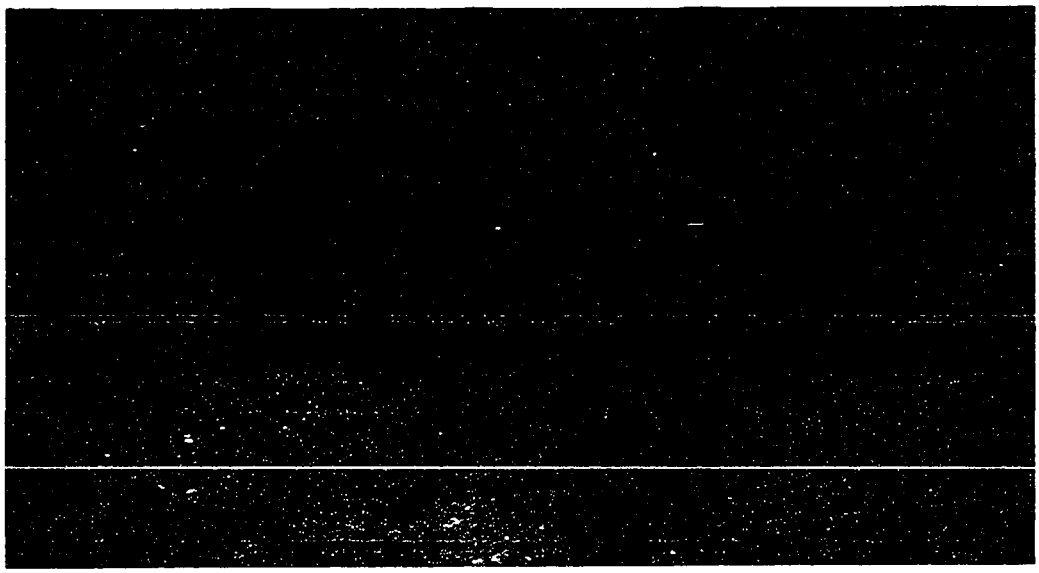

Fig. 3.4. Two ablatometers as established in the field

Surface lowering data from the ablatometers were measured in mV and converted to millimetres (mm). Actual surface lowering was derived by calculating the difference between consecutive readings and summing these differences to provide a cumulative total. These data were then converted into mm using the following calibration determined in the laboratory:

$$16.6732 \text{ mV mm}^{-1} (\pm 0.72 \%)$$

Surface lowering measurements were converted to W m^{-2} for direct comparison with the energy fluxes:

$$Abl(Wm^{-2}) = \frac{Abl(meas) * \rho_i * L_f}{\Delta t} \qquad (3.4.)$$

in which Abl(meas) is mm difference between discreet five minute intervals; ρ_i is ice density (0.89 kg m^{-3} x 10^3); L_f is the latent heat of fusion (333.7 J kg^{-1} x 10^3 at 0 °C); and Δt is a time conversion factor (300 seconds).

3.2.2.2. Weathering Crust Formation

Different techniques were employed to attempt a qualitative analysis of the weathering crust phenomenon. First, ice cores were collected at different times during all seasons and ice densities were calculated based on the volume of the core sample and the water equivalent of the ice in the core. Ice sample densities were calculated according to:

$$\rho_i = \frac{w.e.}{volume} \tag{3.5.}$$

Second, a stereophotographic record of the weathering crust process was obtained. A camera was mounted on a frame that had been drilled into the ice and stereoscopic pairs of photographs were taken at hourly intervals during the 1997 season (Fig. 3.5.).

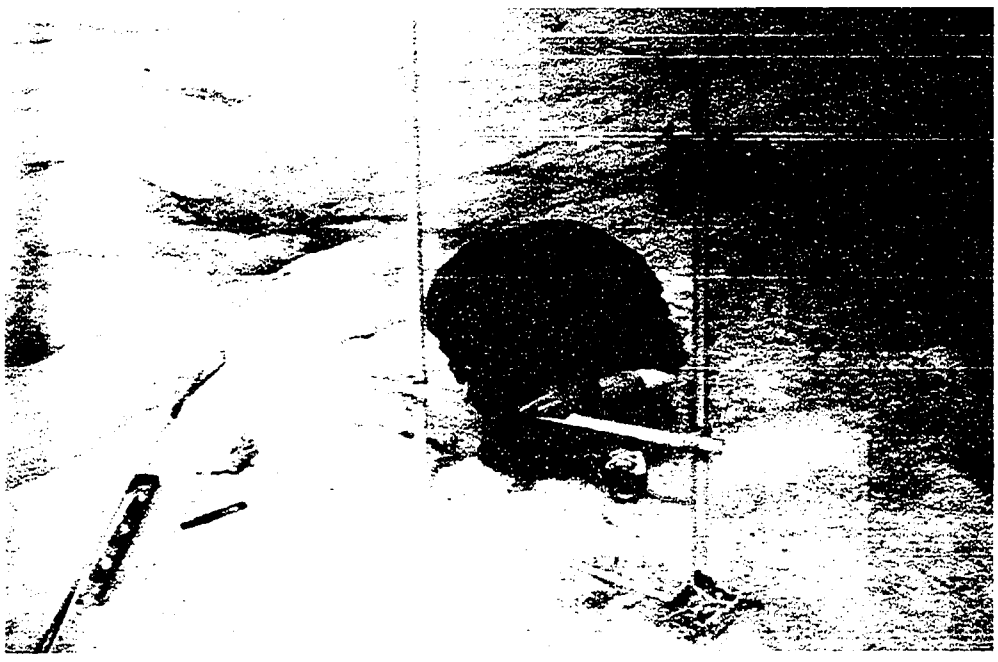

Fig. 3.5. Stereophotographic technique used to examine weathering crust development

3.2.2.3. Discharge

Discharge from the sub-catchments was measured using a V-notch weir. The design of the V-notch weir system evolved over the course of the field seasons. Consecutive days of reasonable discharge data proved difficult to collect, despite constant maintenance. However, the shape of the hydrograph curve for the 1997 field season, based on stage measurements, is relatively free from the issues affecting actual discharge data. As a result, weathering crust development can be compared to the timing of runoff events for lag analysis during the 1997 season.

Stage was recorded in mV and converted to mm using the following calibration:

$$8.056 \text{ mV mm}^{-1} \text{ or } 0.124 \text{ mm mV}^{-1} (\pm 0.41 \%)$$

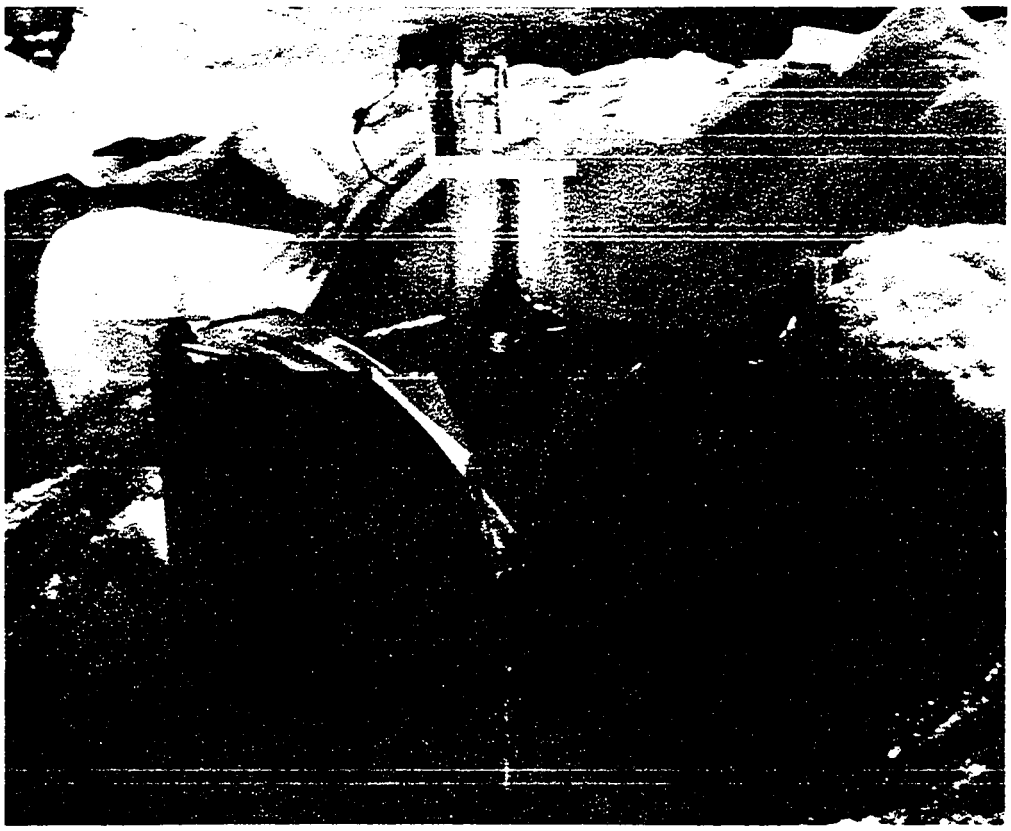

Fig. 3.6. Final weir box design used in 1995 and 1997

The final weir box design was a triangular shape (dimensions 90 x 90 x 90 x 45 cm), as it was found that a triangular shape box was more stable and easier to maintain on the level than a rectangular box (Fig. 3.6.). The box was lined with a heavy duty plastic, less likely to tear, and the joints were more securely formed and well sealed. Two sizes of compound V-notch metal plates were constructed ($22^1/_2$° and 45°; 45° and 90°) that could be interchanged, depending on discharge. The syphons were made from $1^7/_8$ " clear vinyl tubing. The type of tubing was chosen for several reasons. First, its large diameter reduces friction effects on flow within the tube. Second, the vinyl is very smooth, again, keeping friction effects of the tube to a minimum. Finally, being a clear tube, it was very easy to assess whether the syphons were working effectively.

3.2.3. Associated Errors

The following section examines the possible error sources associated with the collection of data in the field. Four logistic problems resulted in gaps in data logger collection: low batteries; loose connections; magnetic tape running out; and lightning disturbance.

3.2.3.1 Meteorology

The errors associated with the various meteorological instruments used are summarised in Appendix III. In general, Konzelmann and Ohmura (1995) quantify overall radiation measurement errors as follows: incoming short-wave radiation ± 4 W m^{-2} ; incoming long-wave radiation ± 10 W m^{-2} ; and net all-wave radiation ± 12 W m^{-2} . In this study, air temperature was measured to ± 0.5 °C, windspeed to ± 1.5 %, humidity to ± 5 % and net radiation to ± 5 %. Errors associated with sensible and latent heat fluxes were calculated as ± 8.9 % and ± 25.5 %, respectively. This results in a total calculated error for energy balance measurements of ± 27.5 %.

In addition to instrument errors, other errors were introduced during data collection. These include equipment malfunctions and logistic problems and usually resulted in data loss. The issues inherent to the data collection processes were kept to a minimum through constant maintenance of the site. This included maintaining instrument levels and keeping radiometers sealed and ventilated.

One source of error associated with the location of the mast was increasing surface roughness during the season. This would have the greatest effect on the radiometer measurements because they were located furthest away from the mast. However, radiometers monitor an area with a radius of ten times their height from the ground. In this case, that describes a field of view of approximately 12 m, which compensates for the developing surface roughness. Changes in surface roughness will also affect turbulent flux calculations. A 10 % change in surface roughness will result in an error of ± 6 % in flux calculations. These errors are greatest at the beginning and end of the season, overestimating fluxes at the beginning of the season and underestimating them at the end of the season.

3.2.3.2. Surface Lowering

The main problem regarding surface lowering measurements was the tendency for the ablatometers to stick and not measure the rate of surface lowering accurately. Unfortunately, some of the ablatometers in use were worse than others. This resulted in sharp jumps in the surface lowering profile but did not affect accuracy of overall surface lowering. This resulted in data loss because all known periods when this occurred were removed from the analysis.

Other problems with the ablatometers included enhanced melt around the support poles. This had the twofold effect of enabling the support poles to shift away from the vertical and

eroding the ice surface under the ablatometer foot. In one case the ablatometer site had to be moved as a result. Investigations into the effects of a non-vertical ablation pole suggest an error of ± 1.5 % for a 10 ° shift away from the vertical.

A further source of error associated with surface lowering measurements is that of spatial representation. Ablatometers record point measurements and as a result may differ from spatially averaged data, such as the energy balance. This study uses data from two sets of ablatometers, which is not sufficient for accurate spatial averaging. However, a comparison enables the calculation of spatial errors. During daytime periods (high energy conditions) spatial errors account for ± 10 W m^{-2} for wood foot ablatometers and 20 W m^{-2} for plastic foot ablatometers. During nocturnal periods (low energy conditions) spatial errors are 69 W m^{-2} for wood foot ablatometers and 30 W m^{-2} for plastic foot ablatometers.

3.2.3.3. Discharge

Discharge data were difficult to obtain. The most persistent problem in collecting the hydrologic data was levelling and re-drilling of the weir box and re-drilling the sump hole for the syphons. The box would melt out fairly rapidly and need re-drilling at least once a week. Between re-drilling, the weir box needed levelling on a daily basis. In the end, even this was not enough to allow for a continuous rating curve. A few times during data collection, the weir box slipped completely and data were lost for a period of time. The weir box also froze up overnight occasionally, during the second and third field seasons. Other problems included: air locks in the syphons which occasionally caused a back up of water in the plots; the stage float sticking; breaching of the plot walls; and the development of surface storage features causing the discharge measurements at the weir to underestimate the amount of melt water being generated. Insofar as

could be determined from visual observations, discharge lost through breaches in the plot walls was small.

3.4. Data Processing

This analysis consisted of calculating the energy partitioning of Q_M between the main energy components; calculating actual differences between measured and potential ablation; calculating a ratio of measured to potential ablation; and calculating ratios between K* and energy available for melt and between $L^*+Q_H+Q_E$ and energy available for melt.

Percentage energy partitioning of Q_M was calculated for Q*, Q_H, Q_E, K* and L*. Each energy source was expressed as a percentage of Q_M. This indicates the dominant source of energy for melt and therefore the type of weathering crust processes occurring.

The actual (mm) difference between measured and potential surface lowering was calculated by subtracting potential surface lowering, calculated from the energy available for melt, from that measured in the field.

In order to be able to identify periods of weathering crust growth and decay a ratio (R) was calculated based on the method used by Müller and Keeler (1969):

$$R = \frac{Q_{M_a}}{Q_{M_p}} \qquad (3.5.)$$

where Q_{Ma} is actual surface lowering, as measured in the field; and Q_{Mp} is potential surface lowering, calculated from the energy available for melt (Q_M).

Weathering crust development will result in a lower Q_{Ma} as compared with Q_{Mp} during periods of crustal growth because of the occurrence of internal melt. During crustal decay periods,

Q_{Ma} will be greater than or equal to Q_{Mp} because the ice surface will have a density less than or equal to 0.89 kg m^{-3} x 10^3. Thus a ratio of measured to expected surface lowering is designed to differentiate between periods of crustal formation and decay. When R values are less than one, weathering crust is developing because the measured surface lowering is less than the expected, so melt must be occurring internally. When R values are greater than one, measured surface lowering is greater than the amount of surface lowering expected to occur, and decay due to melt or mechanical collapse is occurring. Negative R values will occur if Q_M is negative or if surface lowering is negative. When melt is low, particularly in the early morning or late evening, the record of measured surface lowering can fluctuate by a mV in either direction and can register as a negative value. When Q_M is zero the R value cannot be computed.

The ratio of K* to energy available for melt will be equal to, or less than one at all times. It will be closest to one during periods of weathering crust growth. When the ratio is zero, weathering crust growth cannot occur. However, this does not mean that melt of the surface layer is not occurring. In comparison, the ratio of Q_H to energy available for melt will range from zero to greater than one. During the day, the ratio will tend to be less than one and approaching zero, as the dominant supply to Q_M is K*. At night the ratio can be greater than one, depending on how large Q_H is in comparison to Q_M. At night, Q_H has to overcome the energy balance deficit before contributing to Q_M. As a result, if Q_M is positive, Q_H has to be large. When there is no energy available for melt, the ratios will be undefined.

Relative errors associated with this ratio increase with decreasing energy available for melt (Table 3.3). Lower errors are associated with the plastic foot in comparison to the wood foot. This is to be expected as the plastic foot most accurately records weathering crust development.

Table 3.3. Errors associated with typical weathering crust ratios

	Day		Night	
	Clear Sky	Cloud Cover	Cloud Cover	Clear Sky
Wood Foot	R = 0.55 ± 0.23	R = 2.04 ± 0.57	R = 2.0 ± 0.76	R =0.25 ± 1
Plastic Foot	R = 0.85 ± 0.16	R = 1.17 ± 0.35	R = 1.6 ± 0.57	R = 0.3 ± 0.6

4.1. Introduction

Expectations based on weathering crust processes are compared to results gathered in the field. Periods of clear sky, daylight, weathering crust growth; decay, resulting from nocturnal melt and daytime cloud conditions; and clear sky, nocturnal conditions, were identified from the field data and were examined separately. Identification was made on the basis of the measured to potential surface lowering ratio, with the exception of the last category, which was identified through decreased amounts of energy available for melt.

Selected periods from the 1997 data set are further analysed with respect to response times within the system between the onset of melt, weathering crust growth and decay and discharge from the plots. For these periods, associated discharge curves are available which depict the rising and falling limbs of discharge from each artificial sub-catchment.

The juxtaposition of a series of periods of weathering crust growth and decay will have a cumulative effect beyond the driving force of the energy balance. Initial conditions are assumed to be very important with respect to the type and amount of melt that will occur within a period and the likely ratio expected. Thus a diurnal cycle presents itself, superimposed on a longer cycle of weathering crust growth and decay. This is why a theoretical examination of weathering crust processes is also presented. A basic cycle of surface lowering and internal melt is reproduced for a unit area of ice based on energy available for melt with depth, and applied to six layers of increasing ice thickness. The surface layer experiences both surface lowering and internal melt, while the underlying layers are only subject to internal melt. Initial conditions are assumed to be a density of 0.89 kg m^{-3} x 10^3 throughout the column and changing ice densities and volumes are

calculated at five minute intervals using data collected in the field. This enables an examination of progressive ice densities over time and depth, as expected to result from weathering crust development.

4.2. Analysis of the Weathering Crust Ratio

The weathering crust ratio (R) is used in this study to differentiate between periods of weathering crust growth and decay. The ratio between actual and potential surface lowering indicates whether internal melt or surface melt is occurring.

A number of expectations regarding the weathering crust phenomenon existed prior to examination of the data. It was assumed that a clear distinction would exist between day and night conditions, based on the type of energy available for melt under these conditions. As internal melt of the ice surface only occurs within the presence of short-wave radiation, a simple assumption that weathering crust growth would occur under daytime conditions and weathering crust decay would occur under nocturnal conditions was established. The following table demonstrates the effect of additional assumptions invoked under clear sky versus cloud conditions.

Table 4.1. Expected weathering crust processes under basic day versus night and clear sky versus cloud conditions

	Day	Night
Clear Sky	(A) Strong weathering crust growth; $0 \leq R < 1$	(D) Quasi-static - weak weathering crust decay ($R > 1$) or no melt ($R \leq 0$)
Cloud	(B) Transition - combination of weak weathering crust growth and decay; $R \approx 1$	(C) Strong weathering crust decay; $R > 1$

The key to decay is low or no solar radiation input. Under nocturnal conditions, with the absence of solar radiation, the weathering crust cannot develop. However, melt can occur due to the dominance of the sensible heat flux. Under these conditions, surface lowering of the crust will occur overnight through decay. In this manner, nocturnal processes can be like overcast daytime situations. This is an important determinant of initial crustal conditions at the beginning of the following day.

Scenarios (A) and (C) have very clear cut definitions (Table 4.1.). In scenario (A) K* is the dominant energy source. Q_H, Q_E and L* will also contribute to melt and Q_M is the dominant energy sink. As K* is the dominant energy source, three dimensional melt, and thus weathering crust growth, will occur. The R values will be less than one because the calculation of potential lowering does not account for internal melt. It would be expected that, for an ice surface with no established weathering crust, growth would be most intense in the morning, with mainly internal melt occurring, causing an R value close to zero. Ice densities would be highest early in the day. Over the course of the day, internal melt would result in a reduced density surface layer that would begin to ablate later in the day, when surface lowering occurs. If growth is intense enough, it would be expected that, eventually, an equilibrium will be reached where surface lowering and internal melt compensate each other with the result that actual surface lowering will approximate potential surface lowering. This would presumably describe fully developed crustal conditions.

In scenario (C) K* is not present as a source of energy. The energy source is $Q_H + Q_E +$ L↓ and it must be significantly larger than the sink L↑ to overcome the energy deficit and provide energy for melt. The R value is greater than one because the surface that is ablating is at a lower density than the assumed density of 0.89 kg m^{-3} x 10^3 as a result of previous weathering crust growth. Thus it will appear as though greater surface lowering is occurring in the field than is

expected from the amount of energy available for melt. It is to be assumed that the lowest ice densities would exist in the first part of the evening because the weathering crust that developed during the previous day would constitute the topmost layers. As melt continues through the night, surface ice density will increase because the lower density weathering crust will be ablated away, leaving higher density, lower level ice. Thus a ratio significantly higher than one early in the evening would give way to a ratio closer to one as the density of the ice being melted tends towards the 0.89 kg m^{-3} x 10^3 ice density assumed for potential melt.

The remaining two scenarios, (B) and (D), are expected to have the most complicated responses. Scenario (B) is expected to produce a combination of growth and decay. Both will be occurring at the same time, but it is expected that one of the processes will be dominant. K*, Q_H, Q_E and L* will be sources of energy, the relative importance of their contribution to Q_M resulting in growth or decay energy sources fluctuating throughout the day. The weathering crust is in transition and R values will demonstrate small fluctuations around one.

In scenario (D) the R value is expected to be mathematically undefined and little, if any, crustal change is expected to occur (quasi-static). Data values are low and error is likely to be large compared to actual values. R values will fluctuate considerably as a result of low Q_M values. If Q_M is zero or negative, no melt can occur (except through the release of latent heat through re-freezing of melt water). In this case, the R value might be expected to be zero, or negative. By definition in this scenario the Q_H source will generally be less than or equal to the L* sink. There is also a possibility for weak weathering crust decay to occur if Q_H does become larger than the L* deficit, in which case, it might be expected that the R value will be greater than one.

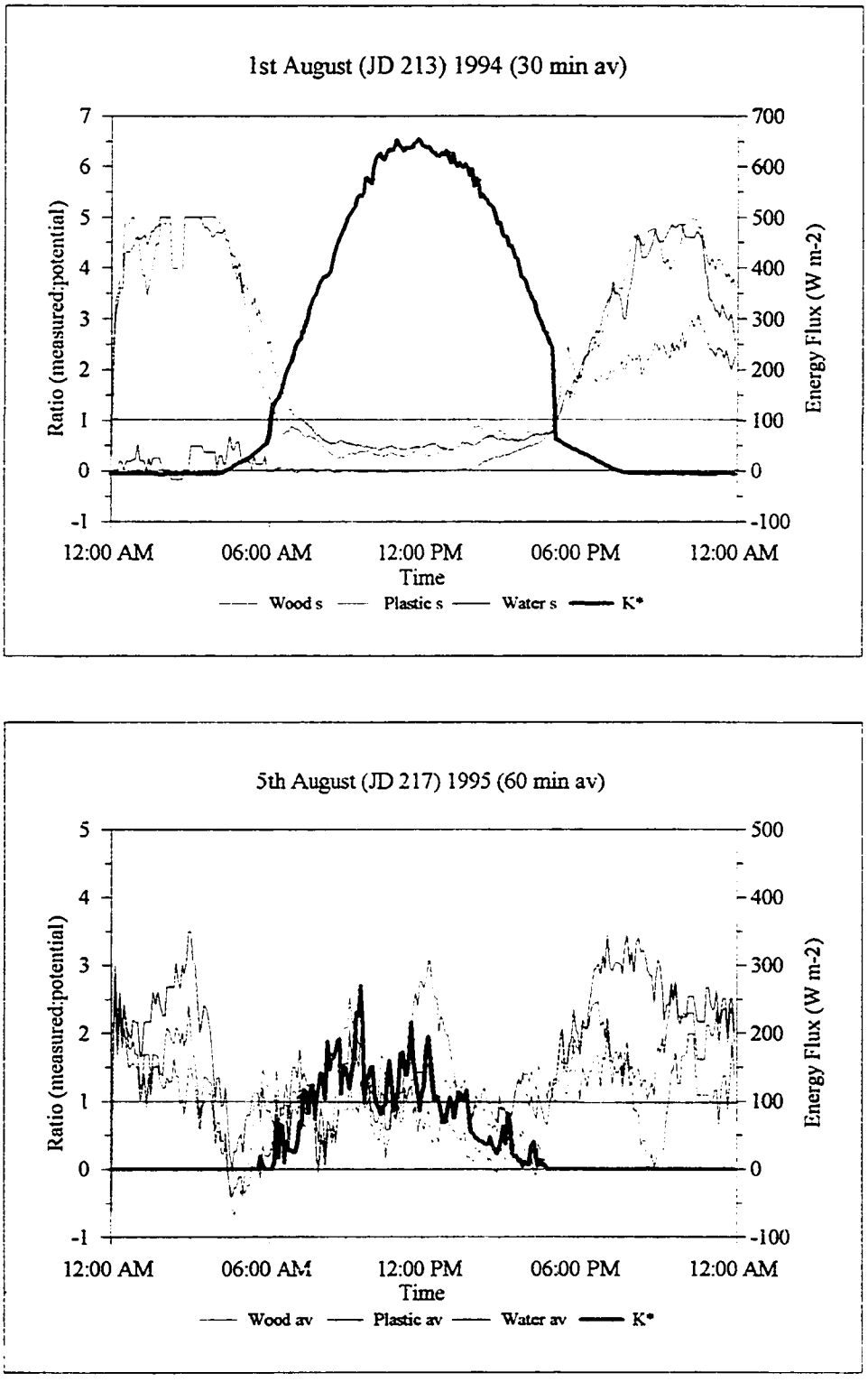

Fig. 4.1. Measured to expected surface lowering ratio and associated short-wave radiation curve for a) August 1st, 1994 (Julian day 213) and b) August 5th, 1995 (Julian day 217)

The above figure demonstrates two daytime periods and their associated weathering crust ratios. The first day is characterised by high short-wave energy inputs and the potential for weathering crust growth is great. It is expected that weathering crust growth will occur for the duration of daylight hours and this is demonstrated by a measured to expected ratio of less than one, as anticipated. It can also be seen that the ratio is closest to zero in the morning, becoming closer to one in the afternoon, suggesting that the strongest weathering crust growth is occurring in the morning.

Fig. 4.1.b. is typical of a cloudy day. Note that maximum solar radiation values are less than 300 W m^{-2} compared with values approaching 700 W m^{-2} in Fig. 4.1.a. Under these conditions, it would be expected that weathering crust growth is reduced. If Q_M is positive it is likely to consist of a greater percentage of energy from the sensible heat flux (Q_H). Under these conditions, the ratio of measured to expected surface lowering is predominantly greater than one because melt is mainly occurring at the surface, wasting away a previously weathered surface.

4.3. Intensive Examination of the Weathering Crust

Based on the ratio of actual to potential surface lowering, several weathering crust conditions can be identified. First, weathering crust growth will occur under melt conditions where K* is the dominant energy source. Second, weathering crust decay will occur during periods when Q_H is the dominant energy source. Third, transition between weathering crust growth and decay will occur during poor weather, daytime periods. Finally, during periods of nocturnal, clear sky conditions, little crustal change will occur. Periods consisting of these conditions are examined. Detailed diaries for selected periods discussed in this section of the analysis are presented in Appendix V. Periods where manual lowering of the ablatometers was undertaken, or where data

were missing, were removed from the analysis. Incidents such as an ablatometer sticking and then righting itself cannot always be distinguished from ice surface collapse and therefore cannot be removed from the analysis.

It should be noted that the small plot in 1994 was intentionally given a lower albedo by scattering debris from a lateral moraine across its surface. Debris, as well as reducing albedo, will enhance melt through cryoconitic processes. The enhanced thermal properties of debris particles and algae intensify melt in their immediate vicinity and cause them to melt more rapidly into the ice surface, thereby altering the microtopography of their immediate surroundings (Fig. 4.2.). The effect of these processes is to decrease the density of the ice surface, presenting a more highly developed crust than would be expected.

Fig. 4.2. An example of cryoconitic melt as a result of algae in the ice

4.3.1. Growth Conditions

Periods of weathering crust growth can be identified by an R value of less than one and constitute scenario (A). Growth will occur when solar radiation dominates the energy available for melt. During periods of growth over 70 % of the energy available for melt is from net short-wave radiation (Table 4.2.). This is expected because it is the property of solar radiation to penetrate the ice surface which results in sub-surface melt and the resultant weathering crust. Average short-wave values are greater than 300 W m^{-2} and mean air temperatures are greater than 4 °C.

In addition to the general characteristics of growth periods gained from examination of all growth periods monitored during data collection, August 1st (Julian Day 213) 1994 and July 28th (Julian Day 209) 1997 were selected for a more detailed analysis. Associated stage records for July 28th 1997 are also discussed. August 1st,1994, is generally a lower energy period than the average for the year (Table 4.2.and 4.3.). This accounts for the lower K* and higher Q_H contributions to Q_M than might be expected. However, surface lowering measurements clearly demonstrate weathering crust growth. In the case of July 28th, 1997, energy inputs are above average, demonstrated by the large contribution of global radiation to Q_M (over 100 %).

Table 4.2. Five minute average summary data for periods of weathering crust growth

	1994	1995	1997
Global (W m^{-2})	520	419	423
K* (W m^{-2})	432	460	323
Q* (W m^{-2})	437	348	236
L* (W m^{-2})	5	-118	-87
Q_H (W m^{-2})	115	45	63
Q_E (W m^{-2})	-7	1	10
Q_M (W m^{-2})	546	394	308
Air Temp (°C)	9.6	4.2	6.6
Vapour Pressure (mb)	5.98	4.66	4.36
Wind Speed (m s^{-1})	5.1	4.0	3.8
Total Ppt (mm)*	0.3	N/A	57.3
Energy Partitioning of Q_M:			
Global (%)	95	106	137
Q* (%)	80	88	76
L* (%)	1	-30	-28
Q_H (%)	21	11	20
Q_E (%)	-1	0	3
K* (%)	79	117	105
$Q_H + Q_E$ +L* (%)	21	-18	-5
Surface Lowering:			
Wood (s) (mm)	0.34	Missing	0.22
Wood (l) (mm)	0.16	0.08	N/A
Water (s) (mm)	0.27	Missing	0.11
Water (l) (mm)	0.14	0	N/A
Plastic (s) (mm)	0.14	0.19	0.11
Plastic (l) (mm)	0.21	0.08	N/A
Potential lowering (mm)	0.55	0.4	0.31
R (avg plastic)	0.32	0.34	0.36
n	696	672	3660

* total, not average

Table 4.3 A comparison of two periods of weathering crust growth

	August 1st (213) 1994	**July 28th (209) 1997**
Growth Period:		
Wood (s)	6:05 AM to 5:00 PM	6:00 AM to 12:35 PM
Plastic (s)	6:15 AM to 5:00 PM	6:00 AM to 4:15 PM
Water (s)	7:05 AM to 5:00 PM	
Global (Avg)	422 W m^{-2}	480 W m^{-2}
K* (Avg)	351 W m^{-2}	360 W m^{-2}
Q* (Avg)	340 W m^{-2}	266 W m^{-2}
L* (Avg)	-11 W m^{-2}	-94 W m^{-2}
Q_H (Avg)	110 W m^{-2}	128 W m^{-2}
Q_E (Avg)	-18 W m^{-2}	5 W m^{-2}
Q_M (Avg)	432 W m^{-2}	340 W m^{-2}
Global (Sum)	23.2 MJ	26.5 MJ
K* (Sum)	19.3 MJ	19.9 MJ
Q* (Sum)	18.7 MJ	14.7 MJ
L* (Sum)	-0.6 MJ	-5.2 MJ
Q_H (Sum)	6.1 MJ	3.8 MJ
Q_E (Sum)	-10.0 MJ	0.3 MJ
Q_M (Sum)	23.7 MJ	18.7 MJ
Air Temp (Avg)	8.5 °C	7.3 °C
Vapour Pressure (Avg)	3.12 mb	3.99 mb
Wind Speed (Avg)	5.4 m s^{-1}	3.9 m s^{-1}
Total Ppt	0 mm	0.1 mm (2:50 PM)
Energy Partitioning of Q_M:		
Global	85 %	106 %
Q*	50 %	69 %
L*	-21 %	-12 %
Q_H	62 %	29 %
Q_E	-11 %	2 %
K*	70 %	81 %
$Q_H + Q_E + L^*$	30 %	19 %
Total surface lowering:		
Water (s)	51.9 mm	
Plastic (s)	14.4 mm	58.1 mm
Potential	79.9 mm	63.1 mm

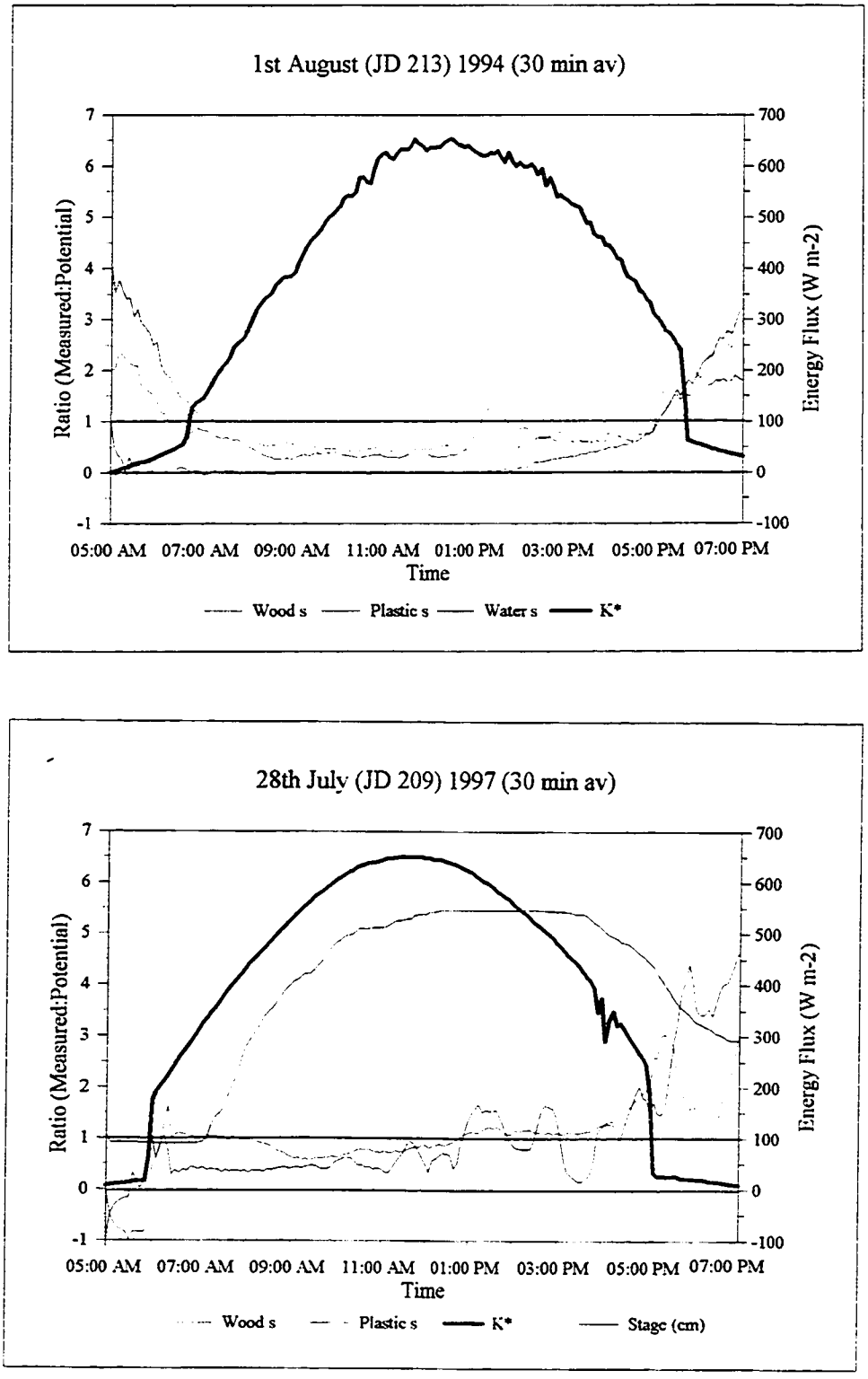

Fig. 4.3. Ratio of actual to potential surface lowering as an indication of weathering crust growth: a) August 1st, 1994 (Julian Day 213); b) July 28th, 1997 (Julian Day 209)

Initial conditions are important for weathering crust development. In the case of July 28th, weathering crust growth is not preceded by nocturnal melt and Q_M becomes positive at 5:55 a.m. As a result, it is likely that weathering crust growth from the previous day still exists. In the case of August 1st, Q_M is already positive due to a dominant positive Q_H flux overnight. In this situation, it is likely that any weathering crust growth will have been depleted overnight through surface lowering, which will melt away the upper, lower density layers.

Weathering crust growth lags behind radiation inputs. Further, differences in thermal properties between the wood and plastic feet mean that the darker wood foot will warm up faster, enhancing local melt, and causing it to respond before the plastic foot. The wood foot has a smaller surface area than the plastic cross shaped foot, exerting more pressure on the ice surface and increasing the likelihood that it will break through a low density ice surface. As a result of its enhanced thermal properties, the wood foot is not a direct indicator of weathering crust, unlike the plastic foot. In some instances early in the day the wood foot actually melts into the ice, producing what appears to be a short period of weathering crust decay. In fact, these periods characterise enhanced melt into the ice surface as a result of the foot's lower albedo.

On August 1st, the wood foot is the first to indicate weathering crust growth at 6:05 a.m., fifteen minutes after Q* becomes positive and at the time when radiation measurements reach 100 W m^{-2} which approximately coincides with the value of the L* deficit. The plastic foot indicates weathering crust growth at 6:15 a.m. The water foot, after a period where potential lowering equals actual lowering and the weathering crust ratio equals one, indicates growth at 7:25 a.m. Data for July 28th demonstrate the onset of weathering crust growth at approximately the same time, although in this case there is no delay of the plastic foot. This implies that the wood foot is melted into the ice surface and that the weathering crust has developed to a point where any

internal melt results in ablation and therefore lowering of the plastic foot. This is supported by clear and sunny conditions during the preceding day, which would promote weathering crust growth and clear, low melt conditions that night, which would maintain crustal conditions from the previous day.

The plastic foot should be the most accurate indicator of weathering crust growth. As can be seen from the weathering crust growth demonstrated by the individual feet (Fig. 4.3.) very little melt occurs with the plastic foot until later in the afternoon, well after solar noon. In fact, until after 2:00 p.m., surface lowering of the plastic foot is zero and on first examination it appears as though melt is zero. However, we know that melt is occurring because Q_M is positive and the other feet indicate surface lowering. This implies that all of the melt that is occurring is internal and is not being measured by the plastic foot ablatometer because, by design, movement of the foot is ablation of the surface. An explanation for this is that the plastic foot rests on top of the crust surface while internal melt is occurring. Then, as the crust density decreases to a critical value, it begins to visually demonstrate weathering crust growth as surface lowering due to melt and crustal collapse occurs. During this phase the plastic foot indicates more intense weathering crust growth than the other two feet (i.e. a ratio closer to zero) for the first 2 hours and 15 minutes. This translates as a very slow rate of lowering of the foot. Following this period, it has a similar ratio of between 0.5 and 0.8 as the other two feet which indicates that the plastic foot ablatometer is experiencing the same rate of surface lowering as the other two ablatometers.

The water foot demonstrates the melt occurring within a stream environment. The response of this foot to melt and weathering crust growth is expected to be slower because the short-wave energy has to travel through the water medium first, having already refracted and exponentially decayed before it reaches the ice surface. Water also flows in channels incised into

the ice surface and local microtopography may reduce the amount of K* incident on the channel bed through localised shadowing. Further, running water will modify effects through erosion and frictional melt of the ice surface. As a result of water turbulence, the surface is unlikely to become pitted as easily. It is assumed that within large channels, these effects would prevent the formation of weathering crust. However, under initial channel formations and small headwater channels, it is assumed that weathering crust growth may occur. Indeed, the development of a weathering crust might propagate channelised flow as water flows within the weathering crust and develops preferential pathways. This may be enhanced by the lower albedo of saturated ice which will locally increase melt rates. R values close to a value of one can indicate melt of ice at 0.89 kg m^{-3} x 10^3.

In the case of August 1st, the channel is quite small and the catchment recently established, so water flow is low and this may explain the appearance of intense weathering crust growth within the channel environment. It is further possible that, in the presence of water, the ratio does not apply with respect to the delineation of weathering crust growth and decay, referring instead to enhanced or decreased lowering as a result of the combination of weathering crust processes and other factors, such as discharge amounts and water temperatures.

Weathering crust growth ends at 5:00 p.m. on August 1st for all three ablatometers. At 5:05 p.m. K* dropped off rapidly below 100 W m^{-2}. Although Q_M was still positive, the source of solar energy had gone and it is to be expected that weathering crust growth will cease at that time, given that only solar radiation can penetrate the ice surface. It is probable that this cessation of K* inputs occurs as a result of shadowing from the surrounding mountains. By 5:00 p.m. in early September, the whole of the glacier tongue is in total shadow.

July 28th demonstrates the weathering crust development that will occur given initial conditions of a partial weathering crust layer. In this case, the plastic foot begins lowering in the morning because the ice has already rotted. The strongest weathering crust growth is seen earlier in the day through a lower ratio value. This begins to change at approximately mid-day even though weathering crust growth is indicated for the greater part of the day.

From 4:45 p.m. to 5:05 p.m., the ratio for the wood foot oscillates around one. Similarly, although there is some weathering crust growth implied by the ratio for the wood foot between 8:50 a.m. and 12:05 p.m., this is not very strong (close to one), which implies that measured surface lowering is equal to potential surface lowering and an equilibrium has been reached. Theoretically, this state of equilibrium would exist once the weathering crust layer had been fully developed with a depth of maximum extent given the extinction of solar radiation with depth and a density at the minimum possible to hold the form of the ice. Further surface melt removes the upper layer of the crust while enabling 'internal' melt of a new layer of ice at the base of the crust. Thus, even though the density of the ice at the surface is significantly less than the assumed density of 0.89 kg m^{-3} x 10^3, the additional melt of the lower ice layer compensates for this.

In the afternoon of July 28th, two periods of weathering crust decay are indicated as the ice surface lowers. The second one, at least, is associated with a rain shower and enhanced cloud cover. At the end of this second period of decay, there is a deep trough shown for the ice plastic foot when the ratio dips back down to almost zero, implying intense weathering crust growth. This occurs immediately after the rainfall event which ended at 2:50 p.m. It is likely that while the rain event occurred, not only would cloud reduce the solar energy receipt at the surface, but the rain itself would degrade the crust through mechanical weathering, especially when there is some thermal energy contribution as well. It is expected that this would have a larger effect on a well

developed crust which already has a lower density and as a result, a less cohesive ice crystal matrix. The growth period ends for the day as cloud cover increases again. Growth is prematurely ended at 4:15 p.m. on July 28th, as noted by the plastic foot, and this is presumed to be a result of increased cloud presence following a rain event at 2:50 p.m. Sunshine charts concur with this, direct sunshine having gone from base camp by 4:30 p.m.

Overall surface lowering for August 1st was 52.7 mm for the wood foot, 51.9 mm for the water foot and 14.4 mm for the plastic foot. Potential surface lowering, based on the energy available for melt was 79.9 mm. This again suggests that the plastic foot was not able to measure internal melt for the initial part of the day as it was not accompanied by any surface lowering. It also suggests that very little, if any, weathering crust existed from the previous day because there was such a large lag between energy inputs and surface lowering of the plastic foot. The reason that the potential lowering is so high is because it is based on the assumption of a constant ice density of 0.89 kg m^{-3} x 10^3. The discrepancy between this and the ablatometers also indicates that weathering crust growth was occurring. It suggests that an equivalent of approximately 27 mm of melt was internal for the wood and water feet, which would have settled into the crust, and 65 mm for the plastic foot, which is designed to rest on top of the crust. Assuming a weathering crust depth of 20 cm and a 1 m^2 surface area, 65 mm of internal melt will result in an ice density of 0.6 kg m^{-3} x 10^3 based on the following equation:

$$\rho = \frac{V_o - V_i}{V_o} \qquad (4.1.)$$

where V_i is the volume of ice melted internally; and V_o is the original ice volume.

For this example, V_o = l*w*h = 100*100*20 cm^3 = 200 000 cm^3
V_i = 100*100*6.5 cm^3 = 65 000 cm^3
therefore, the density of ice ratio = 135 000 / 200 000 = 0.675
so, density = 0.675*0.89 = 0.6 kg m^{-3} x 10^3

For July 28th 1997 overall surface lowering was 65.8 mm for the wood ablatometer and 58.1 for the plastic ablatometer. Potential surface lowering was 63.1 mm. The wood foot lowers more than expected given the energy available for melt. This is to be expected, given that the weathering crust has developed during the previous day and therefore further growth during this period results in a highly developed crust and an equilibrium between surface lowering and internal melt. The plastic foot only demonstrates 5 mm of internal melt, again an indication of a previously developed crust.

In Fig. 4.3.a. it can be seen that the wood foot demonstrates a period of decay, or surface lowering without internal melting, at 1:15 p.m on August 1st. This is not due to actual crustal decay but to the foot dropping at least a centimetre in each of three five minute intervals. This could be for several reasons: first, the foot was stuck up and dropped; second, the foot broke through the crust and into the ice; and third, energy stored within the foot is being released. The ablatometer in the water on July 28th demonstrates the same behaviour. In this case, the foot was manually lowered at 3:38 p.m., because it was elevated, and was consequently removed from this analysis.

The most likely explanation for August 1st is that internal melt had occurred to a point where the enhanced thermal properties and small surface area of the foot, combined with the decreased density of the crust, resulted in a surface layer that could not support itself and so the actual surface of the ice collapsed. This theory is also used to explain the lack of surface lowering of the plastic foot while intensive internal melt is occurring and the subsequent period of lowering as the density decreases to a point where the crust begins to ablate due to melt or collapse.

Stage records are available for July 28th and can be utilised in the examination of lags resulting from weathering crust growth processes. Stage kept falling until 6:00 a.m., suggesting

overnight draining of melt water from the previous day. An initial stage increase occurred at 6:55 a.m. and stage rose 31.2 mm by 9:00 a.m. This is fifty five minutes after weathering crust growth commenced. Maximum stage occurred from 12:20 p.m. to 2:30 p.m., having increased 10.8 mm by 10:30 a.m. and a further 3.6 mm by 12:20 p.m. Maximum discharge preceded the end of weathering crust growth for the plastic foot by one hour and forty five minutes. Stage decreased 4.9 mm by 4:10 p.m. and a further 17.0 mm by 6:05 p.m. Melt continued in the form of weathering crust decay through the night and stage fell slowly through the night.

It is apparent that the lag between melt occurring and increasing stage from the sub-catchment is slightly less than an hour in this case. Records for July 19th, another period of crustal growth, concur with this. Discharge begins to rise at 6:45 a.m. and by 8:35 a.m. stage has risen 8.4 mm. It rises a further 1.5 mm by 9:15 and then a further 0.4 mm to maximum stage. Maximum stage is from 12:50 p.m. to 5:30 p.m. and K* is greater than 600 W m^{-2} between 10:35 a.m. and 2:05 p.m. Initial change in stage lags behind weathering crust growth by fifty minutes. The greatest increase in stage occurs while internal melt of the ice surface is occurring. Then, even though growth is still taking place, the rate of increase decreases significantly. This could reflect the increased storage capacity of the ice surface given its decreased density. For the first two hours increasing amounts of melt water are making their way to the channel system through the ice surface. An equilibrium is reached after approximately two hours where the amount of ice melting and the amount of melt water reaching the channel system are the same and no further rise in stage is recorded. Growth of the weathering crust, as demonstrated by the ice foot record, ends at 5:00 p.m. Half an hour later, the stage begins to fall, suggesting that the system is draining. Melt continues to occur throughout the night, as the weathering crust decays, and explains why stage has only dropped 3.0 mm by 7:15 p.m. and only a further 6.4 mm by 11:40 p.m.

Further to the detailed description of weathering crust growth above, it appears that weathering crust growth is quite sensitive to changes in the radiation energy input. This is clearly demonstrated on August 1st when a cloud system fills the sky and there is a sharp decrease in net short-wave radiation. This type of immediate response is also seen on August 16th, 1994, between 12:00 p.m. and 4:30 p.m. (Fig. 4.4.).

K* falls below 100 W m^{-2} at 1:55 p.m. and is less than 10 W m^{-2} between 3:05 p.m. and 3:30 p.m., rising back up above 100 W m^{-2} at 3:50 p.m. Correspondingly, Q_M is less than 100 W m^{-2} between 2:10 and 3:50 p.m. All three ablatometers in the small plot indicate weathering crust growth at the start of this period and at 1:50 p.m. they all demonstrate weathering crust decay, approximately thirty five minutes after K* decreases. Weathering crust growth begins again at 3:55 p.m. for the plastic foot in the small plot five minutes after both Q_M and K* rise above 100 W m^{-2}. The wood foot in the small plot begins a period of no surface lowering at the same time while the water foot in the small plot remains in a state of decay for most of the period. In the large plot, the wood foot demonstrates growth until 2:00 p.m., ten minutes after the small plot ablatometers respond. It then demonstrates a transitional period of mixed growth and decay, before total decay begins at 2:35 p.m. Growth begins as in the small plot at 3:50 p.m. but decay starts again at 4:20 p.m. The plastic foot demonstrates no lowering between 12:30 p.m. and 1:15 p.m., followed by growth to 2:55 p.m., lagging the ablatometers in the small plot by five minutes. Growth commences again at 3:50 p.m., five minutes earlier than the small plot. The water foot in the large plot has a ratio indicating no lowering with some growth, or decreased lowering, periods until 2:35 p.m. when decay begins, much earlier than the other ablatometers. Decay ends at 3:35 p.m. (again, much earlier than the others) and growth occurs until 4:15 p.m.

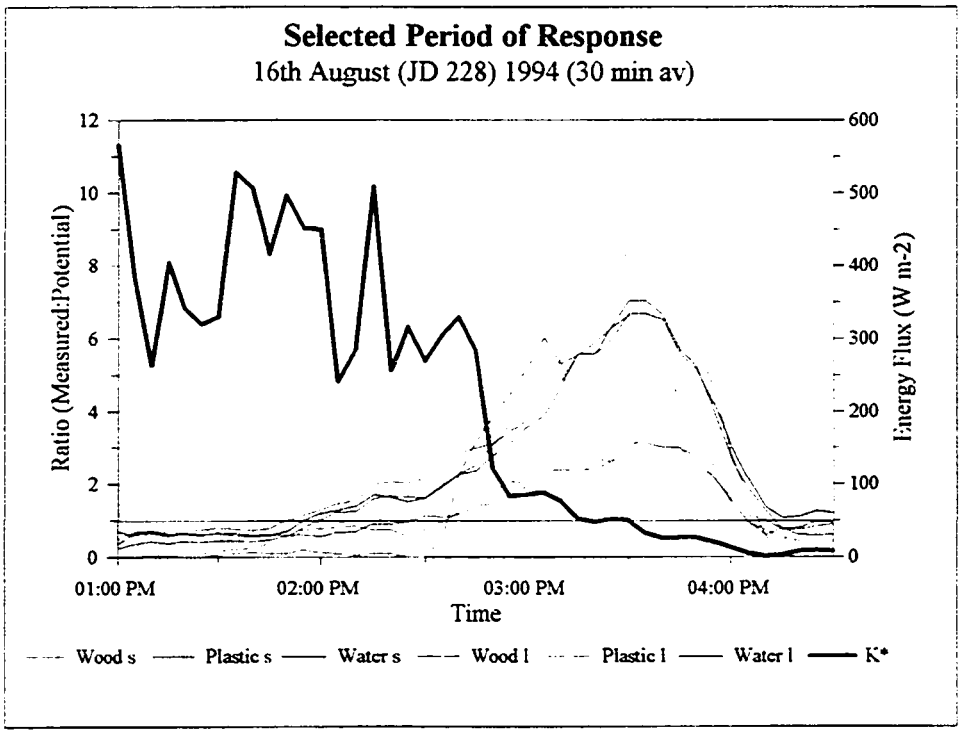

Fig. 4.4. The response of weathering crust processes to changes in the radiation budget

4.3.2. Decay Conditions (Nocturnal)

Weathering crust decay can occur under two broad conditions - warm, usually overcast, nights (scenario C) and overcast days (scenario B). Nocturnal decay will occur when Q_H is dominant and is large enough to overcome the energy deficit of L* and, when necessary, Q_E, for Q_M to be positive. Air temperatures are similar to those during growth periods, as are average windspeeds (Table 4.4.). Further, there is an obvious dominance of Q_H over other energy sources, contributing 100 % of Q_M.

Table 4.4. Five minute average summary of periods of weathering crust decay (nocturnal)

	1994	1995	1997
L* (W m^{-2})	-27	21	-25
Q_H (W m^{-2})	102	44	71
Q_E (W m^{-2})	-2	7	19
Q_M (W m^{-2})	71	45	64
Air Temp (°C)	8.2	4.4	6.9
Vapour Pressure (mb)	3.76	4.8	4.56
Wind Speed (m s^{-1})	5.0	3.7	4.1
Total Ppt (mm)*	0.0	N/A	17.9
Energy Partitioning of Q_M:			
L* (%)	-38	47	-39
Q_H (%)	144	98	111
Q_E (%)	-2	15	29
$Q_H + Q_E + L^*$	104	159	101
Wood (s) (mm)	0.17	0.03	0.11
Wood (l) (mm)	0.17	0.08	N/A
Plastic (s) (mm)	0.18	0.09	0.15
Water (s) (mm)	0.10	0.02	0.04
Water (l) (mm)	0.08	0.00	N/A
Plastic (l) (mm)	0.13	0.05	N/A
Pot lowering (mm)	0.07	0.04	0.07
R (avg plastic)	2.21	1.75	2.14
n	684	648	2388

* total, not average

Three periods were selected for further analysis (Table 4.5.). First, crustal decay is examined as it occurs over the night of August 2nd and 3rd (Julian Day 214 and 215) 1994. A period of transition is examined on July 1st (Julian Day 182) 1997. A further example discussed is the period from July 29th - 31st (Julian Day 210 - 212) 1997. This period encompasses both transition periods and nocturnal decay periods. The latter scenarios are discussed in section 4.3.3. It can be seen that the example of August 2nd and 3rd demonstrates lower energy inputs than average (Table 4.4 and 4.5.). Average air temperature is also slightly lower.

Table 4.5. A comparison of three periods of weathering crust decay and transition

	214–15 (August 2nd -3rd) 1994	**182 (July 1st) 1997**	**210–12 (July 29th - 31st) 1997**
Decay Period:			
Wood (s)	5:00PM to 6:10 AM	5:30 AM to 11:35 PM	2:00 PM (210)to 6:25 AM 2:00 PM (211) to 7:40 AM
Wood (l)	5:00 PM to 6:35 AM		
Water (s)	5:35 PM to 6:40 AM		no melt
Plastic (s)		6:30 AM to 8:15 AM 1:05 PM to 11:40 PM	2:10 PM (210) to 2:30 AM 2:00 PM (211) to 7:25 AM
Plastic (l)	5:05 PM to 6:35 AM		
Global (Avg)	49 W m^{-2}	348 W m^{-2}	92 W m^{-2}
K* (Avg)	44 W m^{-2}	241 W m^{-2}	76 W m^{-2}
Q* (Avg)	20 W m^{-2}	181 W m^{-2}	47 W m^{-2}
L* (Avg)	-24 W m^{-2}	-60 W m^{-2}	-29 W m^{-2}
Q_H (Avg)	122 W m^{-2}	42 W m^{-2}	100 W m^{-2}
Q_E (Avg)	22 W m^{-2}	-13 W m^{-2}	40 W m^{-2}
Q_M (Avg)	163 W m^{-2}	209 W m^{-2}	187 W m^{-2}
Global (Sum)	2.7 M J	25.3 M J	14.3 M J
K* (Sum)	2.4 M J	17.6 M J	11.8 M J
Q* (Sum)	1.1 M J	13.2 M J	7.3 M J
L* (Sum)	-1.3 M J	-4.4 M J	-4.5 M J
Q_H (Sum)	6.6 M J	3.0 M J	15.6 M J
Q_E (Sum)	1.2 M J	-0.9 M J	6.1 M J
Q_M (Sum)	8.9 M J	15.3 M J	29.0 M J
Air Temp (Avg)	9.3 °C	5.2 °C	8.6 °C
Vapour Press (Avg)	3.92 mb	4.65 mb	4.49 mb
Wind speed (Avg)	5.4 m s^{-1}	3.5 m s^{-1}	4.8 m s^{-1}
Total Ppt.	0 mm	0 mm	18.1 mm
Energy Partitioning of Q_M			
Global	17 %	109 %	36 %
Q*	-2 %	63 %	-18 %
L*	-17 %	-14 %	-47 %
Q_H	85 %	47 %	99 %
Q_E	17 %	-10 %	19 %
K*	15 %	78 %	29 %
$Q_H + Q_E + L^*$	85 %	23 %	71 %

Total Surface Lowering:			
Wood (s)	56.1 mm	68.8 mm	126.6 mm
Wood (l)	50.1 mm		
Water (s)	36.6 mm		
Plastic (s)		68.2 mm	140.8 mm
Plastic (l)	45.9 mm		
Potential Lowering	29.6 mm	45.2 mm	10.8 mm

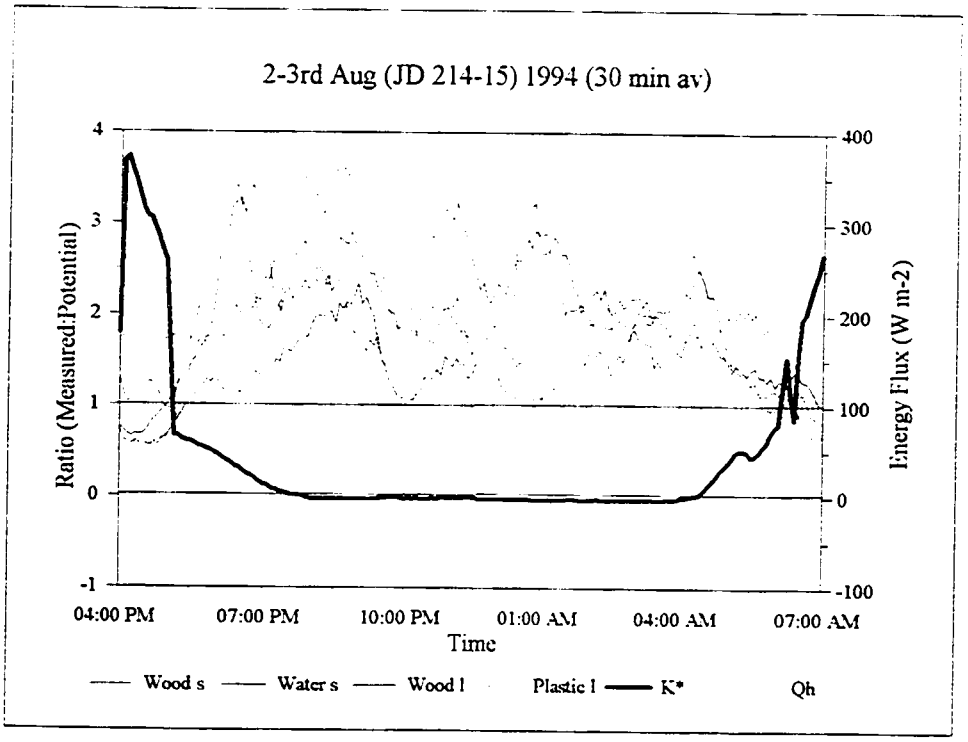

Fig. 4.5. Ratio of actual to potential surface lowering as an indication of weathering crust decay: August 2nd-3rd,1994 (Julian Day 214-15)

It is expected that melt would be reduced under nocturnal or cloudy conditions. Although this is the case, these results clearly demonstrate that significant melt can still occur. The amount of surface lowering occurring between August 2nd and 3rd, 1994 was 56.1 mm in the small plot and 50.1 mm in the large plot, for the wood feet, while the plastic foot in the large plot lowered 45.9

mm. The water foot lowered 36.6 mm in the small plot and expected surface lowering was 29.6 mm.

All of the ablatometers demonstrated greater surface lowering than expected, based on Q_M. This is because the expected lowering is based on a density of 0.89 kg m^{-3} x 10^3. It is to be assumed that previous weathering crust growth has reduced actual ice density to less than this. Thus the actual surface lowering that is occurring is a result of melt of a less dense ice matrix than is assumed for potential lowering. Calculated ice densities for August 1st and 2nd, based on actual and potential surface lowering values, are 0.53 and 0.59 kg m^{-3} x 10^3 for the small and large plot wood ablatometers, respectively; 0.64 kg m^{-3} x 10^3 for the plastic foot in the large plot; and 0.81 kg m^{-3} x 10^3 for the water ablatometer in the small plot. Ice densities within the channel environment are expected to be higher as a result of the decreased likelihood of weathering crust growth within a water environment. Thus it is assumed that the surface beneath a channel is close to a density of 0.89 kg m^{-3} x 10^3.

The nocturnal decay period examined commences at 4:00 p.m. on the 2nd and ends at 7:00 a.m. on the 3rd. The wood and water feet in the small plot and the wood and plastic feet in the large plot were all demonstrating weathering crust growth at the beginning of this period, indicating the ending of daytime melt. The wood foot in the small plot underwent a period of decay between 4:15 and 4:35 p.m. and growth ended at 4:55 p.m. Growth ended for the water foot of the small plot at 5:20 pm; the wood foot in the large plot at 4:35 pm; and the plastic foot in the large plot at 5:00 p.m. K* fell below 100 W m^{-2} at 5:10 p.m. that day and ceased being positive at 7:55 p.m. Between 7:35 p.m. and 9:05 p.m., Q_M was negative. This was partly due to Q_H dropping below 100 W m^{-2} between 8:30 p.m. and 9:05 p.m.

Overnight, the ablatometers were fairly consistent in demonstrating decay processes, with the exception of the water foot in the small plot and the wood foot in the large plot. Decay was demonstrated by the wood foot in the small plot from 5:00 p.m. until 6:00 a.m. and from 5:10 p.m. to 5:30 a.m. by the plastic foot in the large plot. The wood foot in the large plot had a ratio equal to one from 4:50 p.m. to 8:40 p.m., indicating either a fully developed weathering crust or no weathering crust. Decay began at 9:00 p.m. and ended at 6:30 a.m., with five minute periods of weathering crust growth occurring after 5:30 a.m. The water foot in the small plot followed a similar pattern. Decay occurred between 5:25 p.m. and 6:35 a.m. with the exception of growth, or enhanced lowering, at five minute intervals after 3:30 a.m. Growth for the wood foot in the small plot began at 6:15 a.m. and for the plastic foot in the large plot at 6:45 a.m. with the hour from 5:30 a.m. to 6:30 a.m. being a transition period characterised by a mixture of growth, decay and a ratio of one. K* inputs began at 4:10 a.m. and increased above 100 W m^{-2} at 6:10 a.m. on the 3rd.

4.3.3. Transition Conditions

Transition occurs under daytime cloud conditions and is a complex response to both radiant and turbulent energy sources (scenario B). Depending on which energy type is greater, the weathering crust response will be growth or decay, often oscillating over small time periods. K* is still the dominant source of energy available for melt, but Q_H is significant at more than 30 % of Q_M (Table 4.6.). The more extensive and thicker the cloud cover, the greater the contribution of Q_H as compared to K*. The summary for transition periods is a simplification of events as they occurred because, by definition, each period consists of a complexity of growth and equilibrium periods even though they are dominated by decay (Appendix V).

Table 4.6. Five minute average summary of periods of daytime decay transition

	1994	1995	1997
Global (W m^{-2})	135	146	231
K* (W m^{-2})	115	122	180
Q* (W m^{-2})	105	120	72
L* (W m^{-2})	-11	-8	-108
Q_H (W m^{-2})	92	59	66
Q_E (W m^{-2})	8	10	-2
Q_M (W m^{-2})	204	188	136
Air Temp (°C)	9.2	5.3	6.2
Vapour Pressure (mb)	3.67	4.7	4.41
Wind Speed (m s^{-1})	4.0	4.0	4.3
Total Ppt (mm)[†]	0.0	N/A	11.8
Energy Partitioning of Q_M:			
Global (%)	66	77	169
Q* (%)	51	63	53
L* (%)	-5	-4	-80
Q_H (%)	45	31	49
Q_E (%)	4	5	-2
K* (%)	57	65	132
$Q_H + Q_E + L^*$ (%)	43	32	-33
Surface Lowering:			
Wood (s) (mm)	0.45		0.18
Wood (l) (mm)	0.29	0.21	N/A
Water (s) (mm)	0.21	0.04	0.10
Water (l) (mm)	0.10	0.00	N/A
Plastic (s) (mm)	0.46	0.23	0.18
Plastic (l) (mm)	0.29	0.11	N/A
Pot lowering (mm)	0.19	0.19	0.14
R (avg plastic)	1.97	0.89	1.29
n	130	372	1020

[†] total, not average

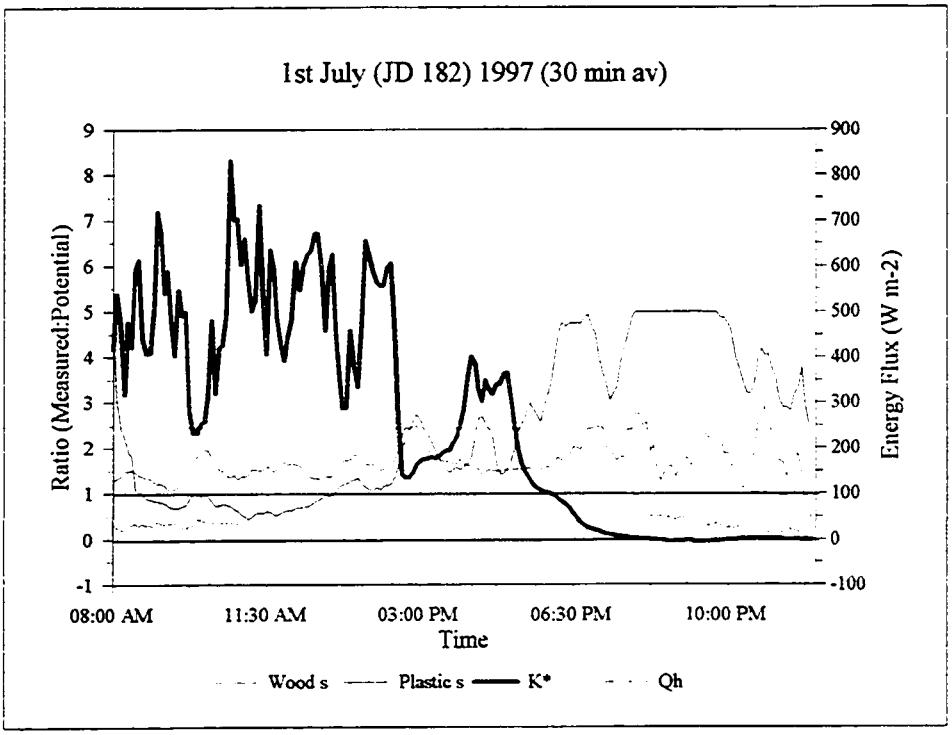

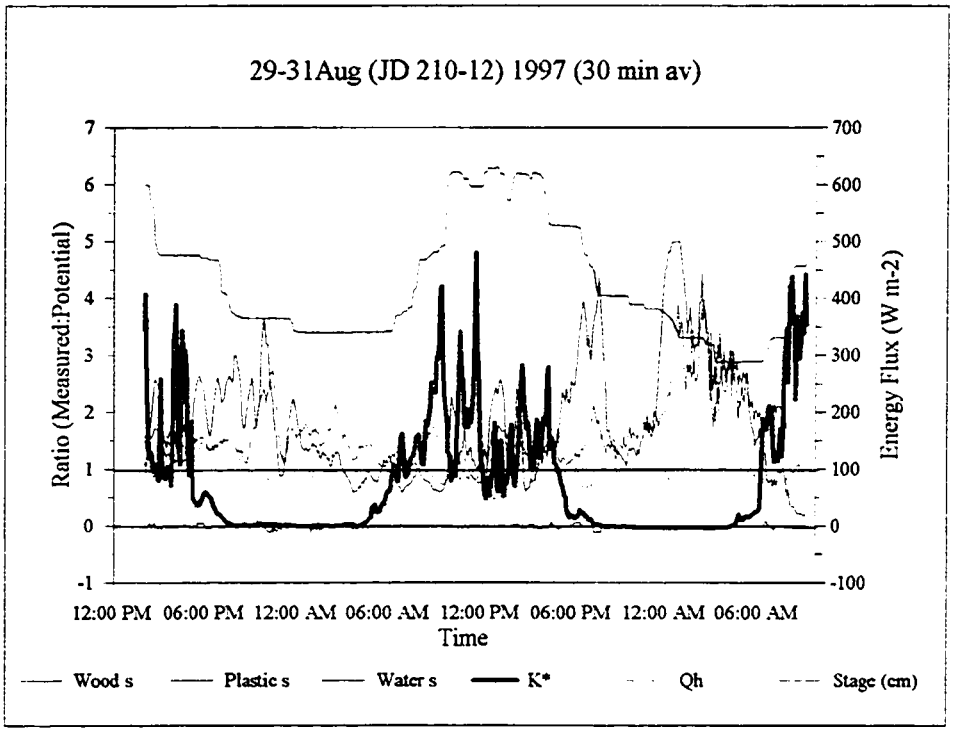

Fig. 4.6. Ratio of actual to potential surface lowering as an indication of weathering crust transition and decay: a) July 1st,1997 (Julian Day 182);
b) July 29th-31st, 1997 (Julian Day 210-12)

July 1st, 1997 is a poor weather period which demonstrates transition between growth and decay. The day began quite cold with the discharge syphons frozen. Although this is a period of dominant decay, previous weather conditions had made the surface rotten. This is probably a result of weathering crust growth combined with remnants of snow frozen to the ice surface. The wood and plastic feet lowered 68.8 mm and 68.2 mm respectively and expected lowering was 45.2 mm (Table 4.5.). The water foot did not demonstrate any lowering. This can be compared to a potential surface lowering of 10.8 mm. Approximate densities, based on measured surface lowering, are 0.88 kg m^{-3} x 10^3 for the wood and plastic ablatometers.

K* reached 100 W m^{-2} at 5:20 a.m. on the 1st and this coincides with the start of a ten minute growth period of the wood foot. The plastic foot shows no lowering before 5:30 a.m. At 6:30 a.m. decay begins, lasting until 8:25 a.m. This is followed by another period of growth until 9:40 a.m. when K* drops from 500 to 284 W m^{-2}. The wood foot demonstrates decay for the first part of the morning. After 10:00 a.m. a mixture of no lowering and a ratio of one continue until the end of the period. The plastic foot exhibits a brief period of growth in the late morning and then decay occurs from 1:05 p.m. until the end of the period.

Between 12:35 and 12:40 p.m. global radiation values are over 1000 W m^{-2}. This demonstrates the effect of multiple reflection off clouds enhancing incoming solar radiation. This is the time when the plastic foot ends a period of weathering crust growth. The wood foot does not demonstrate any growth as a result of this enhanced solar radiation.

During the period from 2:00 p.m. on July 29th to 9: 00 a.m. on July 31st 1997, both daytime transition and nocturnal crustal decay occurs. The wood and plastic feet lowered 126.6 mm and 140.8 mm respectively during this period. Calculated densities are 0.37 and 0.31 kg m^{-3} x

10^3, respectively, for the wood and plastic feet. The water foot demonstrates very little surface lowering, with a total of 5.9 mm, mainly occurring on the 29th between 12:00 p.m. and 1:40 p.m. during what appears to be a period of weathering crust growth. At 1:40 p.m. the radiation input decreases suddenly as clouds move in and K* decreases from 642 W m^{-2} to 256 W m^{-2} while Q_M drops from approximately 600 W m^{-2} to approximately 300 W m^{-2}. The wood and plastic feet oscillate between growth and decay and then, in the early afternoon, move into a period of decay. Radiation inputs remain low for the rest of the day, K* dropping below 150 W m^{-2} at 2:15 p.m. with only short time periods having greater energy inputs. During periods of higher solar energy inputs, the plastic foot demonstrates a ratio of one.

The ice surface ablatometers are generally less variable during the night, as would be expected, because there is no solar energy available for growth to be taking place. The wood and plastic feet demonstrate decay overnight, but for different lengths of time. The plastic foot changes early in the morning to a period where the ratio is approximately equal to one. This suggests that the entire developed weathering crust layer has ablated away, leaving dense ice at the surface which is closer to the ice density used for potential lowering calculations. A period of apparent weathering crust growth commences at 3:10 a.m. This is unusual because, even though Q* and K* become positive at 2:55 a.m., the values are very low, the L* deficit is unlikely to have been compensated for and the glacier would still be in shadow from the surrounding peaks. It is unlikely that the plastic foot will be this sensitive to short-wave radiation with respect to weathering crust growth. Q_M is 160 W m^{-2} at this time but K* is only 1.63 W m^{-2}. The possibility that the foot catches for a short time period has to be considered and is the more likely explanation in this case.

From 4:20 a.m. to 6:15 a.m. on the 30th, the plastic foot ratio remains around one, varying between 0.8 and 1.2 before weathering crust growth begins, five minutes after K* has reached 100 W m^{-2}. Between 7:25 a.m. and 8:25 a.m. for the wood foot and 7:25 a.m. and 7:45 a.m. for the plastic foot, the ratio is approximately equal to one. During a similar period (7:10 - 7:35 a.m., 8:00 a.m. and 8:10 to 8:15 a.m.) K* and Q_H are approximately equal. However, it is not the case every time that the ratio is equal to one. Periods of weathering crust growth and equilibrium are interspersed within the dominant decay processes throughout the morning. At 9:20 a.m. K* drops from 420 to 293 W m^{-2} and this might explain why decay set in soon after on both ice ablatometers. After 12:00 p.m. for the plastic foot and 12:20 p.m. for the wood foot, decay is dominant. At 12:05 p.m. K* drops below 100 W m^{-2} for approximately an hour and then oscillates before dropping off again at 5:05 p.m.

During the afternoon the plastic foot demonstrated a growth period as K* went above 100 W m^{-2} but this was not always the case. K* had increased beyond this threshold earlier in the day and growth did not result. Obviously a more complex driving force exists. It could involve a response to precipitation, as a rainfall event occurred between 12:00 p.m. and 2:25 p.m. that day. Growth also began after an earlier rainfall event between 9:30 a.m. and 10:30 a.m., commencing at 10:35 a.m. and lasting until 11:05 a.m. The wood foot also demonstrated weathering crust growth during this time. The plastic foot did not change from decay for any of the other precipitation events. This may have something to do with the mechanisms of rain falling on an ice surface but is equally likely to be a result of clearing skies after a precipitation event. Other precipitation events occurred between 3:00 p.m. and 3:55 p.m. as well as at 5:45 p.m. and at 5:35 a.m. on the 31st.

The stage record for this period demonstrates an increase in stage after 5:45 a.m. on the 30th. This is juxtaposed against wood foot growth which commenced at 5:25 a.m. and plastic decay which began at 5:35 a.m. This would suggest a lag of between ten and twenty minutes between the onset of melt and a corresponding change in stage. Stage continued to increase until 10:25 a.m., after which it fell slightly. The greatest rise in stage occurred between 9:15 and 10:05 a.m (13.0 mm). The behaviour of the stage record during this period is explained by a precipitation event of 4.1 mm between 9:35 and 10:35 a.m. The rain was most intense between 9:50 and 10:15 a.m. This would suggest that the drop in stage that began at 10:25 a.m. was the end of the precipitation event flowing through the plot. Within the same general time period of the precipitation event, K* decreased to less than 100 W m^{-2} and the wood and plastic feet changed from periods of growth to periods of decay and then back to growth.

Stage continued to increase until 12:25 p.m., then decreased again over the next ten minutes. A second precipitation event occurred between 12:00 p.m. and 1:20 p.m. when 7.8 mm of rain fell. Rainfall was intense between 12:15 p.m. and 12:20 p.m. with 1.3 and 1.2 mm of rain falling per five minute period, respectively. Again, the decrease in stage is probably a response to the most intense rainfall having passed through the system. Another intense precipitation period occurs between 12:40 p.m. and 12:50 p.m. within the same rain event. This would explain the fifteen minute increase in stage after 12:45 p.m. Further precipitation events at 1:40 p.m. and 3:05 p.m. had similar effects on the stage record. The stage began to recede after 5:45 p.m. and continued to fall through the night.

At 12:20 p.m., the wood foot demonstrates weathering crust decay which lasts until 7:40 a.m. on the 31st. Plastic decay begins at 12:00 p.m. and lasts until 7:25 a.m. on the 31st with the

exception of an hour of weathering crust growth between 2:25 and 3:25 p.m. In this case, it is apparent that precipitation events and not melt were the driving force of the stage record.

On the 31st of August energy available for melt was quite low until 6:05 a.m. when it exceeded 100 W m^{-2}. K* became positive at 4:10 and was greater than 100 W m^{-2} by 6:05 a.m. It decreased below 100 W m^{-2} at 5:10 p.m. The plastic foot demonstrated weathering crust growth from 6:00 a.m onwards. Stage decreased by 8.4 mm before 3:10 a.m., draining melt water, and began to increase again at 6:10 a.m., five minutes after weathering crust growth commenced. A small precipitation event had occurred by 5:35 a.m. when 0.1 mm of rain was recorded. By 6:50 a.m. stage had increased to 4.1 mm and between 7:40 a.m. and 8:20 a.m. it increased by 12.6 mm. By 7:45 a.m. the wood foot began a period of transition between decay and growth. Meanwhile the water foot demonstrated no surface lowering for most of the period.

The rate of increase in stage slowed down after 8:50 a.m., increasing by only 0.5 mm between 10:20 a.m. and 10:35 a.m. Maximum discharge for the day was reached at 12:10 p.m. and continued until 3:30 p.m. Between 11:35 a.m. and 1:10 p.m., the ratio for the plastic ablatometer is mainly zero, which indicates total internal melt. The wood foot surface is lowering but weathering crust growth is taking place.

Stage began to fall after 3:30 p.m. Meanwhile, weathering crust decay occurs between 3:15 and 3:45 p.m. for the plastic foot and the wood foot exhibits the same state between 4:10 p.m. and 4:55 p.m. Stage increased again significantly between 10:10 and 10:40 p.m. (6.2 mm), coinciding with an increase in Q_M between 10:05 and 10:20 p.m. L*, Q_H and Q_E were all positive at this time. However, evening stage data cannot be analysed in detail as a result of instrument malfunction.

4.3.4. Quasi-Static Conditions (Low Melt)

The final category examined as part of this analysis is that of low melt conditions. Under these conditions, Q_M is predominantly negative and therefore no energy is available for growth or decay of the weathering crust. Thus a quasi-static condition exists where very little change occurs in the weathering crust. Air temperatures tend to be lower than for other scenarios (Table 4.7.), as do average windspeeds. These periods most closely resemble scenario (D) in the contingency table, although they are not limited to nocturnal periods. Although it might be expected that these periods are a result of lower energy inputs at the beginning and end of the melt season, they actually occur throughout July, August and early September.

Two periods are examined in greater detail within this section. The first is the afternoon of the 6th through to the 7th of September 1997 and the second is the day of July 11th 1997 (Table 4.8., Fig. 4.7.). Both periods are dominated by cold, dry weather, with minimal precipitation during the 11th, and both are closely associated with snowfalls, either the previous or following day.

Table 4.7. Five minute average summary of periods of low melt conditions

	1994	1995	1997
Global (W m^{-2})	0	37	53
K* (W m^{-2})	-4	18	33
Q* (W m^{-2})	-50	11	-21
L* (W m^{-2})	-46	-11	-54
Q_H (W m^{-2})	45	26	38
Q_E (W m^{-2})	-4	-5	-7
Q_M (W m^{-2})	-9	33	9
Air Temp (°C)	5.1	3.0	4.0
Vapour Pressure	4.44	5.62	4.72
Wind Speed (m s^{-1})	3.3	3.2	3.6
Total Ppt (mm)*	0.0	N/A	12.2
Energy Partitioning of Q_M:			
Global (%)	4	113	562
Q* (%)	538	35	-226
L* (%)	494	-34	-568
Q_H (%)	-485	79	401
Q_E (%)	47	-14	-75
K* (%)	44	54	348
$Q_H + Q_E + L^*$ (%)	56	31	-242
Surface Lowering:			
Wood (s) (mm)	0.07	0.04	0.05
Wood (l) (mm)	0.05	0.04	N/A
Water (s) (mm)	0.08	0.02	0.02
Water (l) (mm)	0.06	0.00	N/A
Plastic (s) (mm)	0.02	0.05	0.03
Plastic (l) (mm)	0.08	0.05	N/A
Potential (mm)	-0.01	0.03	0.01
R (avg plastic)	-5	1.3	3
n	168	888	2628

* total, not average

Table 4.8. A summary of selected periods of low melt

	185-86 (4-5th Jul) 1997	**192 (11th July) 1997**
Total Surface Lowering:		
Wood (s)	8.3 mm	16.5 mm
Plastic (s)	23.5 mm	0.1 mm
Potential	0.2 mm	0.3 mm
Global (Avg)	16 W m^{-2}	149 W m^{-2}
K* (Avg)	9 W m^{-2}	75 W m^{-2}
Q* (Avg)	-42 W m^{-2}	14 W m^{-2}
L* (Avg)	-42 W m^{-2}	-61 W m^{-2}
Q_H (Avg)	60 W m^{-2}	28 W m^{-2}
Q_E (Avg)	-17 W m^{-2}	-40 W m^{-2}
Q_M (Avg)	1.2 W m^{-2}	0.8 W m^{-2}
Global (Sum)	0.6 MJ	12.9 MJ
K* (Sum)	0.4 MJ	6.5 MJ
Q* (Sum)	-16.7 MJ	1.2 MJ
L* (Sum)	-1.7 MJ	-5.3 MJ
Q_H (Sum)	2.4 MJ	2.4 MJ
Q_E (Sum)	-0.7 MJ	-3.5 MJ
Q_M (Sum)	0.05 MJ	0.07 MJ
Air Temp (Avg)	5.8 °C	2.0 °C
Vapour Press (Avg)	4.84 mb	4.77 mb
Wind Speed (Avg)	4.1 m s^{-1}	5.5 m s^{-1}
Total Ppt.	0.0 mm	0.9 mm
Energy Partitioning of Q_M:		
Global	Not listed as percentages are large due to negative or very small Q_M	-18 %
Q*		73 %
L*		23 %
Q_H		-132 %
Q_E		158 %
K*		50 %
$Q_H + Q_E + L^*$		50 %

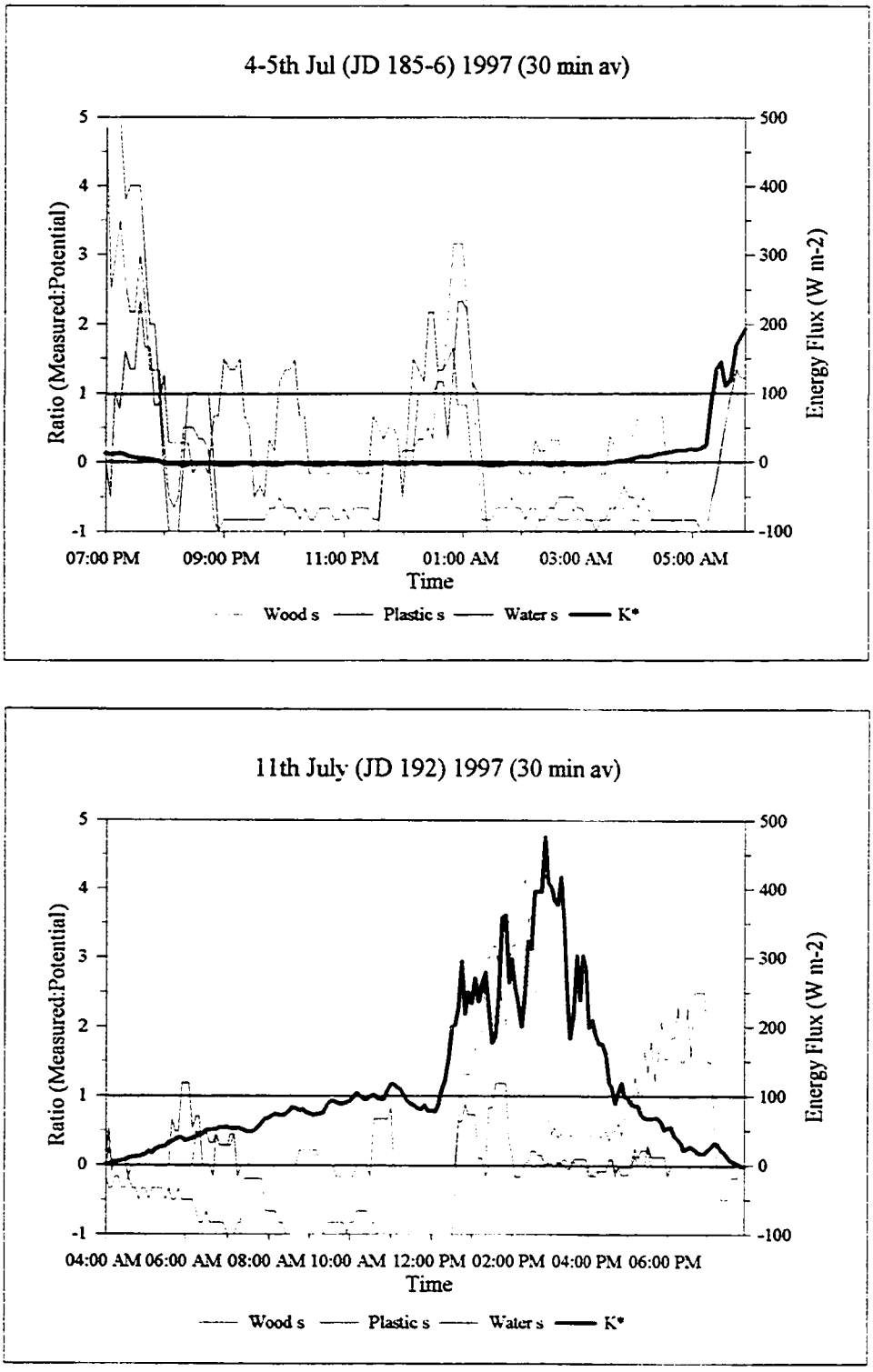

Fig. 4.7. Ratio of actual to potential surface lowering under low melt conditions: a) July 4th - 5th, 1997 (Julian Day 185 - 86); b) July 11th, 1997 (Julian Day 192)

Surface lowering for these periods was quite low, as would be expected. Lowering over the night of July 4th and 5th was 8.3 mm for the wood foot, 23.5 mm for the plastic foot and 1.2 mm for the water foot, compared to an expected lowering of 0.2 mm. On the 11th of July, surface lowering was 16.5 mm for the wood foot, 0.1 mm for the plastic foot and 0 mm for the water foot, while expected lowering was 0.3 mm. This implies that weathering crust decay occurred for the wood foot.

During the nocturnal period of the 4th and 5th of July, Q_M becomes negative at 7:40 p.m. and remains negative for most of the period. K* is positive until 8:00 p.m. The wood and plastic ablatometers demonstrate weathering crust decay at the beginning and end of this period, while the water ablatometer mainly demonstrates a ratio of zero, interspersed with five minute periods of decay. For the majority of the period the ratios are negative as a result of the negative values of Q_M.

On the 11th of July K* reached approximately 100 W m^{-2} at 10:10 a.m. and dropped below 100 W m^{-2} for the night at 5:05 p.m. Fluctuations during the day also dropped K* below 100 W m^{-2}. The only significant activity shown by any ablatometers was by the wood foot which indicated decay between 2:35 and 4:40 p.m. This began when K* was approximately 250 W m^{-2} and as previously explained, is likely to be a direct result of energy absorption by the foot and subsequent melt into the ice. It is assumed that the water foot does not exhibit the same behaviour due to the presence of water and the absence of a weathering crust which prevents melt in of the foot.

Discharge records are not available for these periods because under low melt conditions, ice layers generally formed over channels and in the weir box, freezing the float above the water level.

Fig. 4.8. Ice layers forming in channels

4.3.5. Summary

The experimental results confirm expectations of weathering crust processes. In attempting to summarise weathering crust growth and decay, it has to be recognised that it is a complex set of processes highly dependant on initial conditions as well as the amount and type of energy available for melt. When attempting to determine the processes occurring within the weathering crust, clear sky conditions are relatively simple. It is more difficult to explain how

much growth will occur under given conditions and the ratio of internal to surface melt under those conditions.

Several observations arise from this analysis of weathering crust growth. First, once K* reaches 100 W m^{-2} melt begins to occur. This due to the fact that 100 W m^{-2} approximately equals the energy needed to overcome the L* deficit. For the same reason, weathering crust growth ends once radiation energy falls below 100 W m^{-2}. However, this does not mean that once radiation energy exceeds 100 W m^{-2}, decay does not occur.

It is also demonstrated that when initial weathering crust growth is occurring, ablatometers designed to stay on the surface of the ice will not be able to detect melt, because initial melt is internal. When the density of the surface layer is sufficiently decreased, actual lowering of the surface will occur. This seems to approximately coincide with maximum melt energy amounts for the day, as on August 1st, 1994. After a period of time, an equilibrium is likely to be reached which implies a fully developed weathering crust. In the case of August 1st, this seems to have occurred by the end of the day for the wood foot. Overnight, given continued clear skies, melt is unlikely to occur and the status of the weathering crust is unlikely to change unless a very cold period is experienced when there is the possibility of re-freezing of stored melt water.

Nocturnal periods of melt and periods of low melt are also quite self explanatory. In the case of the former, if energy is available for melt it is usually provided through the sensible heat flux. Weathering crust growth cannot occur because there is no source of short-wave radiation. Therefore if melt occurs overnight, it must result in decay and this is seen in the analysis of nocturnal periods of weathering crust decay. In the case of the low melt periods, melt amounts will be limited by the limited energy available for melt. This is partially complicated by the reaction

time or lag of weathering crust processes during periods of low melt and the occurrence of mechanical collapse of the crust.

Poor weather periods during the day are the most complex regarding weathering crust processes. A source of short-wave energy exists during the day even if it is not very large, so weathering crust growth will occur. However, Q_H is usually quite a large component of the energy available for melt and can only contribute to weathering crust decay. As a result, periods of dominant growth or decay exist interspersed with transition periods. Further study is required in order to be able to determine when decay, as opposed to growth, will occur. Again, initial conditions are important because dominant decay of a fully developed weathering crust will result in large amounts of surface lowering given the same melt energy inputs as compared to a less developed, or no weathering crust, situation with higher surface layer densities. If the weathering crust is not developed at all, and decay is dominant, it would be expected that the ratio of potential to actual surface lowering approximates to one, because both actual and potential ice densities would be 0.89 kg m^{-3} x 10^3. Under field conditions, it is unlikely that this scenario will exist because internal melt will always occur during daylight hours.

Initial conditions are very important. The density of the ice at the beginning of a period will determine how quickly surface lowering will take place and how much time elapses before an equilibrium is reached. Further, surface collapse does not have to coincide with periods of expected melt. Independent of the amount and type of energy being received at the surface, collapse of the ice surface can occur when conditions are such that the ice matrix can no longer support its own weight or the weight of the ablatometer. Thus during a period of growth, an apparent period of decay may exist in the ratio of actual to potential surface lowering when in

reality it depicts a period of crustal collapse. Further, apparent surface lowering may occur under conditions that do not support melt processes. Again, this is assumed to be a result of crustal collapse which is a mechanical response rather than a melt response.

This leads to a redefinition of boundary ratio values. Initially an R value greater than one was defined as describing decay, while a ratio of less than one described growth. A ratio of one was assumed to indicate a fully developed weathering crust and a ratio of zero was assumed to indicate no melt. As a result of this analysis, further assigned ratio interpretations have to be added. First, a ratio of zero can indicate no melt and it is assumed that this is the case if Q_M is also less than zero. However, if Q_M is positive then melt must be occurring and in this situation, a ratio of zero must indicate total internal melt, which is an indication of initial weathering crust growth. Second, during a period of the ratio being equal to one, it was also noticed that K* equalled Q_H. Given this scenario, internal melt could possibly equal surface lowering without a fully developed crust existing. However, it should be noted that this was an isolated incident. An R value of one also defines periods late in nocturnal decay events when the weathering crust layer has been ablated away and the ice being melted away has a density close to 0.89 kg m^{-3} x 10^3. Finally, an R value greater than one can indicate melt of a wood foot into the ice surface, the dropping of a foot, both naturally or manually, after it has become stuck, or mechanical collapse of the ice matrix.

Lags in the system, based on stage hydrographs, appear to be between five and fifty minutes from the onset of melt as demonstrated by the ablatometers. This agrees with a study by Derikx (1975) to determine the response time of small catchments on Peyto Glacier. Using hourly measurements a lag time was not indicated by the data, suggesting that any lags in the system were less than an hour. Increases in lag time are assumed to be a result of decreased crustal densities

which increase storage in the surface layers. This increased storage also lengthens drainage times within the sub-catchments into the evening. This can be compounded by nocturnal weathering crust decay which can produce melt water through the night and will decrease the storage capacity of the weathering crust layer. Precipitation events have a very short lag time of between five and ten minutes. In these small sub-catchments precipitation events tend to supercede melt water as the driving force for changes in stage. This is assumed to be a result of decreased internal melt through the presence of cloud cover as well as the intensity of the rainfall event.

Derikx (1975) suggested that runoff delay in a subcatchment is mainly caused by travel within channels, particularly within the upper reaches where drainage channels are poorly developed. Personal observation in the field would suggest that these areas are facilitated by flow through the weathering crust. Indeed, preferential flow within the weathering crust may be initial stages of headward channel development in a catchment.

4.4. An Examination of Daily Ablation Rates

Continuing on from the above analysis, it is possible to examine differences between actual and potential surface lowering in absolute terms as well as through ratios. This section examines cumulative millimetre differences between daily actual and potential lowering at five minute intervals. This allows for estimation of the potential errors involved in short term manual ablation measurements and determination of when those errors are greatest (Fig. 4.9.).

It is apparent from Fig. 4.9 (a) and (b) that a diurnal cycle exists during periods of weathering crust growth. In the very early morning a negative (falling) or a flat (no change) limb tends to exist. The falling limb demonstrates a period where measured surface lowering is greater

than potential surface lowering, indicating weathering crust decay. As the morning continues, a positive (rising limb) occurs where measured surface lowering is less than potential and weathering crust growth is occurring. At the end of the day another falling (or flat) limb exists, again indicating weathering crust decay (or no change). It can be seen that the plastic foot tends to show a greater difference than the other two feet. This would be expected because the foot is assumed to rest on the surface, and therefore most accurately demonstrates the difference in lowering caused by internal melt.

The strength of the trend varies, as can be seen from July 28th, where the pattern has a very small magnitude. It is probable that this period demonstrates a fully developed weathering crust, where an equilibrium exists between surface lowering and internal melt. This is supported by the results from the wood foot ratio for this period, which approximates one.

a)

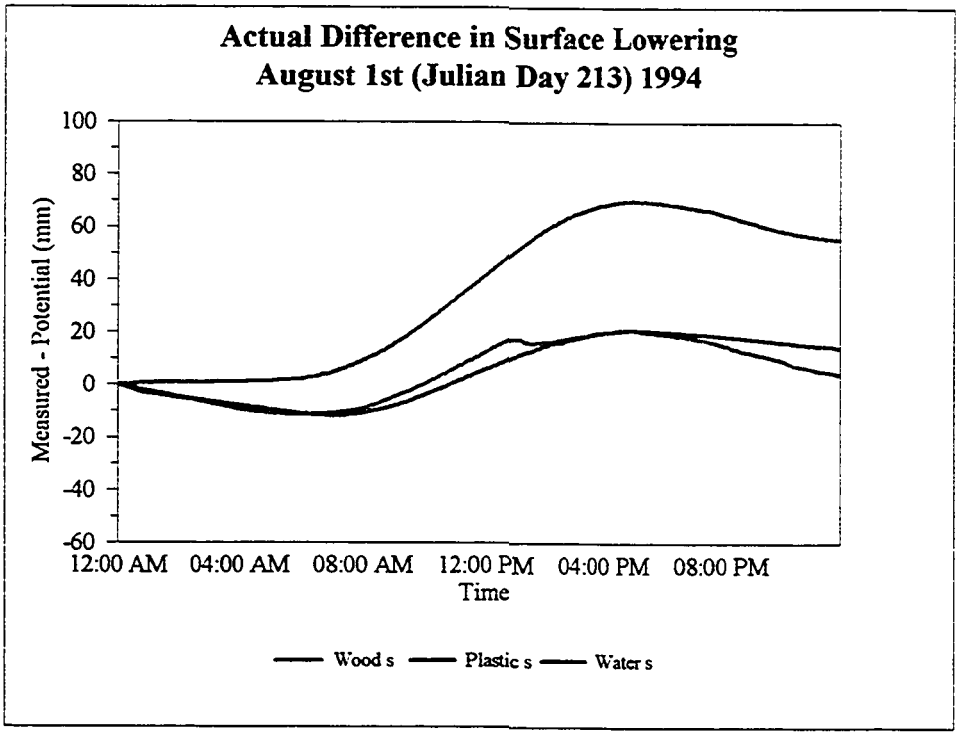

b)

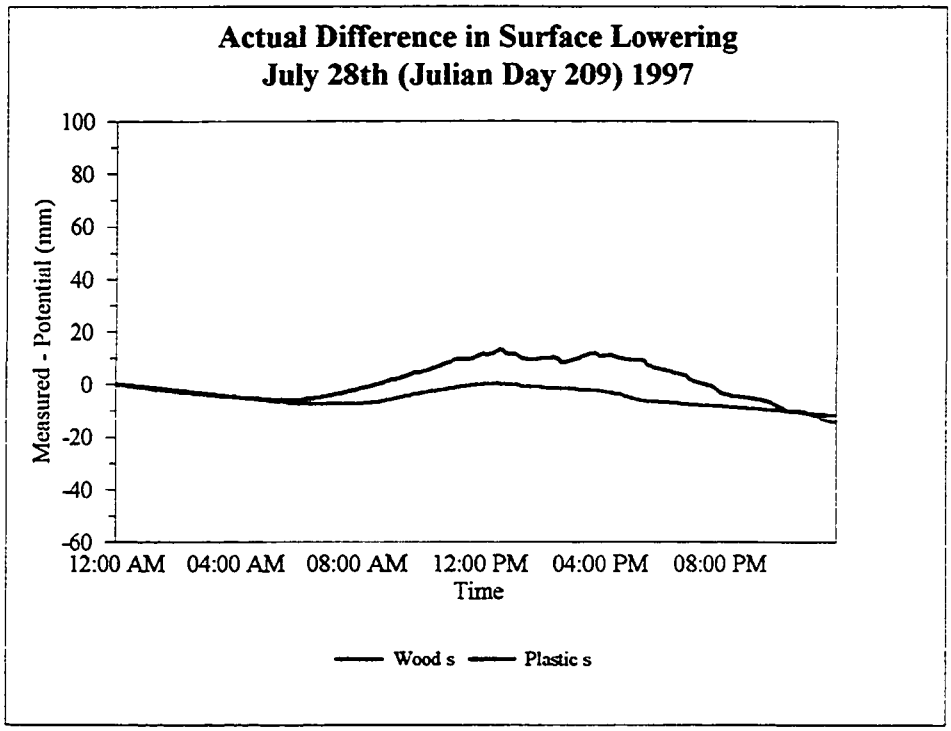
Actual Difference in Surface Lowering
July 28th (Julian Day 209) 1997
Measured - Potential (mm)
100
80
60
40
20
0
-20
-40
-60
12:00 AM
04:00 AM
08:00 AM
12:00 PM
04:00 PM
08:00 PM
Time
Wood s
Plastic s

c)

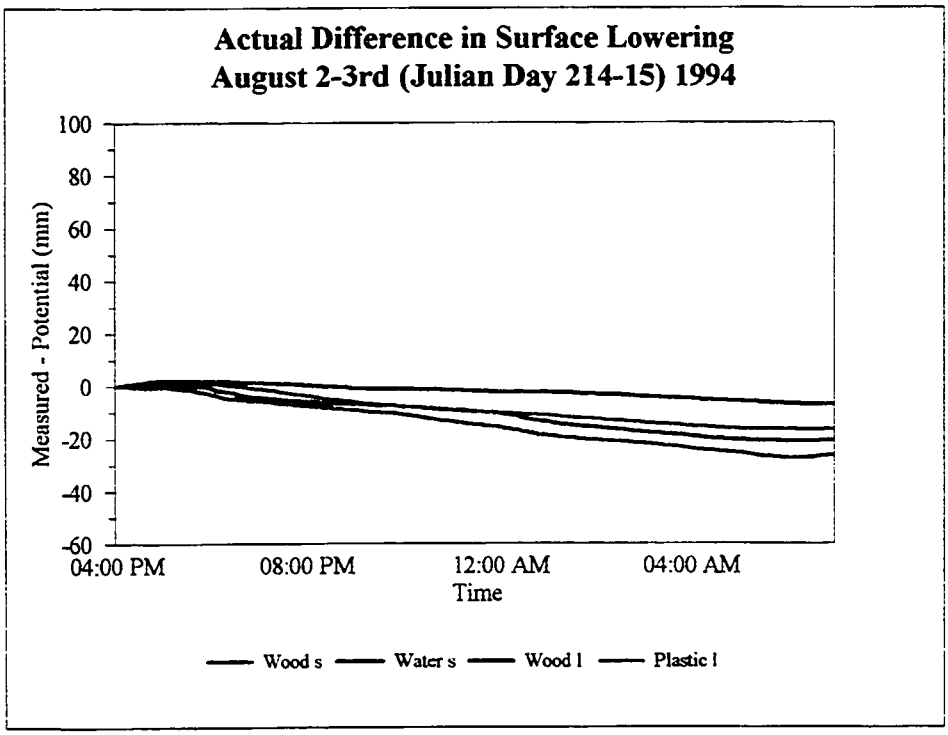
Actual Difference in Surface Lowering
August 2-3rd (Julian Day 214-15) 1994
Measured - Potential (mm)
100
80
60
40
20
0
-20
-40
-60
04:00 PM
08:00 PM
12:00 AM
04:00 AM
Time
Wood s
Water s
Wood l
Plastic l

d)

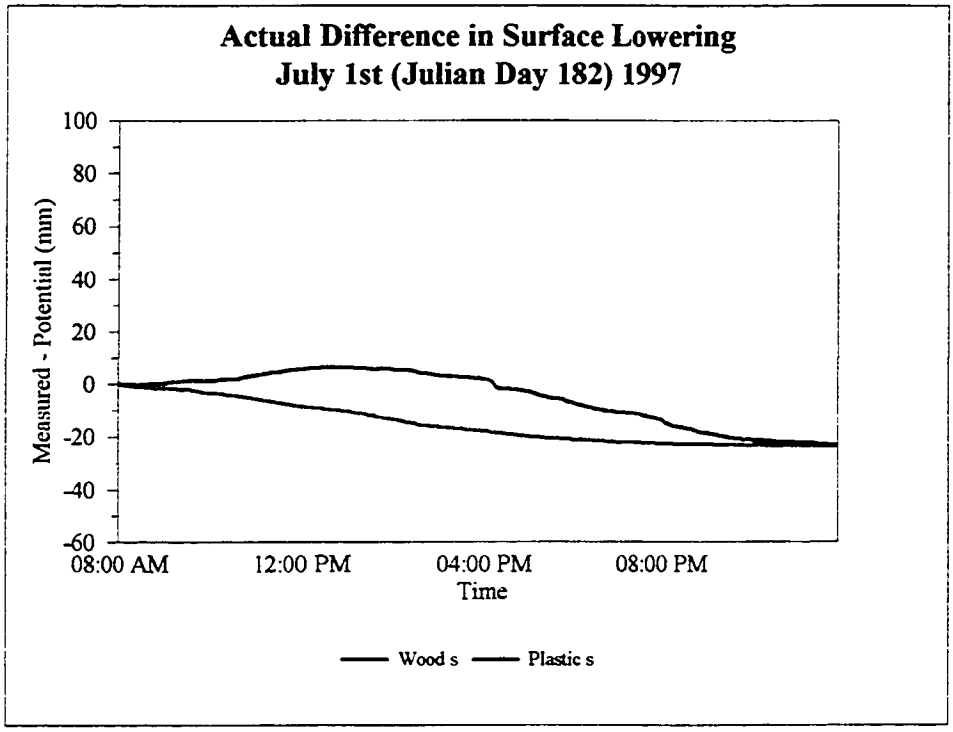
Actual Difference in Surface Lowering
July 1st (Julian Day 182) 1997
Measured - Potential (mm)
100
80
60
40
20
0
-20
-40
-60
08:00 AM
12:00 PM
04:00 PM
08:00 PM
Time
Wood s
Plastic s

e)

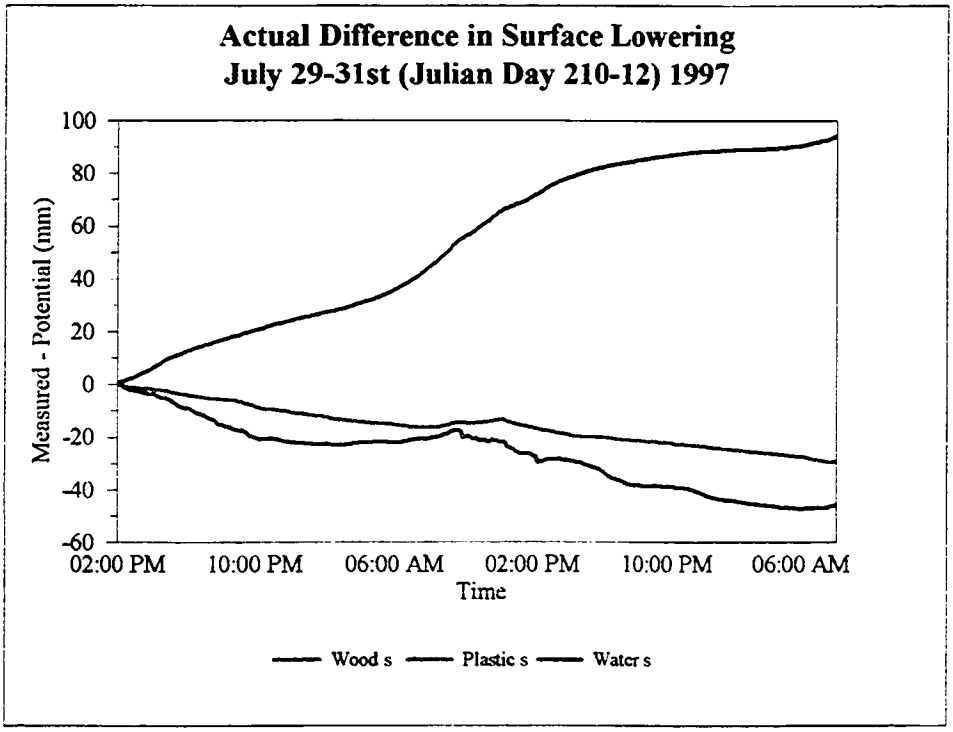
Actual Difference in Surface Lowering
July 29-31st (Julian Day 210-12) 1997
Measured - Potential (mm)
100
80
60
40
20
0
-20
-40
-60
02:00 PM
10:00 PM
06:00 AM
02:00 PM
10:00 PM
06:00 AM
Time
Wood s
Plastic s
Water s

f)

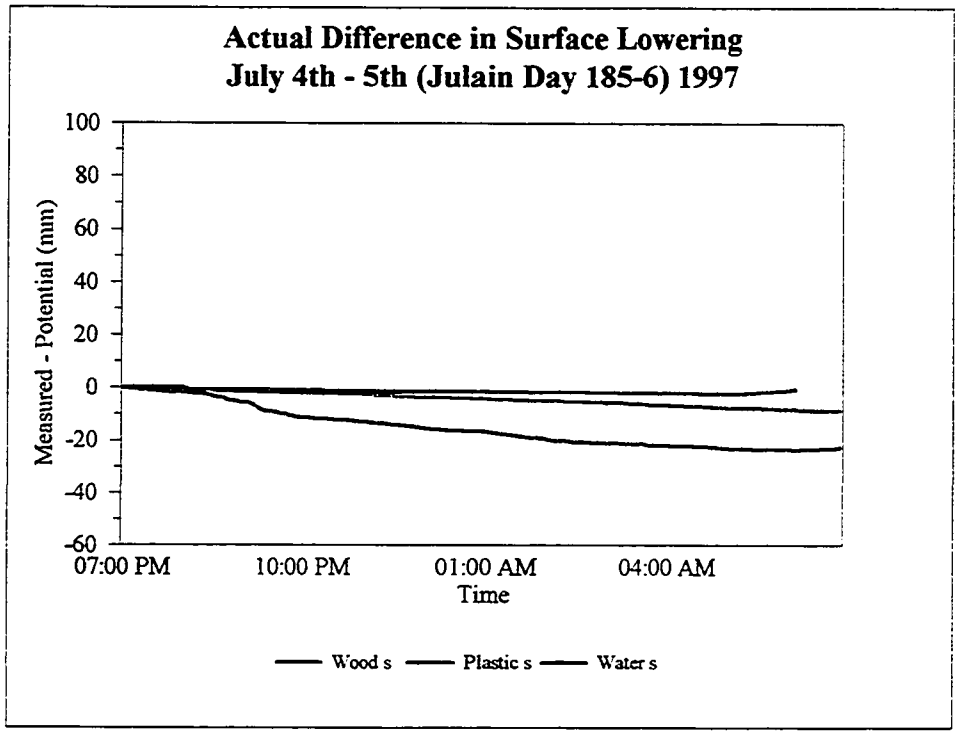

g)

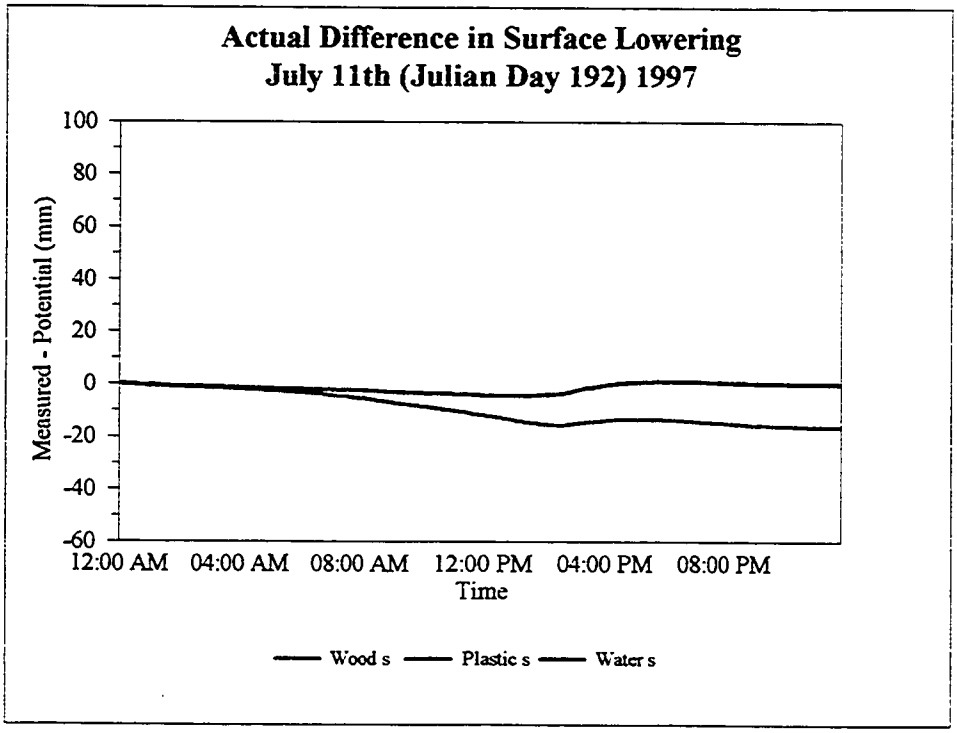

Fig. 4.9. Millimetre differences between measured and potential surface lowering a) August 1st, 1994(Julian Day 213); b) July 28th, 1997 (Julian Day 209); c) August 2nd- 3rd, 1994 (Julian Day 214-15); d) July 1st, 1997 (Julian Day 182); e) July 29th-31st, 1997 (Julian Day 210-12); f) July 4th-5th, 1997 (Julian Day 185-86); g) July 11th, 1997 (Julian Day 192)

The daytime and nocturnal decay periods appear to demonstrate the same diurnal pattern, although at a smaller magnitude which is presumably due to lower total melt rates. For July 1st and August 2nd and 3rd the wood foot just follows a falling trend indicating that the measured is greater than potential and decay is occurring for the whole period. The plastic foot, on the other hand, does indicate weathering crust growth in the late morning and early afternoon of July 1st. Again, this can be explained through different properties of the feet, the plastic foot resting on the surface and most accurately describing weathering crust processes, while the wood foot melts into the ice. During the period July 29th to 31st both feet on the ice demonstrate a very small rise indicating weathering crust growth in the middle of the day. The water foot in this example shows very little surface lowering for the entire period, even though melt is occurring, which explains why the difference continues to increase throughout the period. When surface lowering values are low or zero, the line plotted approximates or equals the inverse of potential lowering during that period.

July 11th 1997, a period of low melt conditions, indicates a very subdued pattern with the identical differences for the water foot and the plastic foot. The wood foot shows greater decay through the morning than the other two feet. Enhanced surface lowering is a result of melt in of the foot due to its enhanced thermal properties.

These results indicate that some error could exist when using short term surface lowering measurements if they are not taken at the same time of day or close to mid-day when differences are likely to be greatest. It can also be seen that differences do not reconcile themselves, at least over the period of a day, particularly in the case of the plastic foot, even though it might be expected that differences between measured and potential surface lowering would cancel themselves out over quite short time periods. It is possible that a combination of different weather

types might extend or shorten this period. An example of a continuous period demonstrates how cumulative differences can increase and decrease over time (Fig. 4.10). Although a reconciliation between measured and potential lowering does not occur within this time period, the fact that models of melt and runoff over whole melt seasons are quite accurate seems to suggest that differences do reconcile themselves eventually.

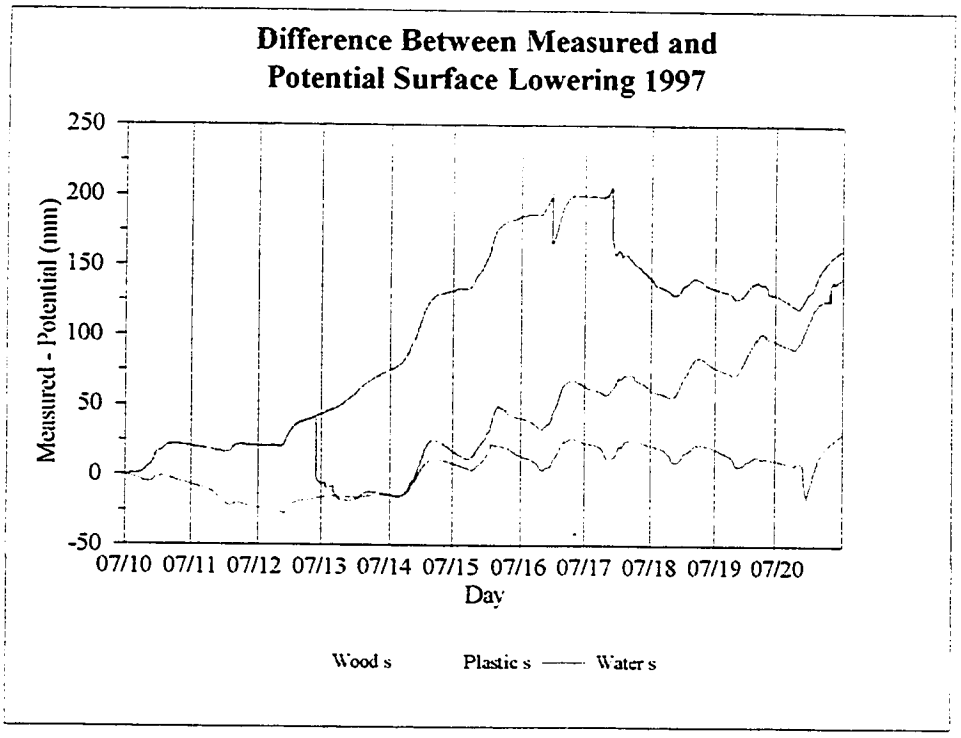

Fig. 4.10. Continuous difference measurements for July 10th-20th (Julian Day 191 - 201) 1997

These plots of actual difference between measured and potential surface lowering further indicate weathering crust processes and demonstrate the diurnal cycle as well as the daily progression of weathering crust growth and decay. They also indicate that in the middle of the day,

particularly during periods of strong weathering crust growth, large differences exist between actual melt and surface lowering measurements.

4.5. An Examination of Ice Densities

The ratio of measured to potential surface lowering that defines weathering crust growth or decay is based on an assumed density of 0.89 kg m^{-3} x 10^3. However, a constant density of 0.89 kg m^{-3} x 10^3 cannot exist if internal melt is occurring. Weathering crust growth was approximated over a 1 m^2 area of ice in an attempt to explore variations in ice density with depth. Initially it was assumed that the weathering crust was 20 cm deep, according to the literature. Only 30 % of K↓ penetrates to this depth below the ice surface. Using average daily Q_M values for selected growth periods, the volume of ice after melt had occurred was calculated. The ratio of this volume to the original volume was calculated to produce a percentage density that can be applied to an assumed density of 0.89 kg m^{-3} x 10^3. This results in a calculated density value reflecting weathering crust growth (Table 4.9.).

Table 4.9. Initial ice density calculations for periods of weathering crust growth

Day	Q_M Avg (W m^{-2})	Day Length (hr)	Original Ice Volume (cm^3)	Melt* (cm^3)	Final Ice Volume (cm^3)	Density %†	Density (kg m^{-3} x 10^3)
1/8/94	432	13	200 000	60 586	139 414	0.7	0.62
14/8/94	549	9	200 000	53 304	146 696	0.73	0.65
28/7/97	340	12	200 000	44 016	155 984	0.78	0.69

*Q_M /333.7*300*12*day length;†final / original;

The results for August 1st, based simply on the internal melt that had occurred, resulted in an ice density of 0.6 kg m^{-3} x 10^3 (section 4.3.1.). As can be seen from the calculations above, the

density is comparable at 0.62 kg m^{-3} x 10^3. The results for July 28th 1997 are not similar to densities based on internal melt. Surface lowering measurements suggest a density of 0.87 kg m^{-3} x 10^3 compared to the above value of 0.69 kg m^{-3} x 10^3. The reason for the discrepancy is the prior existence of a weathering crust. The enhanced lowering of the plastic foot is likely to be a result of crustal collapse.

Improving on this method, an attempt was made to distribute the results over depth and time. A similar technique was used on the same periods of weathering crust growth but average hourly values of Q_M replaced the daily average. These were used to calculate hourly melt over 2 cm depths. Every hour, a new 2 cm ice volume was made available for melt, by adding it to the final volume after melt from the previous time interval. Q_M was applied to the entire new volume and an ice density was calculated for the time period using the ratio of the final volume after melt to the original volume. These results demonstrated an increase in density over the period of melt because they do not account for internal melt below the depth integrated each hour. It is assumed that every new 2 cm depth is at 0.89 kg m^{-3} x 10^3. This is obviously not the case in the field and the results reflected this. Densities increase because, as the energy available for melt is decreasing, the volume of ice affected by this melt is increasing. These results led to a final attempt to reproduce ice densities as they result from weathering crust processes over depth and time.

4.5.1. A Simulation of Expected Ice Densities from Weathering Crust Processes

As a final method to analyse ice densities and their variation over time as a result of weathering crust processes, a physically-based simulation was produced which calculates densities at six ice depths in five minute intervals. A column of ice with a surface area of 1 m^2 is broken

down into units of increasing thickness, beginning with a 1cm thick layer and doubling the thickness of each subsequent layer. Thus level one (L_1) is 1 cm thick, level 2 (L_2) is 2 cm thick, level 3 (L_3) is 4 cm thick, level 4 (L_4) is 8 cm thick, level 5 (L_5) is 16 cm thick and level 6 (L_6) is 32 cm thick, for a total column depth of 63 cm, at which level 2.3 % of K↓ is received. It is assumed that beneath this column is a layer of ice, of infinite depth, with a density of 0.89 kg m^{-3} x 10^5. The model uses five minute energy inputs, as measured in the field, to drive melt.

K* is used to drive internal melt through use of the exponential decay of solar energy with depth for all layers ($L_1..L_6$) resulting in $K^*_{1..6}$ W m^{-2} 5 min^{-1} as energy inputs (Q_{Mi}) for the respective layers (according to Beers Law):

$$K^*_n = (K^* e^{-a^* z_u} - K^* e^{-a^* z_l}) * \Delta t \qquad (4.2.)$$

in which n is the layer number; z_u is the upper boundary of that layer; z_l is the lower boundary; a is the extinction coefficient for K* at depth z (a = 0.006 m (Geiger, 1965; pg.207)); and Δt is a conversion factor (300 seconds).

Q_H, L* and Q_E are used to calculate energy inputs for ablation or surface lowering (Q_{Ma}) of the topmost layer (L_1):

$$Q_{Ma} = L^* + Q_H + Q_E \qquad (4.3.)$$

Using these energy inputs, the mass of melt is calculated at each level:

$$Mi = \left(\frac{Q_{Mi}}{\rho^* L_f} \right) \qquad (4.4.)$$

$$Ma = \left(\frac{Q_{Ma}}{\rho^* L_f} \right) \qquad (4.5.)$$

where ρ is ice density of the layer at the beginning of the time interval; and L_f is the latent heat of fusion (333.7 J g^{-1} at 0 °C).

Total melt mass (M) at L_1 is equal to $M_a + M_i$ and at all other levels M is equal to M_i. These melt masses then become inputs for density calculations at each level. At time interval T_1 after melt has occurred there is a density ρ_1 at depth L_1, ρ_2 at depth L_2 to ρ_n at depth L_n. Densities are calculated as:

$$\rho_n = \frac{M_o - M_a - M_i}{V_o - V_a} \qquad (4.6.a.)$$

where $n = L_1$, and

$$\rho_n = \frac{M_o - M_i}{V_o} \qquad (4.6.b.)$$

where $n = L_{2..6}$

in which, M_o is the original mass of ice (before melt); M_a is the mass of ice lost through surface lowering; Mi is the mass of ice lost through internal melt; Vo is the original volume of ice (constant at 10 000 cm^{-3} for L_1, 20 000 cm^{-3} for L_2, 40 000 cm^{-3} for L_3, 80 000 cm^{-3} for L_4, 160 000 cm^{-3} for L_5 and 320 000 cm^{-3} for L_6); and Va is the volume of ice mass lost through ablation:

$$V_a = \frac{M_a}{\rho} \qquad (4.7)$$

wherein ρ is ice density at the beginning of the time period.

The ice column retains its thickness layers from one time period to the next. Therefore as ablation lowers the surface layer, the residual mass has to be replenished by the volume of ice loss (Va) from L_2 which is then replenished from L_3 and so on until L_6 is replenished with ice at 0.89 kg m^{-3} x 10^3 density. This replenishment occurs before melt is allowed to occur at the next time interval and provides a new ice mass (M_n):

$$M_n = \rho_n(V_{on} - V_a) + \rho_{n+1}V_a \qquad (4.8.)$$

This mass is used to calculate an input density for the next time interval and this density is used in the calculations of M_s, M_i and V_a for that time period.

Dividing equation (4.8.) by volume:

$$\frac{M_n}{V_n} = \frac{\rho_n(V_{on} - V_a) + \rho_{n+1}V_a}{V_n} \qquad (4.9.)$$

Equation (4.9.) can be simplified as:

$$\rho_n = \rho_n(1 - \frac{V_a}{V_n}) + \rho_{n+1}\frac{V_a}{V_n} \qquad (4.10.)$$

Equation (4.10.) has a limiting case when M_s, and therefore V_a is equal to zero. In this situation, internal melt is occurring at all layers but there is no replenishment allowed for in the simulation unless ablation is occurring at the same time. Thus:

$$M_n = \rho_n V_n \qquad (4.11.)$$

This equation will collapse as further internal melt occurs and density values will eventually become negative, simulating the depletion of the surface layer through internal melt. Therefore, a condition is generated where:

$$\rho_n = \rho_{n+1} \tag{4.12}$$

When K^*_1 is positive but Q_{M_2} is negative, the surface layer will be replenished from subsequent layers when necessary. Under these conditions K^*_1 is calculated as in equation (4.2.) but instead of the input being K* it becomes $K^* + Q_H + L^* + Q_E$ to account for energy loss from the surface. This reduces internal melt in the topmost layer of ice but allows internal melt of the other layers to continue as usual. Crustal collapse is invoked when ice density at the end of a time period has a density less than or equal to 0 kg m^{-3} x 10^3 and the surface layer is allowed to be replenished from lower layers. This replenishment is calculated in the following manner:

$$M_{on} = \rho_n(V_o - 10000) + (10000 * \rho_{n+1}) \tag{4.13.}$$

This forms the basis of the initial simulation produced to calculate ice densities at five minute intervals and increasing depth beneath the ice surface, given the effects of weathering crust processes. The simulation is initialised with an ice density of 0.89 kg m^{-3} x 10^3.

The results from this simulation (Fig. 4.11.) are encouraging because even though density measurements do not exist to corroborate the model, it performs in a physically plausible manner. Before discussing the results it should be emphasised that initial crustal conditions have been forced equal to 0.89 kg m^{-3} x 10^3 which does not account for the effects of previous weathering crust processes.

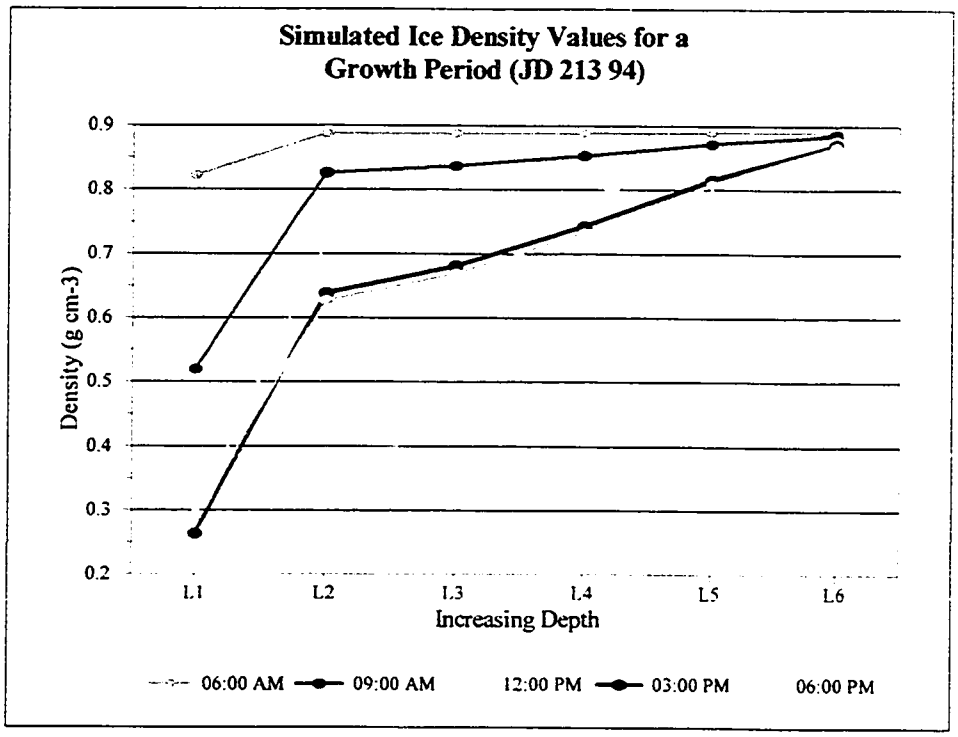

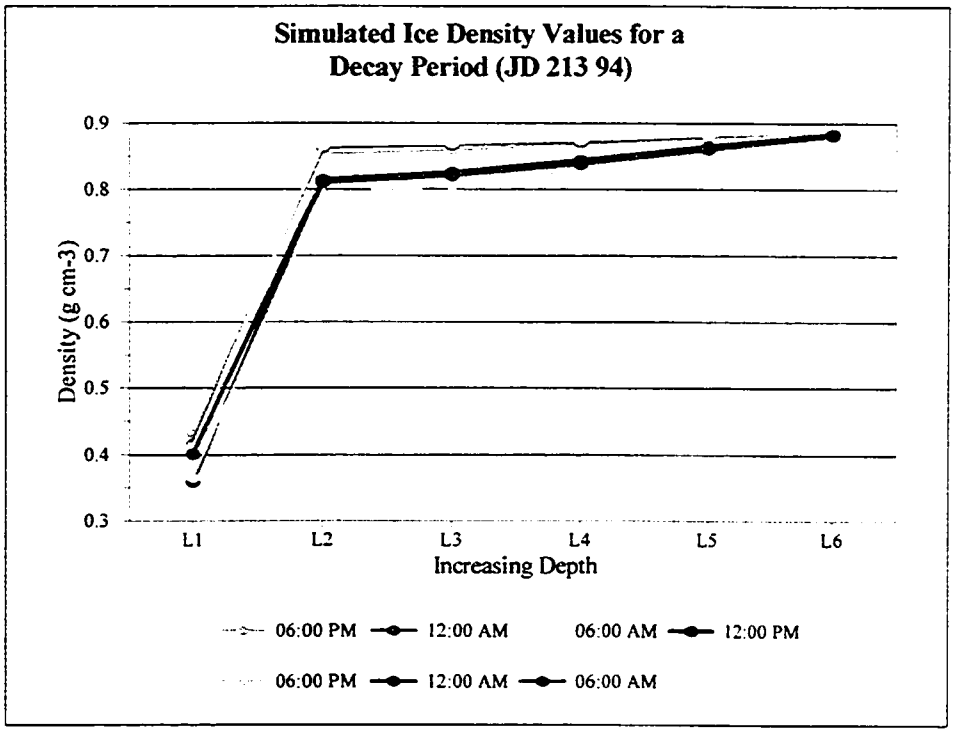

Fig. 4.11. Simulation output results for a) a period of weathering crust growth; and b) a period of weathering crust decay

During a period of weathering crust growth the model suggests that surface densities decrease fairly rapidly in the early part of the day and then level off in the afternoon before beginning to increase again into the evening. This conforms to measurements in the field which suggest that internal melt is greatest early in the day and then, as densities reach a critical point, lowering or collapse of the crust begins. This would maintain a fairly uniform density layer as the simulation predicts. Deeper layers show a similar, but more muted, pattern with the deepest layer demonstrating very little change in density through the period. Again this fits expectations because it is assumed in the field that the weathering crust is underlain by ice at a density of 0.89 kg m^{-3} x 10^3. The depth of this weathering crust is slightly greater in the model than suggested from the literature.

Modelled densities for a period of weathering crust decay (Fig. 4.11.b.) demonstrate little variation in density through time. Internal melt occurs at the beginning of the period but does not affect lower levels in the ice column. Densities may increase slightly overnight which would be expected if the top layer is ablating away, but they do not change as much as might be expected. During the day decay and growth are obviously quite balanced because density does not decrease very much as a result of internal melt, which would suggest that ablation is wasting away the lower density ice as it develops.

Although weathering crust densities appear to be simulated quite accurately, based on expectations derived from observations and data gathered in the field, it does not deal with a negative energy budget and the effect that this might have on density values. The method assumes that if energy available for melt is less than zero, no melt will occur and therefore densities will not change. This is unlikely to be the case under real conditions. Re-freezing of liquid water from previous melt is likely to occur, increasing ice densities.

The simulation was altered to reflect re-freezing of melt water by imposing three assumptions. First, liquid water is present at all times for re-freezing to occur. Second, liquid water is not stored in the top layer of ice so any re-freezing begins at L_2. Third, water is re-frozen at a density of 0.89 kg m^{-3} x 10^3. This method freezes an amount of water calculated from the amount of negative energy available. This is converted into a mass and added to the existing ice mass in the layer and then converted to a new bulk density. Once the density of a layer being re-frozen reaches 0.89 kg m^{-3} x 10^3, re-freezing occurs in the subsequent layer.

This new approach was used to simulate the same periods as in the initial model. Identical density results were produced by both methods for the weathering crust growth period and decay period. This was expected because neither types encompass periods of a negative energy budget (by definition). Both simulation approaches were then used to calculate ice densities for a continuous data period encompassing Julian Day 214 to 226 (August 2nd to 14th) 1997 (Fig. 4.12.) and melt under low melt conditions (Fig. 4.13.).

The continuous data period encompasses all types of weathering crust processes. The simulations recreate priming of lower surface layers during periods of internal melt with a negative Q_{M2} surface budget. Even though the surface layer has a negative energy budget and therefore melt cannot occur, the lower layers still receive solar radiation, which results in internal melt. As a result, the density of L_2 can become lower than that of L_1 until the energy balance of L_1 becomes positive. Then, the density of L_1 quickly falls below that of L_2. This phenomenon is a direct result of long-wave radiation being lost from the ice surface and not from within a volume, and is clearly seen on three occasions during the above period, when the density of L_2 is less than L_1 in the morning before the surface layer has overcome this deficit. It is known as the solid state

greenhouse effect (Brandt and Warren, 1993) and results in short-wave heating at depth and long-wave cooling at the surface.

Greater variations in density are also demonstrated for the lower layers in this longer period of simulation. This emphasises the importance of initial conditions on ice densities as a result of weathering crust processes. As can be seen, both methods produce similar results (Fig. 4.12.). The effect of re-freezing on density values is to increase densities within the lower layers, as would be expected, but the mass gains from re-freezing are minimal. The greatest effect is the reduction of the thickness of the weathering crust layer, with densities in L_6 for the simulation with refreezing remaining close to 0.89 kg m^{-3} x 10^3. Temperate glaciers are assumed to have an ice surface temperature of 0 °C throughout the melt season and so re-freezing should be negligible.

The simulations were altered slightly for this longer period of calculation by constraining crustal collapse to a density of 0.1 kg m^{-3} x 10^3 rather than to 0 kg m^{-3} x 10^3. The reason for this alteration is that a density of less than 0.1 kg m^{-3} x 10^3 can be reduced to a negative density within a five minute melt period. This does not create problems on small time scales, when initial conditions are forced to 0.89 kg m^{-3} x 10^3, but it can result in unrealistic negative density values at larger time scales, when early morning densities later in the simulation are lower than 0.89 kg m^{-3} x 10^3.

Simulation of a period of low melt by each of the methods also produce almost identical density values throughout the period, with the exception of the lowest layer which remains close to 0.89 kg m^{-3} x 10^3 in the re-freezing simulation (Fig. 4.13.).

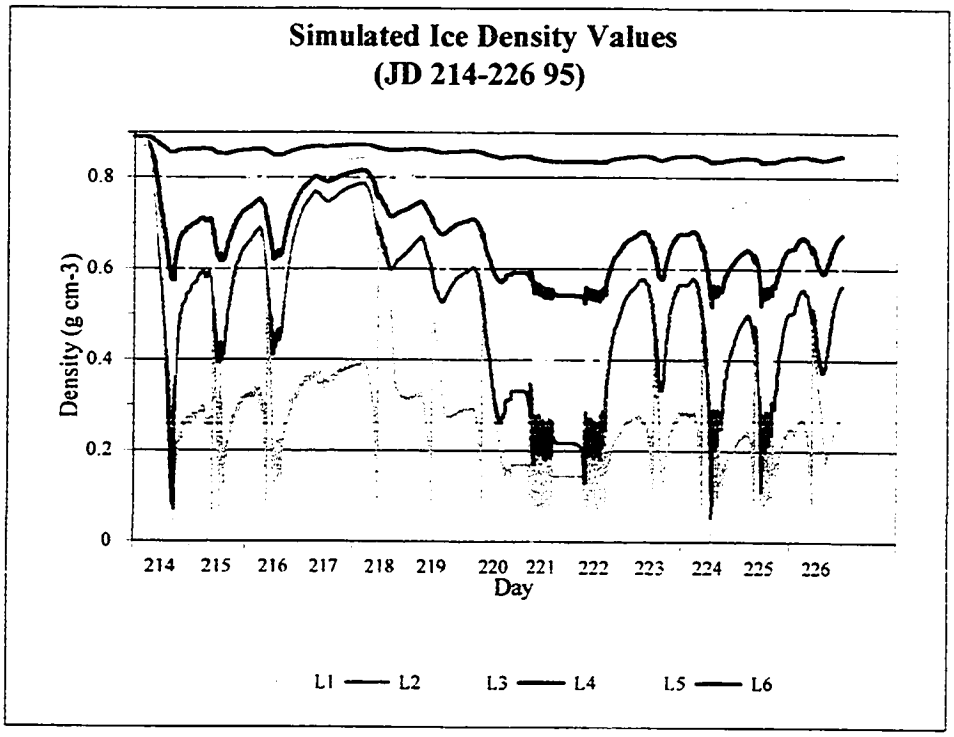

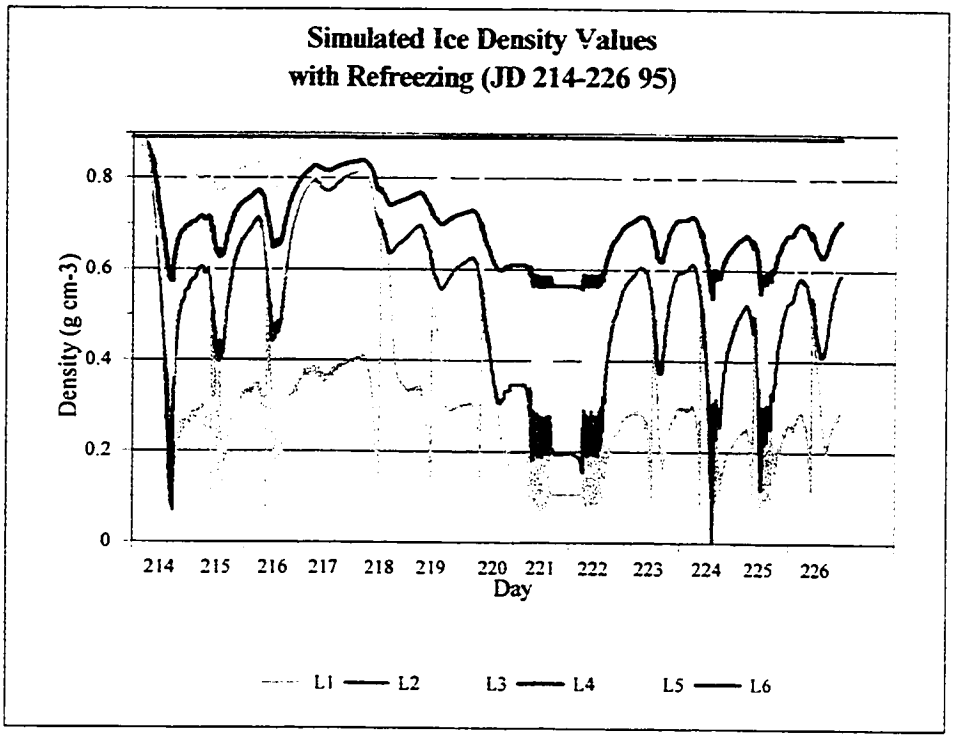

Fig. 4.12. A comparison of outputs from a) method one and b) method two for a continuous data period

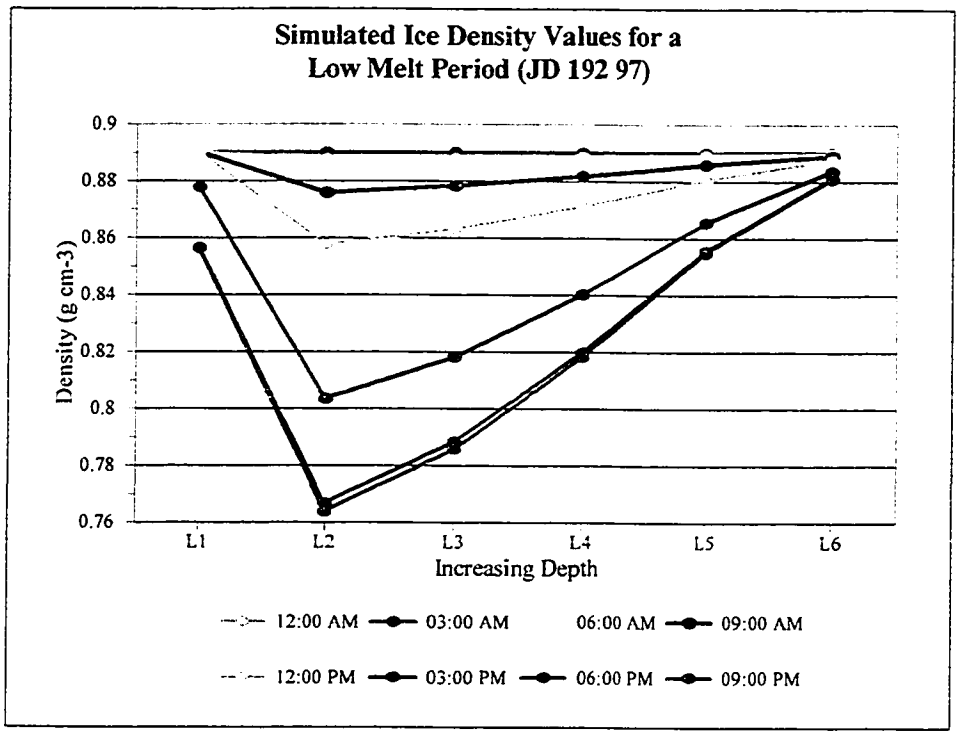

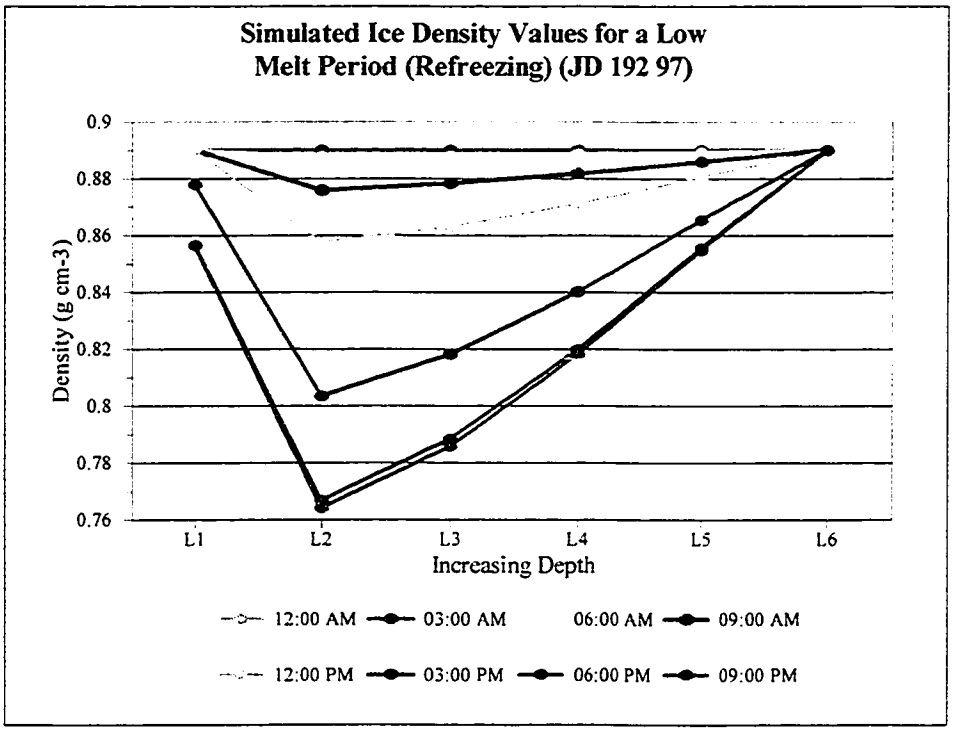

Fig. 4.13. A comparison of outputs from a) method one and b) method two for a period of low melt

The performance of each of the models was further examined in comparison to manual measurements (Table 4.10.). Two runs were made under each of the simulations. In the first run, densities were forced to 0.42 kg m^{-3} x 10^3 at 11:45 a.m. in the upper two layers. For the second run ice densities were initialised at 0.89 kg m^{-3} x 10^3 at 12 a.m. on September 2nd.

Before discussing density values from the different methods it should be noted that the manual density measurement is not a very accurate measurement technique because it is difficult to obtain a uniform core of ice and the cores have to be taken at different locations due to the destructive nature of the method, encompassing local spatial variations in the results. Both simulations produce almost identical densities for both data runs. Slight differences in densities exhibit themselves in the lower layers, so the deeper the ice core depth, the more likely that differences will exist between the two methods. Core depths greater than 3 cm include ice from L_3 and this explains the apparent increase in density in both manual measurements and simulations at times when they would be expected to be decreasing as a result of weathering crust growth. At 7:25 a.m., on September 3rd, the recorded manual density is 0.74 kg m^{-3} x 10^3 while the first run simulations (a) provide a density of 0.72 kg m^{-3} x 10^3. Even though the densities do not coincide on an hourly basis, the simulations obviously recreate similar conditions overnight, in the upper layers, to approximate initial conditions in the field. Apart from 7:25 a.m., simulated densities do not match measured densities until 1:15 p.m. on the 3rd when measured density is 0.64 kg m^{-3} x 10^3 and simulated density is 0.66 kg m^{-3} x 10^3. However, they do approximate the increases and decreases in density.

Density values from the second run of the simulations (b) are higher than the first run early on the 2nd. After this, they are lower because the second run allows for a longer period of energy inputs. As a result, surface density values are lower than for the first run while the lower layers

are more dense than for the first run. This suggests that a weathering crust layer existed prior to this time period, explaining the less dense subsurface layers. The underestimation of the surface layer density in the first run is likely to be a result of the average density used to initiate the simulation.

Table 4.10. Model simulations compared to manual density measurements

Day	Time	Simulation 1 (kg m^{-3} x 10^3)		Simulation 2 (kg m^{-3} x 10^3)		Manual Density (kg m^{-3} x 10^3)	Depth (cm)
		a	b	a	b		
2/9	11:45 AM	0.48	*0.64*	0.48	*0.64*	**0.42**	3.5
	12:40 PM	0.6	*0.66*	0.6	*0.66*	**0.66**	4.5
	01:40 PM	0.7	*0.67*	0.7	*0.67*	**0.63**	5.5
	02:40 PM	0.71	*0.66*	0.71	*0.66*	**0.57**	4.5
	3:05 PM	0.75	*0.69*	0.75	*0.69*	**0.58**	6
3/9	07:25 AM	0.72	*0.68*	0.72	*0.68*	**0.74**	3.5
	08:10 AM	0.61	*0.57*	0.61	*0.57*	**0.41**	2
	09:05 AM	0.68	*0.64*	0.69	*0.64*	**0.62**	3.5
	10:05 AM	0.63	*0.59*	0.63	*0.59*	**0.55**	3
	11:10 AM	0.61	*0.67*	0.61	*0.67*	**0.35**	7.5
	12:00 PM	0.64	*0.6*	0.64	*0.6*	**0.71**	4.5
	1:15 PM	0.66	*0.62*	0.66	*0.62*	**0.64**	5
	2:15 PM	0.68	*0.64*	0.68	*0.64*	**0.85**	6.5
	3:10 PM	0.67	*0.64*	0.67	*0.64*	**0.79**	5.5
	3:50 PM	0.65	*0.62*	0.65	*0.63*	**0.49**	4.5
RMS Error		0.14	*0.15*	0.14	*0.15*		

a - density L_1 and L_2 set at 0.42 kg m^{-3} x 10^3 at 11:45 AM

b - density 0.89 kg m^{-3} x 10^3 at 12:00 AM

4.6. Summary

Weathering crust processes are complex and driven by the type of energy contributing to Q_M. Short-wave energy produces internal melt while the long-wave and turbulent heat fluxes produce surface melt. When the contribution of energy is from one source (clear sky days with a negative Q_{Ma} at the surface or nocturnal periods with a positive Q_M), the weathering crust processes occurring are distinct. However, when a combination of both energy types contribute to Q_M the resultant combination of processes is difficult to determine.

Qualitative results from the field demonstrate the high variability of weathering crust characteristics over space and time. The ice surface layer termed the weathering crust is not simply a result of weathering crust processes, although these play a major role. It is also a result of other factors including cryoconitic melt, melt water flow and crystal size, shape and orientation.

This chapter has demonstrated weathering crust processes occurring in the field through the use of the measured to potential surface lowering ratio and has used examples of these processes to further examine energy inputs associated with these periods at five minute intervals. This examination of processes in the field indicates that, under intensive weathering crust growth conditions, melt is solely internal early in the morning if initial formation of the weathering crust is slight. Surface lowering does not commence until the ice surface density has decreased significantly. Thus, even if an ablatometer is measuring no melt, significant melt water generation can be occurring. Under daytime decay periods, the most complex combination of processes occurs. Lowering of the surface layer and internal melt are simultaneous and densities are likely to remain stable as newly melted internal ice is ablated away. In the presence of thick cloud cover densities may even increase as the surface lowering component becomes more significant than the internal melt component.

Further analysis of the effect of weathering crust processes demonstrated a diurnal pattern in the discrepancy between actual and potential surface lowering that was greatest around mid-day under strong weathering crust growth conditions. This has implications for surface lowering measurements, particularly on a diurnal scale, as a surrogate for melt outputs. Although there is no evidence from the field data collected, it is assumed that these errors compensate over time. However, there is an indication from the field data that this could be a period exceeding ten to twelve days, depending on weather conditions.

Finally, an attempt was made in this section to approximate ice densities over depth and time which may occur as a result of weathering crust processes. Although data are not available from the field to assess the accuracy of these simulations, it would appear as though simulation of ice densities is quite accurate with respect to analysis undertaken on the weathering crust phenomenon, observations in the field and scientific expectations. It is interesting that when negative energy is given an opportunity to re-freeze melt water within the crust, densities are not significantly different to when no change in state is imposed.

5.1. Summary

This thesis presents an overview of the surface of a glacier as an interface between the energy balance and the hydrology of the glacier. It concentrates on weathering crust processes at small spatial and temporal scales, examining the processes and circumstances leading to growth and decay over time during the melt period in order to better understand the phenomenon. The thesis began with an introduction into the study and an overview of the components of the energy balance that pertain to surface melt and the weathering crust phenomenon. Data used to describe and explain the weathering crust phenomenon were collected on the Peyto Glacier, Alberta during the melt seasons of 1994, 1995 and 1997.

The data collection and analysis presented in this thesis demonstrates the most detailed study of the weathering crust phenomenon to date. It provides both quantitative and qualitative descriptions of weathering crust processes; possible impacts of the weathering crust on the accuracy of surface lowering measurements as a surrogate for total ice ablation; an examination of probable lags within the system as a result of the weathering crust; and a method for simulating densities over time and depth as a surrogate for actual measurements which cannot be made easily in the field at the present time.

It was anticipated that weathering crust processes and their effects would approximate to a microcosm of larger scale glacial drainage processes, with preferential flow paths, storage features and varying lag times. It was further anticipated that its inclusion within hydrological modelling of glacier surface melt would increase the accuracy of modelled melt water generation and in particular surface lowering at small time scales. Finally, the information gathered from this

analysis was used to produce a simulation of ice densities over depth and time based on energy inputs measured in the field. The conclusions drawn from these analyses are presented, along with recommendations for further work, in the following sections.

5.2. Conclusions

Weathering crust development is the result of two processes - growth and decay. The growth component is driven by K* which provides internal melt of the ice surface. Decay is driven by $Q_H + Q_E + L^*$ which, when positive, provides for melt at the surface. The result is a surface layer of ice of varying thickness and density. The weathering crust layer can be considered to behave in a similar manner to larger scale glacial and hydrological phenomenon. Preferential pathways or channels will develop in a mature weathering crust and cracks will transfer water deeper into the weathering crust layer. In highly developed crusts, a saturated layer can exist, storing water and smoothing out variations in runoff.

It is possible to draw hydrological comparisons between the weathering crust and the firn layer. The firn layer is a porous transition layer between winter snow and glacier ice and varies in thickness and density over time. It is underlain by an impermeable ice layer which can result in a saturated layer at its base. The firn layer is a larger scale phenomenon than the weathering crust, but hydrologic similarities exist between the two, such as increased porosity, the saturated layer at the base which is a temporary water store and the variation in dimensions over time. Further, the hydraulic conductivity of a fully developed weathering crust is similar to those of a firn layer (Fountain and Walder 1998), although this is considered in the literature to be coincidental and contrary data do not exist.

Nevertheless, the two arise from different processes. Moreover, the weathering crust

exists on a significantly smaller scale and as a result, it will not significantly affect the entire glacier system over long time periods as in the case of the firn layer. However, it is significant at smaller time scales. Thus in many ways the weathering crust layer, and therefore processes occurring within the layer, is a microcosm of larger scale hydrological processes.

This thesis has provided an intensive examination of the weathering crust phenomenon on small spatial and temporal scales using different techniques, including some which have not been used previously such as stereophotographs and simulated densities. It demonstrates and explains the processes which lead to the existence of a weathering crust at the ice surface of a glacier using continuous ablation measurements at five minute intervals. This allows for use of a ratio of measured to potential surface lowering on a continuous basis, re-defining the implications of R values under different conditions. It also enables the examination of nocturnal conditions and the processes contributing to those conditions, which have not previously been analysed. Further, the provision of an examination of the diurnal weathering crust cycle may enable increased accuracies when modelling surface melt and runoff at this scale within hydrological models.

From this analysis of the weathering crust phenomenon, it is suggested that ablation in a water environment cannot be categorised in the same manner as that occurring on ice surfaces. The presence of flowing water and channel morphology result in the ice surface beneath these channels receiving lower amounts of energy than the surrounding ice surface and preventing the growth of a weathering crust. Flowing water will also erode loose ice, further preventing development of a weathering crust layer. Thus the ratio of actual to potential surface lowering is considered capable of identifying periods of enhanced or reduced surface lowering with respect to energy inputs within a channel environment, but not able to indicate weathering crust growth or decay processes, as it is assumed that these processes are modified by the presence of water and

lower energy inputs. Data do not exist to be able to examine this further.

Lags in the system based on stage hydrographs appear to be between five and fifty minutes from the onset of melt, as demonstrated by the ablatometers. Precipitation events have a very short lag time of between five and ten minutes. In these small sub-catchments precipitation events tend to supercede melt water as the driving force for changes in stage. This is assumed to be a result of decreased melt through the presence of cloud cover as well as the intensity of the rainfall event.

The density simulations enhanced analysis of field data through the indication of subsurface processes. Subsurface priming occurs when a large negative long-wave and turbulent heat flux budget (which applies only to the surface of the ice) exists during the day. This negative energy is lost from the surface layer only and under these conditions melt of the surface layer will not occur. However a short-wave radiation source exists, so penetration into lower layers and therefore internal melt of those layers will occur. Thus the density of the ice beneath the surface can become less than that of the surface layer. This is another way in which melt from an ice surface can be underestimated for modelling purposes. However the condition is short-lived because as soon as the topmost layer has a positive energy budget, the increased energy at this level will lower the density beyond that of the lower layers fairly quickly.

The simulations also demonstrate the probable importance of re-freezing within the weathering crust, at least during the melt season when on a temperate glacier the surface is usually at 0 °C. A comparison between a simulation allowing for re-freezing of meltwater and one which ignores re-freezing within the layers, demonstrates a small increase in densities in the lower layers, where re-freezing was allowed to occur, in the former.

It is concluded that the weathering crust is key to understanding the conversion of energy

inputs into melt water amounts and the timing of discharge of that melt water through the supraglacial channel system.

5.3. Future Work

This study provides a detailed examination of weathering crust processes on an ice surface. It demonstrates the complexities involved in the weathering crust phenomenon, while giving an insight into those complexities in order to facilitate understanding of the processes occurring. However, this does not supply all of the answers.

It is recommended that further data collection is undertaken, again on small spatial and temporal scales, concentrating on ablatometer measurements and nocturnal processes. A weir box with hydraulic jacks to maintain the level would enhance this study through the comparison of actual amounts of melt water generated and expected amounts based on weathering crust processes. It would provide for better analysis of the lags in the system as well.

Stereophotographs provide detailed information on the state of the weathering crust at a particular point in time. It is recommended that a longer scale study is undertaken using this method of analysis. The creation of a reference grid above the ice would link subsequent photographic pairs to each other.

Finally, linking simulated density profiles to a hydrological model through generation of melt water as density decreases and flow of that water through the weathering crust layer and into a channel system would provide further insight into how the weathering crust affects melt water runoff. A comparison of this to discharge and surface lowering measurements made in the field would also aid in ratification of the simulated density profiles.

C	specific heat of water	$J\ kg^{-1}\ K^{-1}$
I	ice melt	$kg\ m^{-3} \times 10^{3}$
K*	net short-wave radiation	$W\ m^{-2}$
K^*_n	energy available for internal melt at level n	$W\ m^{-2}$
K↓	incoming short-wave radiation	$W\ m^{-2}$
K↑	outgoing short-wave radiation	$W\ m^{-2}$
L	latent heat, of fusion (L_f), of vaporisation (L_v or λ)	$J\ kg^{-1}$
	Monin-Obukhov length scale	
L*	net long-wave radiation	$W\ m^{-2}$
L↓	incoming long-wave radiation from the atmosphere	$W\ m^{-2}$
L↑	outgoing long-wave radiation from a surface	$W\ m^{-2}$
M	mass	g
Q*	net all-wave radiation	$W\ m^{-2}$
Q_E	turbulent latent heat flux density	$W\ m^{-2}$
Q_G	sub-surface heat flux density	$W\ m^{-2}$
Q_H	turbulent sensible heat flux density	$W\ m^{-2}$
Q_M	energy available for melt	$W\ m^{-2}$
Q_{Ma}	actual surface lowering flux	$W\ m^{-2}$
	surface lowering flux	$W\ m^{-2}$
Q_{Mi}	internal melt flux	$W\ m^{-2}$
Q_{Mp}	potential surface lowering flux	$W\ m^{-2}$
Q_R	rate of heat supply by rainfall	$W\ m^{-2}$
T	temperature, air (T_a), ice (T_i), water (T_w), wet (T_W), dry (T_D), mean daily (T_j), precipitation (T_p)	°C
T*	temperature scalar	
V	volume	cm^{-3}
a	extinction coefficient	m^{-1}
c_p	specific heat of air at constant pressure	$J\ kg^{-1}\ K^{-1}$
e	vapour pressure, saturation vapour pressure (e_w), saturation vapour pressure at 100 % (e_s)	mb
	base of natural logarithms	
g	acceleration due to gravity	$m\ s^{-2}$

h	height of an object	m
k	thermal conductivity	$W m^{-1} K^{-1}$
	von Kármán's constant	m
p	precipitation	mm
	atmospheric pressure	mb
u	horizontal wind speed	$m s^{-1}$
u*	friction velocity	$m s^{-1}$
z	vertical distance	m
z_o	roughness length for windspeed	m m
z_t	roughness length for temperature	m
z_e	roughness length for humidity	m
α	surface albedo	
	empirical constant	
γ	psychrometric constant	
ε	surface emissivity	
	ratio of molecular weight of water vapour to air	$Pa K^{-1}$
ρ	density of a substance, air (ρ_a), ice (ρ_i), water (ρ_w)	$kg m^{-3}$
σ	Stefan Boltzmann constant	$W m^{-2} K^{-4}$
a	air	
i	ice	
	internal	
l	lower boundary	
n	layer number	
	time interval	
o	surface	
	reference height	
u	upper boundary	
w	water	
min	minimum value	
max	maximum value	

APPENDIX II STEREOPHOTOGRAPHS OF THE WEATHERING CRUST

The following stereophotographs were taken at 9:30 a.m., 12:30 p.m. and 3:00 p.m. on September 2nd and 7:00 a.m., 11:00 a.m. and 3:00 p.m. on September 3rd.

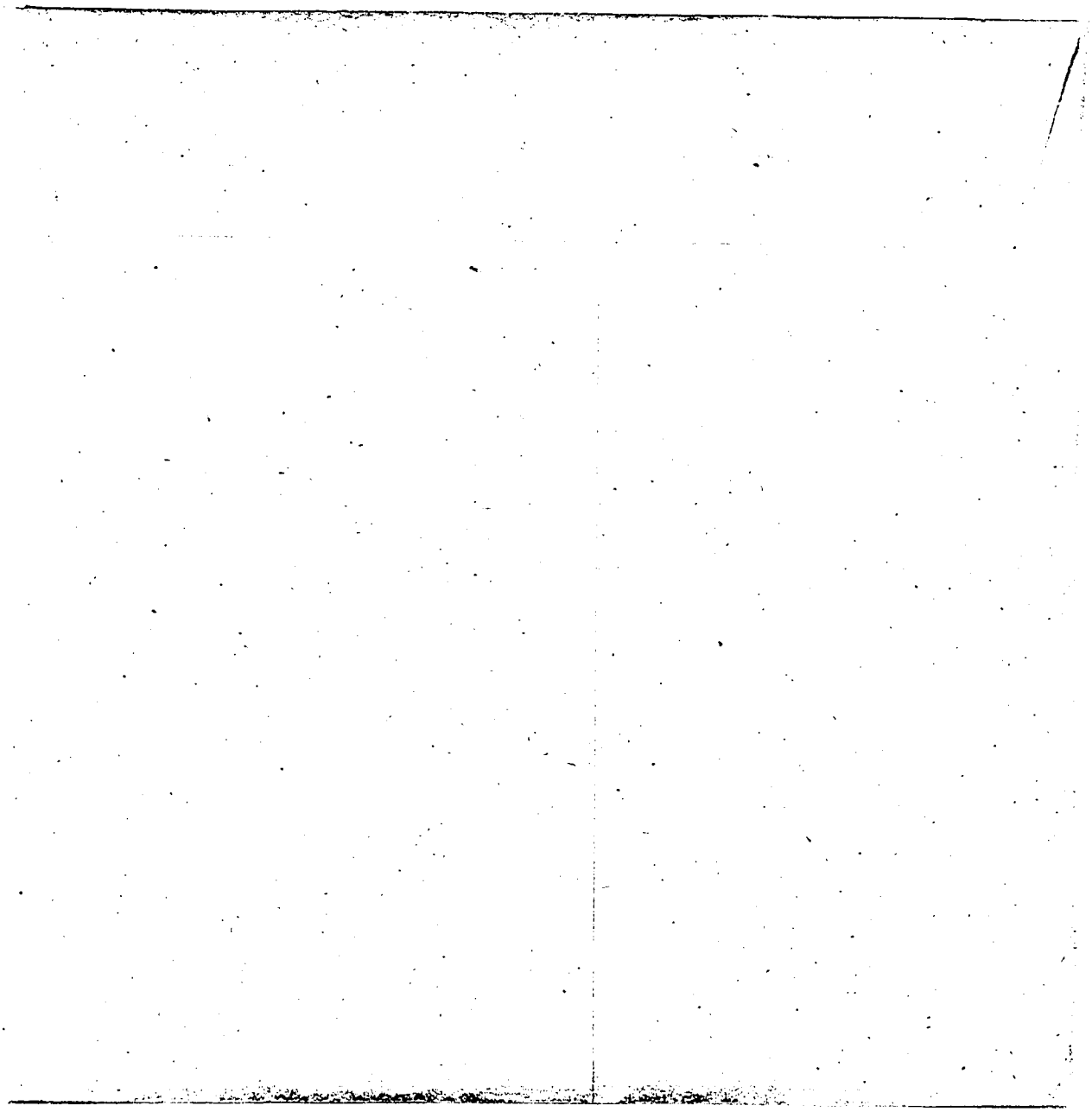

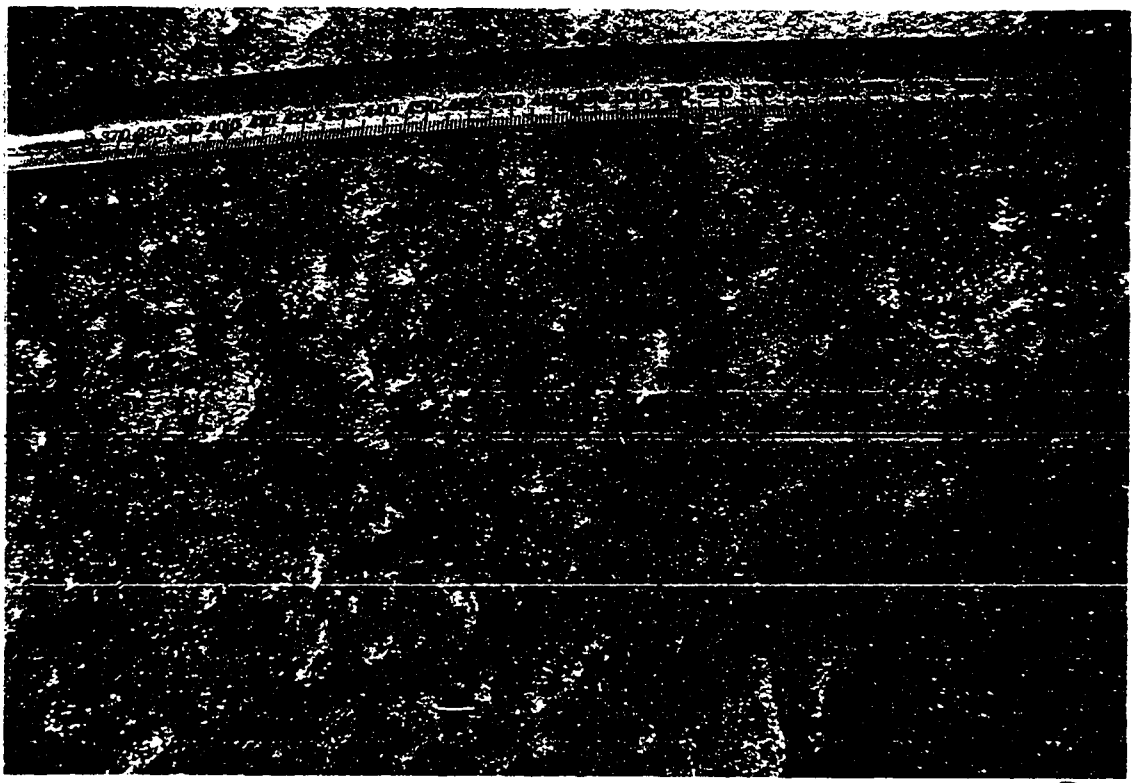

2/9 9:42 AM (A)

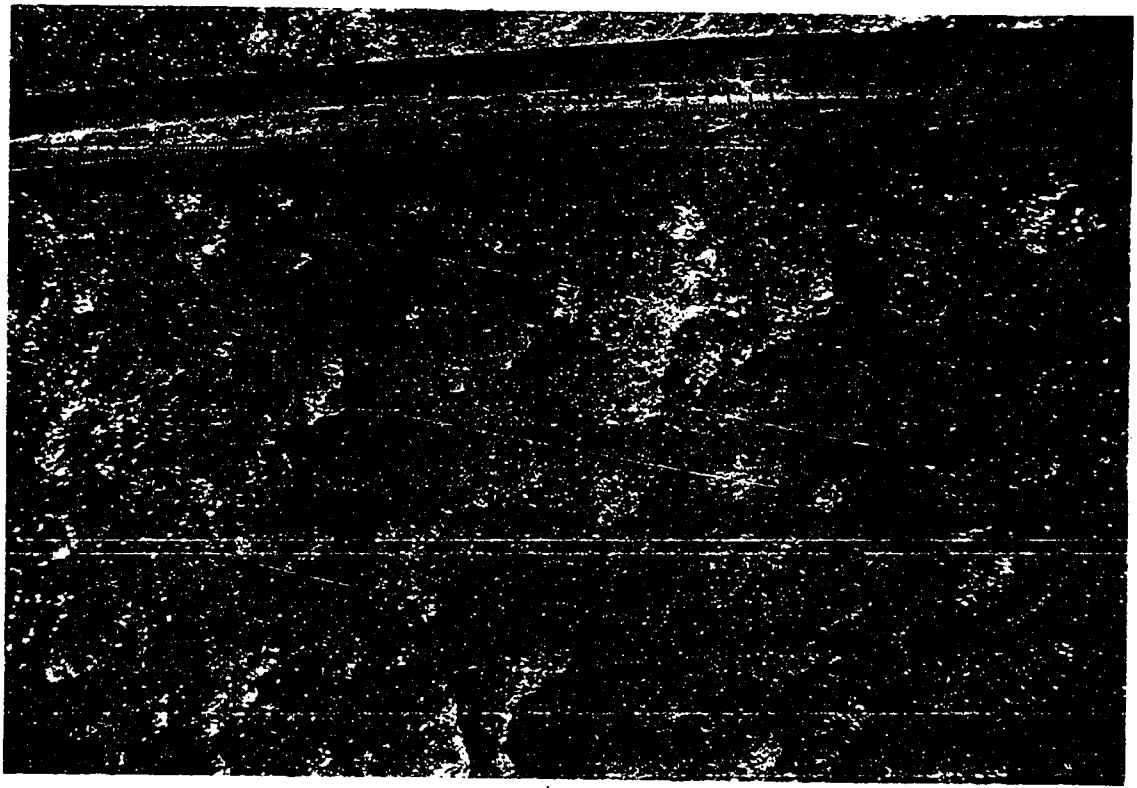

2/9 9:42 AM (B)

2/9 12:30 PM (A)

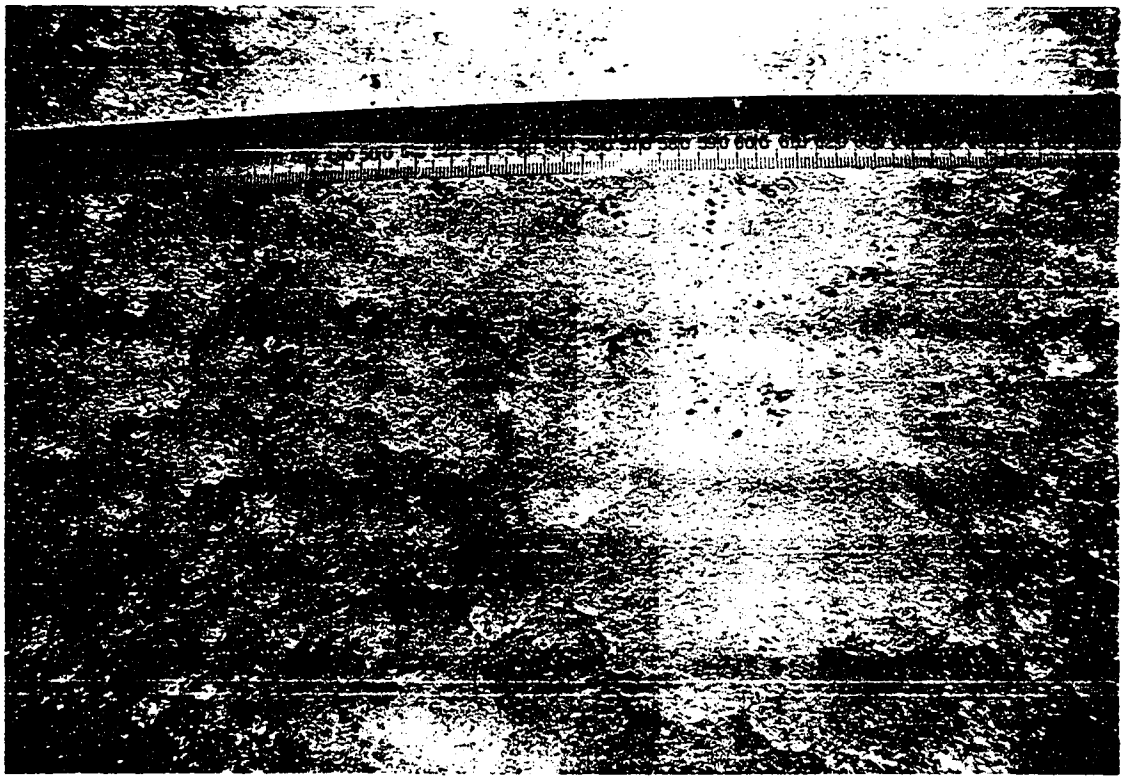

2/9 12:30 P.M (B)

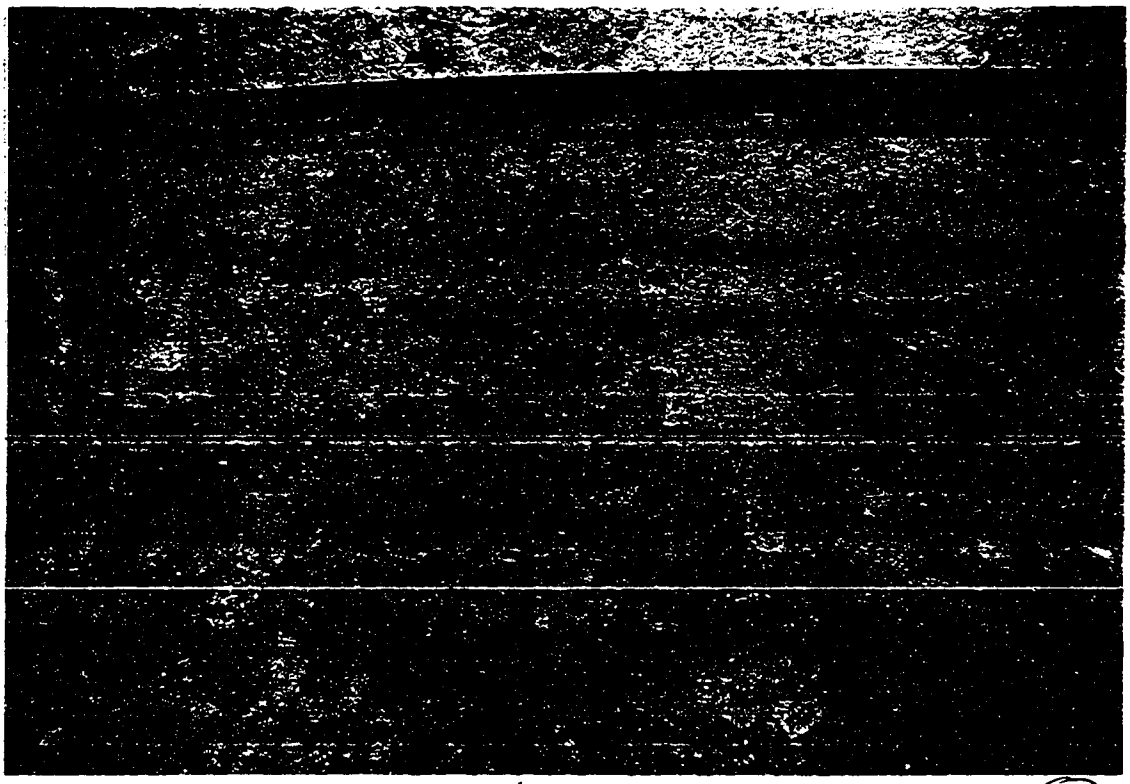

2/9 3:05 pm (A)

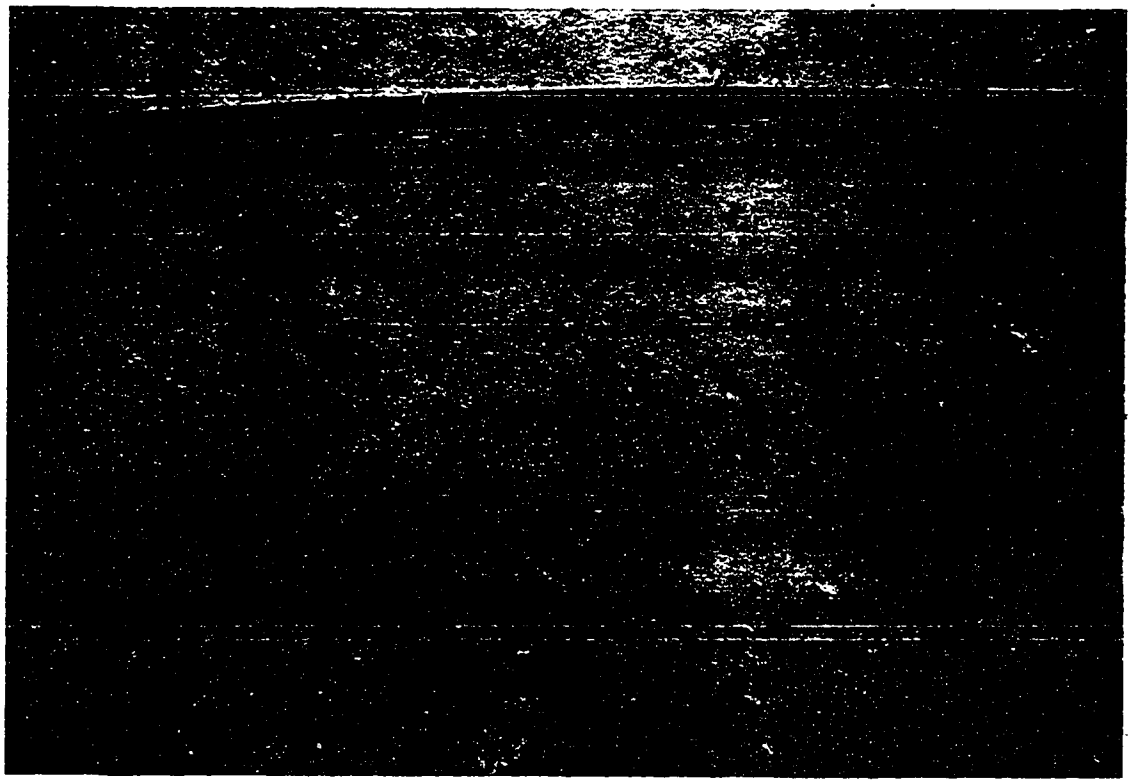

2/9 3:05 pm (B)

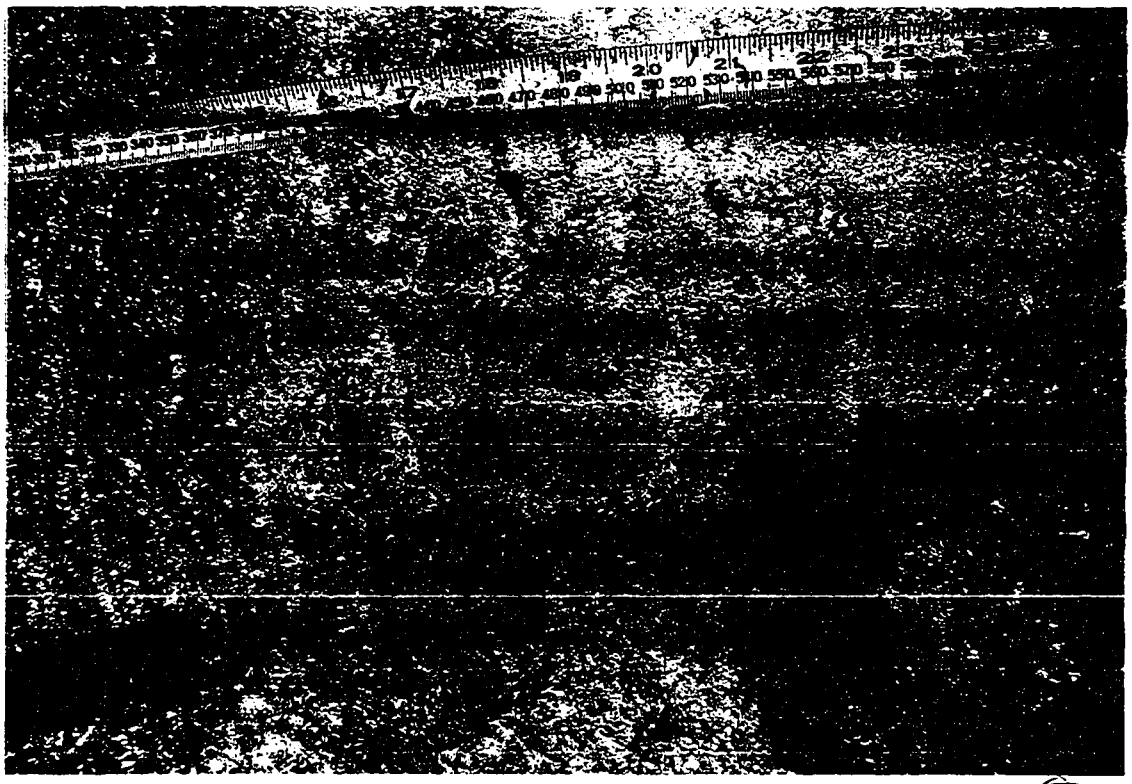

3/9 7:00 Am (A)

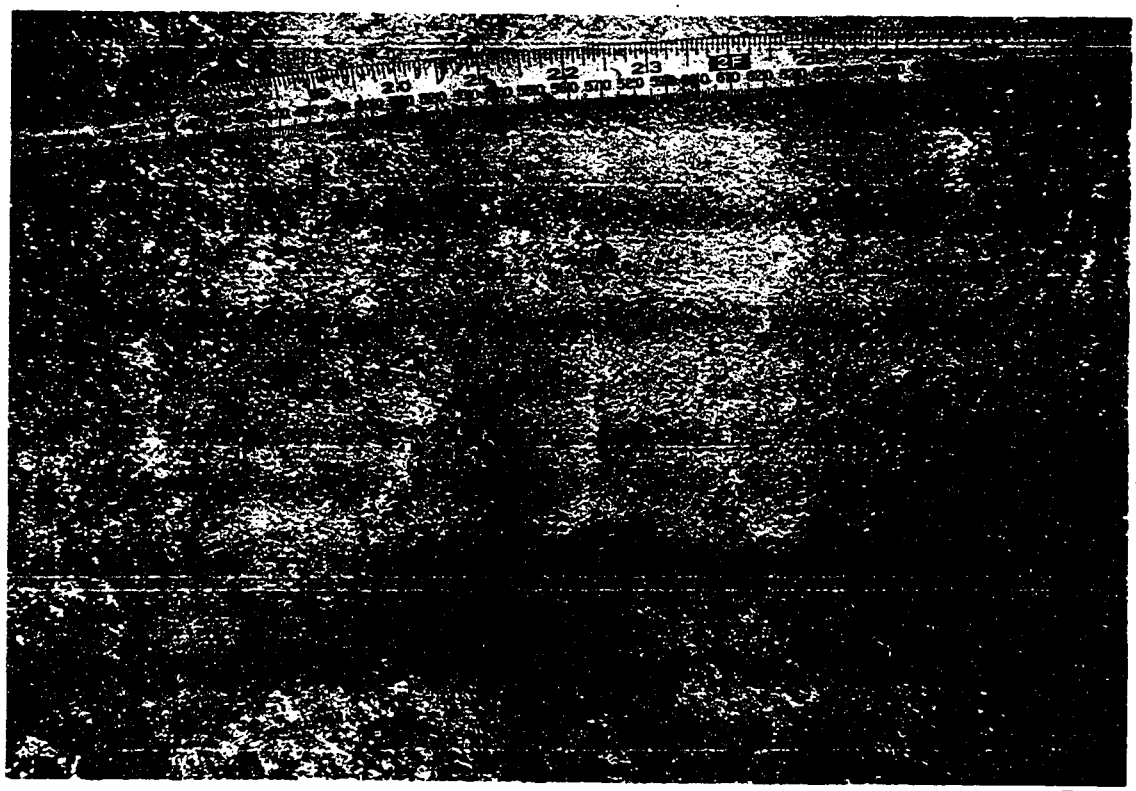

3/9 7:00 Am (B)

3/9 11:00 Am (A)

3/9 11:00 Am (B)

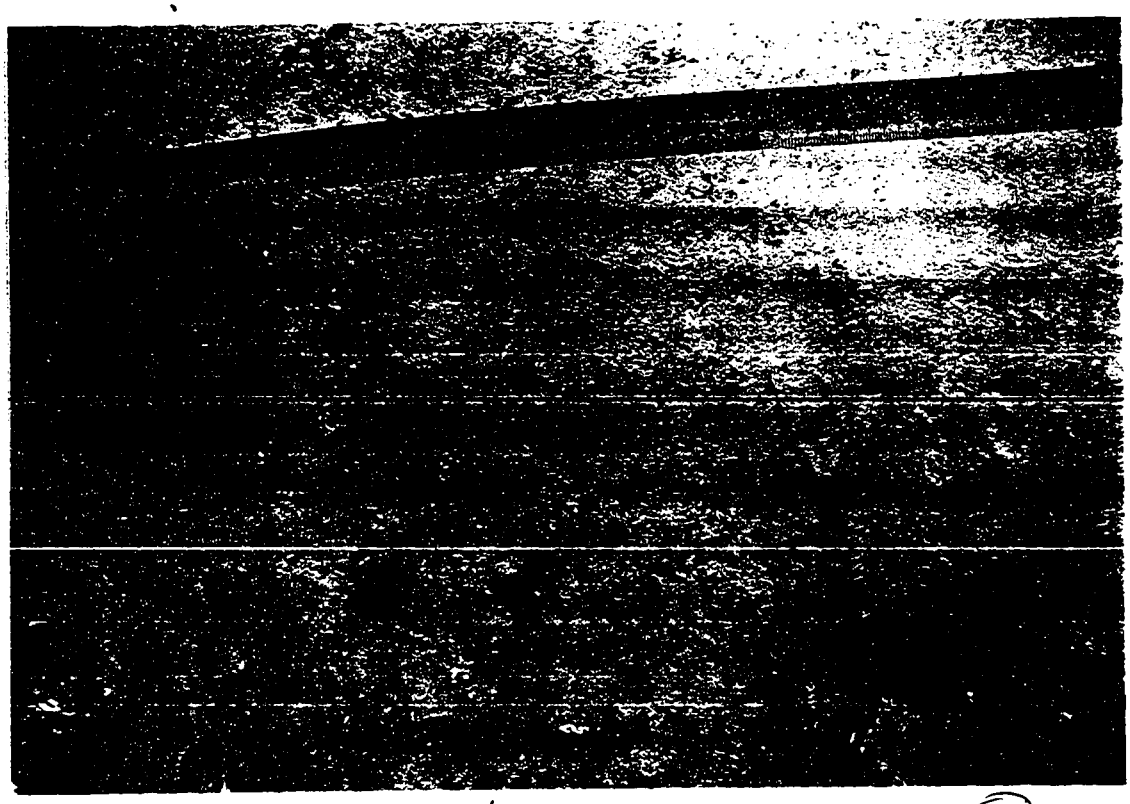

3/9 3:00 PM (A)

3/9 3:00 PM (B)

Table A.III.1. Meteorological variables measured and instrumentation types for each field season

	1994	1995	1997
Q*	net radiometer, plastic domes (CN1-R, Middleton, Carter-Scott Design, Australia)	net radiometer, plastic domes (CN1-R, Middleton, Carter-Scott Design, Australia)	net radiometer, plastic domes (SW-1 Swissteco, Switzerland)
K*	net radiometer, glass domes (CN1-R, Middleton, Carter-Scott Design, Australia)	net radiometer, glass domes (CN1-R, Middleton, Carter-Scott Design, Australia)	net radiometer, glass domes (SW-1 Swissteco, Switzerland)
K↓	pyranometer (CM11 Kip Zonen, Netherlands)	pyranometer (CM11 Kip Zonen, Netherlands)	pyranometer (Li-200SZ, Li-cor, USA)
T_a, RH	Vaisala probe (HMP45c, Campbell Scientific, USA), 1 m above ice	Vaisala probe (HMP45c, Campbell Scientific, USA), 1 m above ice	---
T_W, T_D	---	---	Copper-constantan thermocouple, 0.5 m and 1 m above the ice+)
U	Anemometer (014a, Geneq Inc., Campbell Scientific, USA), 1 m above ice	Anemometer, (014a, Geneq Inc., Campbell Scientific, USA) 1 m above ice	Anemometer, (014a, Geneq Inc., Campbell Scientific, USA) 1 m above ice
Rainfall	Tipping bucket rain gauge (TE525, Campbell Scientific, USA)	Tipping bucket rain gauge (TE525, Campbell Scientific, USA)	Tipping rain gauge bucket (P-1000, Geneq Inc., Canada)

+designed and constructed by Dr. D.S. Munro, University of Toronto, Erindale campus

Table A.III.2. Summary of meteorological instrument precision

Component Measured	Instrument	Calibration Error
Net short-wave radiation (K*)	Middleton Net Radiometer	< ± 3 % up and downwards < ± 5 % short and long-wave
	Swissteco Net Radiometer	± 2.5 % accuracy of calibration
Net all-wave radiation (Q*)	Middleton Net Radiometer	< ± 3 % up and downwards < ± 5 % short and long-wave
	Swissteco Net Radiometer	± 2.5.% accuracy of calibration
Incoming short-wave radiation (K↓)	Kip Zonen Pyranometer	± 5 %
	Li-cor Pyranometer	± 5 %
Temperature (T_W, T_D)	Vaisala Probe HMP35C	<± 0.5°C over -36 to +50 °C range <± 0.1°C over -33 to +48 °C range
	Copper-Constintan Thermocouple	± 0.4°C over -33 to +48 °C range[§]
Relative Humidity (RH)	Vaisala Probe HMP35C	± 2 % (0 - 90 %) ± 3 % (90 - 100 %)
	Campbell Scientific CS500 Temperature-Humidity Probe	± 2 % at 10 % ± 3 % at 90 %
Windspeed (U)	Geneq Inc. Anemometer	± 1.5 %
Rainfall	Campbell Scientific Tipping Bucket	± 1 tip (0.01") or 1 % at ≤ 2" $hour^{-1}$
	Geneq Inc. Tipping Bucket	3 % per 100 mm

[§] based on Campbell Scientific thermocouple 107

APPENDIX IV **FORTRAN PROGRAM FOR METEOROLOGICAL DATA EXTRACTION**

```
C   THIS FILE CALCULATES THE ENERGY BALANCE FOR 1997 BASED ON
MEASURED
C   NET ALL-WAVE, SHORT-WAVE AND GLOBAL
    OPEN (1, FILE='/usr/local/data/schu7373/ebtest.txt', STATUS='OLD')
    OPEN (2, FILE='/usr/local/data/schu7373/ebtest.prn',
   /STATUS='UNKNOWN')
    ZOU=.00246
C   SURFACE ROUGHNESS
    AZOU=ALOG(ZOU)
C   LOG SURFACE ROUGHNESS FOR THE PURPOSE OF CALCULATING QH AND QE
    Z=1.
C   INSTRUMENT HEIGHT (M) (TEMP AND U)
  1 CONTINUE
C   TO CALCULATE EN BAL INCLUDING QH AND QE
    READ(1,*,END=999)DAY,TIME,QN,SN,GBL,T1,RH1,U1
    GO TO 2
  2 CONTINUE
    GBL=GBL*126.9
    SN=SN*23.98
    QN=QN*22.09
C   CONVERTING SIGNALS FOR GBL,SN,QN TO W M^-2 BASED ON INSTRUMENT
/CALIBRATIONS
    ALB=0.
    IF(GBL.LE.1.)GO TO 50
C   IF INCOMING SW NEGATIVE, ALBEDO = 0, OTHERWISE,
    ALB=(GBL-SN)/GBL
C   CALCULATING ALBEDO (RATIO K OUT/K DOWN)
 50 CONTINUE
    RL=QN-SN
C   NET LW = NET ALL-WAVE - NET SHORT-WAVE
    RD=RL+310.
C   INCOMING LW = NET LW +310 (OUTGOING LW ASSUMED FROM BLACK BODY
AT 0C)
    IF(RH1.EQ.-9.9)RH1=0.
C   IF RH MISSING, RH ASSUMED 0
```

```
C   CALCULATING QH AND QE USING BULK HEAT TRANSFER METHOD
    E1=RH1*6.1078*EXP((17.269*T1)/(T1+237.3))
C   CALCULATING VAPOUR PRESSURE (e=RH*es where es is saturation vapour pressure at
100 %)
    ZM=0.
    ZH=0.
    DO 200 I=1,3
C   SETS UP ITERATION LOOP
    CM=.41/(ALOG(Z/ZOU)+ZM)
    TAU=U1*CM
    REN=ALOG(TAU)+AZOU-ALOG(.0000175*(1.+T1/546.)**1.81)
    ZOR=.317-.565*REN-.183*REN*REN
    ZOH=ZOU*EXP(ZOR)
    CH=.41/(ALOG(Z/ZOH)+ZH)
    QH=972.*U1*T1*CM*CH
    ZL=972.*TAU*TAU*TAU*(273.+T1)/(.41*QH*9.8)
    ZM=5./ZL
    ZH=5./ZL
 200 CONTINUE
    CME=CM/.41
    CMX=ALOG(Z/ZOU)
    CHE=CH/.41
    CHX=ALOG(Z/ZOH)
    ZER=.396-.512*REN-.180*REN*REN
    ZOE=ZOU*EXP(ZER)
    CE=.41/(ALOG(Z/ZOE)+ZH)
    CEX=ALOG(Z/ZOE)
    CEE=CE/.41
    ZM=0.
    ZH=0.
    QE=18.9088*U1*(E1-610.78)*CM*CE
    WRITE(2,*)DAY,TIME,GBL,SN,QN,QH,QE,T1,RH1,U1
    GO TO 1
 999 CONTINUE
    STOP
    END
```

APPENDIX V CALENDER OF EVENTS DURING SELECTED ANALYSIS PERIODS

A.V.1. Growth Periods

Calendar of events for JD 213 (August 1st) 1994

Q_M is already positive

6:05 a.m. global, K* and Q* greater than 100 W m^{-2}; wood foot weathering crust growth

6:15 a.m. plastic weathering crust growth

6:30 - 7:25 a.m. water foot approximately equal to 1

7:25 a.m. water foot weathering crust growth

1:00 p.m. plastic foot weathering crust growth

3:50 p.m. wood foot approximately equal to 1 (5 minutes)

4:45 - 5:05 p.m. wood foot approximately equal to 1

5:05 p.m. global, K* and Q* drop below 100 W m^{-2} after this; wood, plastic and water feet weathering crust decay

Calender of events for JD 209 (July 28th) 1997

5:55 a.m. Q_M becomes positive

6:00 a.m. global, K* and Q* greater than 100 W m^{-2}; wood foot begins weathering crust growth

6:05 a.m. plastic foot begins weathering crust growth

6:10 - 8:15 a.m. wood foot weathering crust decay

8:20 a.m. - 12:30 p.m. wood foot weathering crust growth

11:15 - 11:30 a.m. plastic foot weathering crust decay

12:35 p.m. wood foot weathering crust decay for the rest of the period

12:45 - 1:45 p.m. plastic foot weathering crust decay

2:30 - 2:45 p.m. plastic foot weathering crust decay

2:50 p.m. precipitation has occurred before now (time of bucket tip)

3:50 -3:55 p.m. plastic foot weathering crust decay

4:05 p.m. drop in global, K* and Q*

4:20 p.m. plastic foot weathering crust decay for the rest of the period

5:05 p.m. global, K* and Q* drop below 100 w m^{-2} after this

A.V.2. Decay Periods

Calender of Events for JD 214 - 215 (August 2nd - 3rd) 1994

4:00 - 8:25 p.m. $Q_H > 100$ W m^{-2}

4:00 onwards no melt for water large foot all period; Q_M positive all period

4:00 - 4:10 p.m. plastic small growth

4:00 p.m. wood small ice decay

4:00 - 5:20 p.m. water small growth except 5:05 p.m. =1

4:00 - 4:35 p.m. wood large growth

4:00 - 5:00 p.m. plastic large growth

4:00 - 7:30 p.m. $Q_M > 100$ except 7:25

4:05 - 4:10 p.m. wood small growth

4:10 p.m. onwards plastic small foot no melt through most of the period

4:15 - 4:35 p.m. wood small ice decay

4:40 - 4:55 p.m. wood small ice growth

4:40 p.m. wood large = 1

4:45 p.m. wood large growth

4:50 - 8:40 p.m. wood large = 1 except 5:05 decay

5:00 p.m. - 6:10 a.m. wood small decay

5:05 p.m. plastic large = 1

5:10 p.m. - 5:30 a.m. plastic large decay except 12:55 a.m. = 1; 5:20 a.m. = 1

5:10 p.m. global, K* and Q* < 100

5:25 p.m. 6:45 a.m. water small decay except 6:05 p.m. growth; 6:45 p.m. = 1; 6:55 p.m. = 1; 9:25 p.m. growth; 9:50 p.m. growth; 9:55 p.m. growth;10:05 p.m. growth; 10:20 p.m. = 1;10:35 p.m. = 1; 11:55 p.m.= 1;12:05 a.m. growth; 12:10 a.m. =1; 12:15 a.m. =1; 12:35 a.m. growth; 1:00 a.m. growth; 1:15 a.m. = 1; 2:20 a.m. = 1; 3:35 a.m. growth; 5:05 a.m. = 1; 5:25 a.m. = 1; 5:50 a.m. = 1; 6:30 a.m. = 1; 6:45 a.m. growth

7:35 - 9:05 p.m. $Q_M < 100$ except 8:05

7:55 p.m. K* negative

8:30 - 9:05 p.m. $Q_H < 100$

8:35 p.m. Q_E positive to end of period

8:45 p.m. wood large growth

8:50 p.m. wood large decay

8:55 p.m. wood large = 1

9:00 p.m. - 6:35 a.m. wood large decay except 9:10 p.m. = 1; 11:00 p.m. = 1; 5:40 a.m. growth; 6:05 a.m. growth; 6:20 a.m. growth; 6:35 a.m. = 1

9:10 - 10:35 p.m. $Q_H > 100$ except 10:25 p.m.

9:10 p.m. to end of period $Q_M > 100$ except 10:40 p.m. and 3:55 a.m.

10:40 - 11:35 p.m. $Q_H < 100$ except 11:15 and 11:25

11:40 p.m. - 6:00 a.m. $Q_H > 100$ except 11:50 p.m.; 12:50 a.m.; 1:45 a.m.; 1:50 a.m.; 2:00 a.m.; 3:55 a.m.; 5:15 a.m.; 5:55 a.m.

4:10 a.m. K* positive

5:35 - 5:45 a.m. plastic large growth

5:50 - 5:55 a.m. plastic large = 1

6:00 - 6:05 a.m. plastic large decay

6:05 - 6:30 a.m. $Q_H < 100$

6:10 a.m. global, K* and Q* > 100 W m^{-2}

6:10 a.m. plastic large growth

6:15 a.m. wood small growth to end
6:15 - 6:20 a.m. plastic large decay
6:25 a.m. plastic large = 1
6:30 a.m. plastic large decay
6:35 a.m. Q_H > 100 onwards
6:35 - 6:40 a.m. plastic large = 1
6:40 a.m. wood large ice growth to end
6:45 a.m. plastic large growth to end
6:50 a.m. water small =1 to end

A.V.3. Transition Periods

Calender of Events for JD 182 (July 1st) 1997

very little melt of the water foot all day
5:20 a.m. global, K* and Q* >100 W m^{-2} ; Q_M becomes positive
5:20 – 5:30 a.m. wood growth
5:30 – 8:55 a.m. wood decay
5:30 a.m. plastic growth (5 min)
5:35 a.m. plastic decay (5 min); Q* < 100 W m^{-2}
5:40 a.m. plastic no melt
5:45 – 6:25 a.m. plastic growth
6:30 - 8:25 a.m. plastic decay (except for 6:50 a.m. and 8:20 a.m. plastic growth)
7:25 – 7:35 a.m. Q* <100 W m-2
7:25 – 7:30 a.m. Q_M < 100 W m-2
7:45 – 7:50 a.m. K* <100 W m-2
8:30 – 9:40 a.m. plastic growth
9:00 – 9:15 a.m. wood foot approximately equals 1
9:20 a.m. – 10:00 p.m. wood decay (except for 5:40 p.m. growth; 8:05 p.m. growth; 8:15 p.m. growth; 8:30 p.m. growth; 9:00 p.m. =1)
9:45 – 9:50 a.m. plastic decay
9:55 – 10:00 a.m. plastic growth
10:05 a.m. plastic foot approximately equal to 1
10:10 a.m. – 12:40 p.m. plastic growth (except at 12:30 p.m. =1)
11:20 a.m. global radiation > 1000 W m^{-2}
12:35 – 12:40 p.m. global radiation >1000 W m^{-2}; plastic growth
12:45 p.m. plastic =1
12:50 p.m. plastic decay
12:55 p.m. plastic growth
1:00 p.m. plastic = 1

1:05 p.m. – end of period plastic foot decay except 1:40 p.m. – 1:45 p.m. growth; 1:50 p.m. – 1:55 p.m. =1; 2:15 p.m. – 2:20 p.m. =1

2:10 p.m. jump in water foot because at 2:09 p.m. it was manually lowered

2:30 – 2:45 p.m. $Q^* < 100$ W m^{-2}

4:10 p.m. $Q_H > 100$

5:25 p.m. to end of period $Q^* < 100$ W m^{-2}

6:00 p.m. to end of period $K^* < 100$ W m^{-2}

6:15 p.m. to end of period $Q_M < 100$

6:20 p.m. to end of period global < 100 W m^{-2}

8:25 p.m. K* negative

10:05 p.m. wood growth (5 min)

10:10 p.m. wood no melt

10:15 p.m. wood decay

10:15 – 11:20 p.m. K* positive (up to 2 W m^{-2})

10:20 p.m. wood growth

10:25 – 10:50 p.m. wood decay

10:55 – 11:15 p.m. wood =1

11:20 - 11:50 p.m. wood decay except 5 min at 11:40 p.m. – no melt

11:45 p.m. Q_M negative for rest of period

11:55 p.m. wood foot no melt

Calender of Events for JD 210 – 212 (July 29th - 31st) 1997 (Decay and Transition)

12:00 – 2:25 p.m. $Q_H > 100$ W m^{-2} except for 1:35 p.m. when it drops below 100 W m^{-2}

12:15 p.m. plastic decay (5 min)

12:45 p.m. plastic decay (10 min)

1:00 p.m. plastic decay (5 min)

1:15 – 1:40 p.m. plastic foot negative due to increase of approximately 5 mm; decay begins (ice foot)

1:25 p.m. K* suddenly decreases

1:40 p.m. wood and water both exhibit decay for 5 min

1:45 p.m. no melt on any feet

1:50 – 2:55 p.m. wood decay

2:00 p.m. plastic foot approximately equals 1

2:05 p.m. plastic foot growth (5 min)

2:10 – 3:50 p.m. plastic foot decay except for 3:00 p.m. when 5 min of growth occurs

2:15 – 2:20 p.m. $Q^* < 100$ W m^{-2}

2:30 – 2:55 p.m. $Q^* < 100$ W m^{-2}

2:30 p.m. $Q_H < 100$ W m^{-2} (5 min)

2:40 – 2:50 p.m. $Q_H < 100$ W m^{-2}

2:50 – 2:55 p.m. global and $K^* < 100$ W m^{-2}

3:00 p.m. wood and plastic feet growth

3:05 – 3:25 p.m. Q*<100 W m^{-2}

3:05 – 3:10 p.m. wood foot decay

3:05 – 3:50 p.m. plastic foot decay

3:10 – 3:20 p.m. global <100 W m^{-2}

3:10 – 3:25 p.m. K* <100 W m^{-2}

3:15 p.m. wood growth (5 min)

3:20 – 3:35 p.m. wood decay

3:35 – 3:45 p.m. K*<100 W m^{-2}

3:35 – 3:50 p.m. Q*< 100 W m^{-2}

3:40 p.m. wood foot growth (5 min)

3:45 – 4:20 p.m. wood foot decay

3:55 – 4:00 p.m. plastic foot approximately equal to 1

4:05 p.m. plastic growth

4:10 – 4:40 p.m. plastic decay

4:20 p.m. Q* < 100 W m^{-2} (5 min)

4:25 – 4:30 p.m. wood growth

4:35 – 8:15 p.m. wood decay

4:45 p.m. plastic growth (5 min)

4:50 – 5:00 p.m. Q* <100 W m^{-2}

4:50 – 10:30 p.m. plastic decay (except for 5 min growth at 9:10 p.m.)

4:55 p.m. global and K* <100 W m^{-2} (5 min)

5:10 p.m. global, K* and Q* <100 W m^{-2} (5 min)

8:00 p.m. K* negative (5 min)

8:20 – 8:25 p.m. wood foot growth

8:30 – 10:50 p.m. wood decay (except for wood growth 5 min at 8:35 p.m.)

8:45 – 9:00 p.m. Q_H <100 W m^{-2}

9:25 – 9:35 p.m. Q_H < 100 W m^{-2}

9:45 p.m. Q_H < 100 W m^{-2} (5 min)

9:55 – 10:00 p.m. Q_H < 100 W m^{-2}

10:10 – 10:15 p.m. Q_H < 100 W m^{-2}

10:25 – 10:35 p.m. Q_H < 100 W m^{-2}

10:35 p.m. plastic foot approximately equal to 1

10:40 – 10:50 p.m. plastic growth

10:55 p.m. wood growth

10:55 p.m. - 2:30 a.m. plastic decay except 1:15 a.m. growth; 1:40 - 1:45 a.m. growth; 1:55 a.m. growth; 2:05 a.m. growth

11:00 p.m. wood decay

11:05 p.m. wood growth

11:10 p.m. - 4:55 a.m. wood decay except 11:50 p.m.; growth; 3:20 - 3:20 a.m. = 1; 4:45 - 4:50 a.m. = 1

11:10 - 11:50 p.m. Q_H < 100 W m^{-2}

11:50 p.m. K* negative
11:55 p.m. - 12:45 a.m. $Q_H > 100$ W m^{-2}
12:50 - 1:00 a.m. $Q_H < 100$ W m^{-2}
1:05 - 1:25 a.m. $Q_H > 100$ W m^{-2}
1:30 - 3:25 a.m. $Q_H < 100$ W m^{-2} except 1:45 a.m. and 2:05 a.m.
2:35 - 5:00 a.m. plastic growth except 3:05 a.m. decay; 4:10 a.m. = 1; 4:25 a.m. decay; 4:35 a.m. decay;
2:55 - 3:45 a.m. K* positive (max 2 W m^{-2})
3:30 - 3:45 a.m. $Q_H > 100$ W m^{-2}
3:50 - 5:00 a.m. $Q_H < 100$ W m^{-2} except 4:35 a.m. and 4:45 a.m.
3:50 - 4:00 K* negative
4:05 a.m. K* positive
5:00 - 5:30 a.m. wood = 1
5:05 - 10:00 a.m. $Q_H > 100$ W m^{-2} except for 5:55 a.m.; 6:35 a.m.; 7:05 a.m.
5:05 - 5:20 a.m. plastic = 1
5:25 - 5:55 a.m. plastic decay except 5:40 - 5:45 a.m. = 1
5:35 a.m. wood growth
5:40 a.m. wood = 1
5:45 a.m. wood decay
5:50 a.m. wood growth
5:55 - 6:50 a.m. wood decay
6:00 - 7:20 a.m. plastic growth except 6:10 - 6:15 a.m. = 1; 7:05 a.m. = 1
6:05 a.m. Q* > 100 W m^{-2} for 5 min
6:15 a.m. global, K* and Q* > 100 W m^{-2}
6:20 - 6:30 a.m. K* < 100 W m^{-2}
6:25 - 6:30 a.m. global and Q* < 100 W m^{-2}
6:35 a.m. global, K* and Q* > 100 W m^{-2}
6:55 a.m. wood growth
6:55 - 7:15 a.m. K* < 100 W m^{-2}
7:00 a.m. global < 100 W m^{-2}
7:05 a.m. global > 100 W m^{-2}
7:00 a.m. wood = 1
7:05 a.m. wood growth
7:10 - 7:15 a.m. wood decay
7:20 - 8:25 a.m. wood = 1 except 8:05 a.m. growth
7:25 - 7:45 a.m. plastic = 1
7:50- 9:30 a.m. plastic growth except 8:15 a.m. = 1
8:30 - 9:35 a.m. wood growth
9:35 - 9:40 a.m. plastic = 1
9:40 - 9:55 a.m. wood = 1
9:45 - 9:55 a.m. plastic decay

10:00 - 10:15 a.m. plastic growth

10:00 - 10:20 a.m. wood decay

10:05 - 10:40 a.m. $Q_H < 100$ W m^{-2}

10:20 - 10:30 a.m. plastic decay

10:25 a.m. - 12:10 p.m. wood growth except 11:10 - 11:15 a.m. = 1

10:35 - 11:05 a.m. plastic growth except 10:45 - 10:50 a.m. decay

10:45 - 10:55 a.m. $Q_H > 100$ W m^{-2}

11:00 - 11:45 a.m. $Q_H < 100$ W m^{-2} except 11:15 a.m.

11:10 - 11:25 a.m. plastic decay

11:30 - 11:35 a.m. plastic growth

11:40 a.m. plastic = 1

11:45 a.m. - 2:20 p.m. plastic decay except 11:55 a.m. growth; 1:20 p.m. growth; 1:30 p.m. growth; 1:40 p.m. growth; 1:55 p.m. growth;

11:50 a.m. - 12:20 p.m. $Q_H > 100$ W m^{-2}

12:15 - 5:25 p.m. wood decay except 4:45 p.m. growth

12:25 - 1:50 p.m. $Q_H < 100$ W m^{-2} except 12:35 p.m. and 1:45pm

1:55 - 3:10 p.m. $Q_H > 100$ W m^{-2} except 2:20

2:25 - 3:30 p.m. plastic growth except 3:10 p.m. decay;

3:10 - 5:05 p.m. $Q^* < 100$ W m^{-2}

3:25 - 4:30 p.m. $Q_H < 100$ W m^{-2} except 3:45 p.m.

3:35 p.m. - 7:25 a.m. plastic decay except 3:50 - 3:55 p.m. no melt; 4:45 p.m. no melt; 5:00 p.m. growth; 8:05 p.m. growth; 8:20 p.m. growth; 8:35 p.m. growth; 8:40 p.m. = 1; 9:05 - 9:10 p.m. growth; 9:25 p.m. growth; 9:40 p.m. growth; 9:55 p.m. growth; 10:05 p.m. growth; 10:15 p.m. growth; 10:25 p.m. growth; 10:40 p.m. growth; 10:50 p.m. growth; 1:35 a.m. no melt; 3:45 a.m. no melt; 4:10 a.m. no melt; 5:20 a.m. = 1; 5:40 a.m. = 1; 5:50 a.m. growth; 6:00 - 6:10 a.m. growth; 6:45 a.m. growth; 6:50 a.m. no melt; 7:00 a.m. no melt; 7:20 a.m. no melt

4:35 - 4:45 p.m. $Q_H > 100$ W m^{-2}

4:50 - 8:20 p.m. $Q_H < 100$ W m^{-2} except 5:20 p.m.; 6:00 p.m.; 6:10 p.m.; 7:55 p.m.; 8:05 p.m.

4:55 p.m. $K^* < 100$ W m^{-2}(5 min)

5:05 p.m. global and $K^* < 100$ W m^{-2}

5:30 - 5:50 p.m. wood growth except 5:40 p.m. decay

5:55 p.m. - 7:40 a.m. wood decay except 8:00 p.m. growth; 8:45 p.m. growth; 9:20 p.m. growth; 9:45 growth; 10:50 p.m. growth; 2:20 a.m. no melt; 3:00 a.m. no melt; 4:10 a.m. no melt; 4:20 a.m. no melt; 5:10 a.m. = 1; 5:50 a.m. growth; 6:05 a.m. = 1;

7:55 p.m. K* negative

8:25 - 8:50 p.m. $Q_H > 100$ W m^{-2} except 8:45 p.m.

8:55 - 9:40 p.m. $Q_H < 100$ W m^{-2} except 9:05 p.m. and 9:20 p.m.

9:45 - 10:00 p.m. $Q_H > 100$ W m^{-2}

10:00 - 10:10 p.m. $Q_H < 100$ W m^{-2}

10:15 - 10:20 p.m. $Q_H > 100$ W m^{-2}

10:25 - 10:30 p.m. $Q_H < 100$ W m^{-2}

10:35 - 10:55 p.m. $Q_H > 100$ W m^{-2}

11:00 p.m. to end of period Q_H < 100 W m^{-2} except 11:15 p.m.; 11:45 p.m.; 11:50 p.m.; 12:25 a.m.; 1:10 a.m.; 5:20 a.m.; 5:30 a.m.

2:20 a.m. Q_M negative and plastic negative

2:45 a.m. Q_M negative and plastic negative

2:55 a.m. Q_M negative and plastic negative

4:10 a.m. K* positive

6:05 a.m. global and K* > 100 W m^{-2}

7:30 a.m. to end of period plastic growth except 8:25 a.m. no melt; 8:45 a.m. no melt; 8:55 a.m. no melt

7:35 a.m. Q* > 100 W m^{-2}

7:45 a.m. to end of period wood foot growth except 8:10 a.m. decay; 8:20 a.m. decay; 8:35 - 8:40 a.m. =1

8:20 a.m. Q* < 100 W m^{-2}(5 min)

A.V.4. Quasi-Static Periods (Low Melt)

Calender of Events for JD 185 - 186 (July 4th - 5th) 1997

7:00 p.m. Q_E negative all period; water ablatometer ratio = 0 most of period with 5 minute intervals of decay and negative ratios

7:00 p.m. - 7:40 p.m. wood and plastic ablatometers decay

7:40 p.m. Q_M negative to end of period

7:45 p.m. - 12:30 a.m. wood and plastic negative except 12:10 - 12:15 a.m.

8:00 p.m. K* negative

12:35 a.m. - 12:55 a.m. wood and plastic decay

1:00 a.m. - 5:15 a.m. wood and plastic negative with 5 minute intervals of ratio = 0

3:40 a.m. K* positive

5:20 a.m. Q* positive; global >100 W m^{-2}; wood and plastic decay to end of period

5:25 a.m. K* > 100 W m^{-2}; Q* >100 W m^{-2}; Q_M >100 W m^{-2}

Calender of Events for JD 192 (July 11th) 1997

12:00 a.m. Q_E negative all period; no melt on ablatometers except wood

4:00 a.m. K* positive

4:55 a.m. Q* positive

6:10 a.m. - 2:35 p.m. wood decay = 1

6:30 a.m. global > 100

7:55 a.m. - 12:50 p.m. Q* negative except 10:30 - 10:40 a.m.; 12:15 p.m.; 12:35 - 12:45 p.m.; 12:50 p.m.

10:10 a.m. K* > 100 W m^{-2} (5 min)

10:35 a.m. K* > 100 W m^{-2} (5 min)

10:55 a.m. K* > 100 W m^{-2} (5 min)

12:35 - 12:45 p.m. Q_M positive

12:50 - 1:00 p.m. Q_M negative

12:55 - 6:45 p.m. Q* positive except 1:00 p.m.; 1:30 p.m.; 6:20 p.m.; 6:25 p.m.

1:05 - 1:20 p.m. Q_M positive
1:25 - 1:30 p.m. Q_M negative
1:35 - 6:15 p.m. Q_M positive
2:25 - 4:25 p.m. $Q^* > 100$ W m^{-2}
2:40 - 4:55 p.m. wood growth
4:40 p.m. $K^* < 100$ W m^{-2}(5 min)
5:00 - 10:10 p.m. wood decay = 1
5:00 p.m. $K^* < 100$ W m^{-2}
5:25 p.m. global < 100 W m^{-2}
6:20 - 6:25 p.m. Q_M negative
6:30 - 6:45 p.m. Q_M positive
6:50 p.m. Q_M negative to end of period
7:50 p.m. K* negative; Q* negative to end of period
10:15 p.m. wood no melt to end of period

REFERENCES

Ambach, W., 1963, Untersuchungen zum Energieumsatzin der Ablationszone des grönlandischen Inlandeises, *Medd. Grønland*, vol. 174, 4

Ambach W. and Hoinkes H.C., 1963, The heat balance of an Alpine snowfield, *International Association of Hydrological Science Publication*, no. 61

Arnold, N.S., Richards, K.S. Willis, I.C. and Sharp, M.J., 1998, Initial results from a distributed, physically based model of glacier hydrology, *Hydrological Processes*, vol. 12, p.191-219

Barry, R.G., 1992, *Mountain Weather and Climate*, 2nd ed., Routledge, pp.402

Brandt, R.E. and Warren, S.G., 1993, Solar-heating rates and temperature profiles in Antarctic snow and ice, *Journal of Glaciology*, vol. 39, no. 131, p.99-110

Campbell, W.J. and Rasmussen, L.A., 1973, The production, flow and distribution of melt water in a glacier treated as a porous medium, *Symposium on the Hydrology of Glaciers. September 1969. Commission of Snow and Ice*, IAHS-AISH, Publ. No. 95, p.11-27

Cutler, P.M. and Munro, D.S., 1996, Visible and near-infrared reflectivity during the ablation period on Peyto Glacier, Alberta, Canada, *Journal of Glaciology*, vol. 42, 141, p.333-40

de la Cassinière, A.C., 1974, Heat exchange over a melting snow surface, *Journal of Glaciology*, vol. 13, 67, p.55-72

Derikx, L., 1973, Glacier discharge simulation by groundwater analogue, *Symposium on the Hydrology of Glaciers. September 1969. Commission of Snow and Ice*, IAHS-AISH, Publ. No. 95, p.29-40

Derikx, L., 1975, The heat balance and associated runoff from an experimental site on a glacier tongue, *Snow and Ice Symposium.* August 1971 (Moscow) in *I*AHS/AISH publ. no. 104, p.59-69

Dilley, A.C., 1968, On the computer calculation of vapour pressure and specific humidity gradients from psychrometric data, *Journal of Applied Meteorology*, vol. 7, p.717-19

Escher-Vetter, H., 1985, Energy balance calculations for the ablation period 1982 at Vernagtferner, Oetzel Alps, *Annals of Glaciology*, vol.6, p.158-160

Föhn, P.M., 1973, Short-term snow melt and ablation derived from heat- and mass-balance measurements, *Journal of Glaciology*, vol. 12, 65, p.275-289

Fountain, A.G. and Walder, J.S., 1998, Water flow through temperate glaciers, *Reviews of Geophysics*, vol. 36, 3, p.299-328

Geiger, R., 1965, *The Climate Near the Ground*, Cambridge, Harvard University Press, pp. 611, pg. 207

Golubev, G.N., 1975, The water regime of the glaciological zones, *Snow and Ice Symposium.* IAHS/AISH, Publ. No. 104, p.111-122

Granger, E.M. and Lister, H., 1966, Wind speed, stability and eddy viscosity over melting ice surfaces, *Journal of Glaciology*, vol.6, p.101-127

Gratton, D.J., Howarth, P.J. and Marceau, D.J., 1993, Using Landsat-5 Thematic Mapper and digital elevation data to determine the net radiation field of a mountain glacier, *Remote Sensing Environments*, vol. 43, p.315-331

Gratton, D.J., Howarth, P.J. and Marceau, D.J., 1994, An investigation of terrain irradiance in a mountain-glacier basin, *Journal of Glaciology*, vol. 40, 136, p.519-26

Hannah, D.M. and McGregor, G.R., 1997, Evaluating the impact of climate on snow- and ice-melt *Journal of Glaciology*, vol. 43, 145, p.563-68

Hoinkes, H., 1955, Measurements of ablation and heat balance on alpine glaciers, *Journal of Glaciology*, vol. 2, p.497-501

IAHS, UNEP, UNESCO, 1998, *Fluctuations of Glaciers 1990 - 1995*, Vol. VII, pg. 184

Konzelmann, T. and Ohmura, A., 1995, Radiative fluxes and their impact on the energy balance of the Greenland ice sheet, *Journal of Glaciology*, vol. 41, 139, p.490-502

Kraus, H., 1975, An energy balance model for ablation in mountainous areas, *Snow and Ice Symposium.* IAHS/AISH Publ. No. 104, p.74-82

LaChapelle, E., 1959, Errors in ablation measurements from settlement and sub-surface melting, *Journal of Glaciology*, vol.3, 6, p.458-467

LaChapelle, E., 1961, Energy exchange measurements on the Blue Glacier, Washington, *Snow and Ice Commission*, IAHS-AISH, Publ. No. 54, p.302-310

Lang, H., 1973, Variations in the relation between glacier discharge and meteorological elements, *Symposium on the Hydrology of Glaciers. September 1969. Commission of Snow and Ice*, IAHS/AISH, Publ. No. 95, p.85-94

Lang, H., 1986, Forecasting melt water runoff from snow-covered areas and from glacier basins, in *River Flow Modelling and Forecasting*, eds. Kraijenhoff, D.A. and Moll, J.R., p.99-127

Lawson, D.E., 1993, *Glaciohydrologic and Glaciohydraulic Effects on Runoff and Sediment Yield in Glacierised Basins*, CRREL Monograph 93-2, Hanover, NH, US Army Corps of Engineers, Cold Regions Research and Engineering Laboratory

Lettau, H.H.,1969, Note on aerodynamic roughness parameter estimation on the basis of roughness element description, *Journal of Applied Meteorology*, vol. 8, p.828-32

Lewkowicz, A.G., 1985, Use of an ablatometer to measure short-term ablation of exposed ground ice, *Canadian Journal of Earth Sciences*, vol. 22, p.1767-73

Lliboutry, L., 1996, Temperate ice permeability, stability of water veins and percolation of internal melt water, *Journal of Glaciology*, vol. 42, 141, p.201-11

Male, D.H. and Granger, R.J., 1981, Snow Surface Energy Exchange, *Water Resources Research*, vol. 17, 3, p.609-627

Martin, S., 1975, Wind regimes and heat exchange on Glacier de Saint-Sorlin, *Journal of Glaciology*, vol. 14, 70, p.91-105

Morris, E.M., 1989, Turbulent transfer over snow and ice (review paper), *Journal of Hydrology*, vol. 105, p.205-223

Müller, F., 1985, Review paper on the radiation budget in the Alps, *Journal of Climatology*, vol. 5, p.445-462

Müller, F. and Keeler, C.M., 1969, Errors in short term ablation measurements on melting ice surfaces, *Journal of Glaciology*, vol. 8, 52, p.91-105

Munro, D. S., 1989, Surface roughness and bulk heat transfer on a glacier: comparison with eddy correlation, *Journal of Glaciology*, vol.35, 121 p.343-348

Munro, D.S., 1990, Comparison of melt energy computations and ablatometer measurements on melting ice and snow, *Arctic and Alpine Research*, vol. 22, 2, p.153-162

Munro, D.S., 1991, A surface energy exchange model of glacier melt and net mass balance, *International Journal of Climatology*, vol. 11 p.689-700

Munro, D.S. and Young, G.J., 1982, An operational short-wave radiation model for glacier basins, *Water Resources Research*, vol. 18,2, p.220-230

Oke, T.R., 1987, *Boundary Layer Climates*, Methuen, pp.435

Ommanney, C.S.L., 1990, Peyto Glacier, extract from *Glaciers of the Canadian Rockies*, NHRI Contribution no. 90059 to the Satellite Image Atlas of Glaciers to be published by U.S.G.S.

Owens, I.F., Sturman, A.P. and Ishikawa, N., 1992, High rates of ablation on the lower part of the Franz Josef Glacier, South Westland, *Proceedings of the Inaugural Joint Conference of the New Zealand Geographic Society and the Institute of the Australian Geographers. Auckland*, p.576-582

Röthlisberger H. and Lang, H., 1987, Glacial hydrology, in *Glacio-fluvial Sediment Transfer*, Gurnell, A.M and Clarke, M.J. (eds.), London: Wiley, ch.10, p.207-84, pp.524

Streten, N.A. and Wendler, G., 1968, The midsummer heat balance of an Alaskan maritime glacier, *Journal of Glaciology*, vol. 7, 51, p.431-440

Van de Wal, R.S.W., Oerlemans, J. and Van der Hage, J.C., 1992, A study of ablation variations on the tongue of Hintereisferner, Austrian Alps, *Journal of Glaciology*, vol. 38, 130, p.319-324

Wendler, G.A. and Ishikawa, N., 1973, Experimental study of the amount of ice melt using three different methods: a contribution to the International Hydrological Decade, *Journal of Glaciology*, vol. 12, 66, p.399-410

Young, G.J., 1991, Hydrological interactions in the Mistaya basin, Alberta, Canada, in *Snow. Hydrology and Forests in High Mountain Areas*, IAHS/AISH Publ. No. 205, p.237-244